The cryptotephra record of the Marine Isotope Stage 12 to 10 interval (460–335 ka) at Tenaghi Philippon, Greece: Exploring chronological markers for the Middle Pleistocene of the Mediterranean region

Polina Vakhrameeva[1], Andreas Koutsodendris[1], Sabine Wulf[1,2], William J. Fletcher[3], Oona Appelt[4], Maria Knipping[5], Ralf Gertisser[6], Mario Trieloff[1], Jörg Pross[1]

[1] Institute of Earth Sciences, Heidelberg University, Im Neuenheimer Feld 234-236, D-69120 Heidelberg, Germany
[2] Department of Geography, University of Portsmouth, Buckingham Building, Lion Terrace, Portsmouth, PO1 3HE, United Kingdom
[3] Department of Geography, School of Environment, Education and Development, University of Manchester, Manchester, M13 9PL, United Kingdom
[4] Helmholtz Centre Potsdam, GFZ German Research Centre for Geosciences, Section 4.3 Chemistry and Physics of Earth Materials, Telegrafenberg, D-14773 Potsdam, Germany
[5] Institute of Botany, University of Hohenheim, Garbenstraße 30, D-70593 Stuttgart, Germany
[6] School of Geography, Geology and the Environment, Keele University, Keele, Staffordshire, ST5 5BG, United Kingdom

Keywords: Tephrostratigraphy; Italian and Aegean Arc volcanism; Marine Isotope Stages 10, 11 and 12; Eastern Mediterranean; land-sea correlation; Tenaghi Philippon

Highlights:

- 18 cryptotephra layers identified for the 460–335 ka interval at Tenaghi Philippon.
- Major- and trace-element compositions reveal Italian and Aegean Arc sources.
- One cryptotephra can be traced to the Santorini Cape Therma 1 eruption.
- Nine cryptotephras originate from a yet unknown Eastern Mediterranean source.
- Cryptotephra ages derived from orbitally tuned high-resolution pollen data.

Abstract

Precise chronologies that allow direct correlation of paleoclimate archives are a prerequisite for deciphering the spatiotemporal characteristics of short-term climate variability. Such chronologies can be established through the analysis of tephra layers that are preserved in the respective sedimentary archives. Here we explore the yet untapped tephrochronological potential of the Eastern Mediterranean region for the Middle Pleistocene, specifically for the interval spanning Marine Isotope Stages (MIS) 12–10 (460–335 ka). High-resolution cryptotephra analysis was carried out on peat cores spanning the MIS 12–10 interval that have been recovered from the iconic climate archive of Tenaghi Philippon, NE Greece. Eighteen primary cryptotephras were identified, and major- and trace-element analyses of single glass shards from all cryptotephras were performed in order to correlate them with their eruptive sources. The results suggest origins from both Italian and Aegean Arc volcanoes. Specifically, one cryptotephra layer could be firmly correlated with the Cape Therma 1 eruption from Santorini, which makes it the first distal tephra finding for this eruptive event. While eight further cryptotephras could be tentatively correlated with their volcanic or even eruptive sources, the provenance of another nine cryptotephras as yet remains unknown. The relatively large number of cryptotephras that could not be assigned to specific volcanic sources and eruptive events reflects the still considerable knowledge gap regarding the geochronology and geochemistry of proximal tephra deposits from the Middle Pleistocene of the Central and Eastern Mediterranean regions. Due to the lack of well-dated Middle Pleistocene eruptions, we provide age estimates for all cryptotephra layers identified in the MIS 12–10 interval at Tenaghi Philippon based on high-resolution pollen data from the same cores. While eight of the identified cryptotephras were deposited within MIS 12 (~438–427 ka), one cryptotephra was deposited at the onset of MIS 11 (~419 ka), five

cryptotephras during the younger part of MIS 11 (~391–367 ka), and four cryptotephras during MIS 10 (~359–336 ka). The high number of cryptotephras from multiple sources as recorded in the MIS 12–10 interval at Tenaghi Philippon highlights the key role of this archive for linking tephrostratigraphic lattices for the Middle Pleistocene of the Central and Eastern Mediterranean regions.

1 Introduction

The Middle Pleistocene period, spanning Marine Isotope Stages (MIS) 19 to 6 (c. 781–126 ka; Cohen et al., 2013), contains some of the arguably most interesting episodes of Quaternary climate evolution. It includes interglacials that represent the two best orbital analogues for the Holocene (i.e., MIS 11 and 19) and as such allow insight into the natural evolution of the present interglacial without human influence (e.g., Past Interglacials Working Group of Pages, 2016). At the same time, it comprises the two strongest glaciations of the past 800 ka (i.e., MIS 12 and 16; Lisiecki and Raymo, 2005).

Over the past decades, Middle Pleistocene climate dynamics have been studied in a number of proxy records from marine (e.g., Barker et al., 2015; Herbert et al., 2010), terrestrial (e.g., Cheng et al., 2016; Melles et al., 2012) and ice-core (e.g., Jouzel et al., 2007; Loulergue et al., 2008) archives that comprise multiple glacial/interglacial cycles. The synchronization of the datasets from these archives is a prerequisite for a mechanistic understanding of short-term climate variability, notably for the quantification of leads and lags between different components of the climate system. This is, however, hindered by the often considerable uncertainties in the age models that exist for the individual archives (Bronk Ramsey et al., 2015; Lowe et al., 2015).

An interesting avenue for the direct synchronization of geological archives is provided by tracing, dating and fingerprinting of tephra layers (Lowe, 2011; Lowe et al., 2015). Tephra layers represent time-sensitive marker horizons because of their geologically

instantaneous eruption and deposition. They circumvent chronological uncertainties as they are intrinsically connected to the application of absolute dating techniques. The geochemical composition of tephra glass shards represents their connection to a source volcano/individual eruption. Therefore, once a particular tephra layer has been geochemically characterized, it can be used to link, synchronize and potentially date sedimentary archives where it has been found. Ideally, a tephra layer can be dated via correlation to a previously dated eruptive event. Alternatively, it can be dated directly by K-Ar, Ar-Ar, U-series, and fission-track methods, or indirectly via dating of the host sediments (Bronk Ramsey et al., 2015). Identification of non-visible ash layers (i.e., cryptotephras) in distal localities has greatly extended the geographical area over which some eruptions can be traced (e.g., Davies, 2015). This approach has greatly boosted the establishment of tephrostratigraphic frameworks for the Late Pleistocene and Holocene in many parts of the world.

The Eastern Mediterranean is a key region for paleoenvironmental research. Due to its intermediate position between the climate systems of the higher and lower latitudes, it exhibits particularly high climatic and environmental variability (Lionello et al., 2012). At the same time, it has particular relevance for paleoanthropological, protohistorical and archeological research. It can help shed light on the dispersal dynamics of archaic and modern humans from Africa into Eurasia (e.g., Lowe et al., 2012; Müller et al., 2011; Zanchetta et al., 2018), and at the same time it represents the cradle of ancient civilizations (Freeman, 2014).

Although the Eastern Mediterranean region has yielded long sedimentary archives both from the marine (e.g., ODP Sites 964, 967, and 968 – e.g., Grant et al., 2017; Lourens, 2004; Fig. 1) and the terrestrial realm (e.g., Tenaghi Philippon – Pross et al., 2015; Lake Ohrid – Wagner et al., 2017; Lake Van – Litt et al., 2014) that cover the Middle Pleistocene, the precise correlation of these archives has remained challenging. For such

efforts, the massive explosive volcanism in the Eastern Mediterranean region as it has occurred from the Eocene onwards (Peccerillo, 2017) has great potential via the generation of a tephrostratigraphic lattice (Keller et al., 1978). However, the tephrostratigraphic framework for the Eastern Mediterranean region as available today does not extend beyond the past ~200 ka (e.g., Aksu et al., 2008; Wulf et al., 2018), and the vast majority of the Middle Pleistocene has yet remained unexplored (Leicher et al., 2016). In light of these limitations, a 'deeper-time' extension of tephrostratigraphic research in the Eastern Mediterranean region is required in order to facilitate precise correlation of already existing and newly emerging paleoclimate records of the Middle Pleistocene.

Within this context, the climate archive of Tenaghi Philippon (NE Greece; Fig. 1) plays a pivotal role. This archive, which lithologically consists predominantly of peat, spans the past 1.35 Ma continuously (Pross et al., 2015, and references therein). It has unique potential for a tephrostratigraphic approach not only because of its stratigraphic length and completeness, but also the favorable geographical setting with regard to the proximity of numerous volcanic sources (including Italy, the Aegean Arc and Anatolia; Fig. 1), and the peat-dominated lithology that warrants good preservation and straightforward detection of (crypto)tephra layers (St. Seymour et al., 2004; Wulf et al., 2018). Here we present a detailed cryptotephra study that has been carried out on new core material from Tenaghi Philippon covering the time interval between c. 460 and 335 ka, broadly corresponding to MIS 12–10 as defined by previously published and new high-resolution pollen data.

2 Tenaghi Philippon as a tephrostratigraphic archive

The Philippi peatland, which harbors the study site, is located in the southeastern part of the intramontane Drama Basin on the SE Balkan Peninsula (Fig. 1). Mostly referred to as

‘Tenaghi Philippon’, the Philippi peatland has emerged as a unique paleoclimate archive for the Quaternary in Europe. The succession consists of a nearly 200 m thick sequence of fen peat and lignite with intercalated lake marls and calcareous clays, making it the thickest known peat-dominated succession worldwide (Christanis et al., 1998). Based on pollen data from early drill cores, the succession spans the past ~1.35 Ma continuously (Pross et al., 2015; Tzedakis et al., 2006; Van der Wiel and Wijmstra, 1987; Wijmstra and Smit, 1976). New, high-quality cores were recovered from the 50–200 m interval of the Tenaghi Philippon archive in 2009 (Pross et al., 2015), providing the material for this study. Importantly, Tenaghi Philippon is located within the dispersal areas of many major explosive eruptions produced by the Italian and Aegean volcanic provinces, which makes it the only known long terrestrial archive from the Balkan Peninsula that documents tephras of both volcanic provenances (Wulf et al., 2018).

The exceptionally favorable conditions for (crypto)tephrostratigraphic studies at Tenaghi Philippon have yielded considerable information on tephrostratigraphic markers for the Upper Pleistocene and Holocene (c. 130–3 ka) of the Eastern Mediterranean region (e.g., Albert et al., 2015; Lowe et al., 2012; Pross et al., 2015; St. Seymour et al., 2004; Wulf et al., 2018). These studies demonstrate that the archive of Tenaghi Philippon is exceptionally well suited to expand the tephrostratigraphic framework for the Middle Pleistocene of the Central and Eastern Mediterranean region.

3 Potential tephra sources in the Eastern Mediterranean region during MIS 12–10

Considering the distance to the Tenaghi Philippon site and the prevailing westerly winds in the Eastern Mediterranean region, the potassium-rich Italian (820–870 km W of Tenaghi Philippon) and calcalkaline Aegean Arc volcanic provinces (370–550 km S of Tenaghi Philippon) can be expected as the main sources for tephra material at Tenaghi Philippon during the Middle Pleistocene (Fig. 1). The most prominent Italian volcanic

provinces that were explosively active during that time are the Roman and Ernici-Roccamonfina Provinces (Peccerillo, 2017) including the volcanoes of Vulsini, Vico, Sabatini, Colli Albani, Ernici, and Roccamonfina (Fig. 1), which produced particularly large explosive eruptions (e.g., Giaccio et al., 2013a; Marra et al., 2014; Nappi et al., 1998; Rouchon et al., 2008). A number of other Italian volcanic provinces exhibited explosive volcanism during MIS 12–10, including the Sicily Province with the volcanic centers of Etna, Pantelleria and Ustica, and potentially the Aeolian Islands with older volcanoes of Lipari, Salina and Filicudi (Peccerillo, 2017) as well as the Campanian Volcanic Zone (De Vivo et al., 2001; Rolandi et al., 2003).

In the Aegean Arc, the most voluminous and frequent explosive activity during the Middle Pleistocene took place at Santorini volcano (Fig. 1). For the MIS 12–10 interval, this activity is documented by at least one major and numerous minor pyroclastic units of the first explosive cycle of the Thera Pyroclastic Formation as well as the cinder cones of the Akrotiri Peninsula and subordinate tuffs of the preceding Peristeria volcano in the Santorini volcanic complex (Druitt et al., 1999). Other volcanic centers that experienced explosive volcanism during MIS 12–10 include Milos and Antimilos (Fytikas et al., 1986b; Marinos, 1959), Methana (Fytikas et al., 1976, 1986a; Gaitanakis and Dietrich, 1995; Matsuda et al., 1999; Pe, 1974) and probably Kos (Bachmann et al., 2010; Dalabakis and Vougioukalakis, 1993; Pasteels et al., 1986) (Fig. 1). The Middle Pleistocene tephrostratigraphy of Aegean Arc volcanoes has remained poorly studied; better age constraints and glass geochemical data to characterize proximal pyroclastic deposits sufficiently are needed even for Santorini, which arguably represents one of the best studied volcanoes in this region (e.g., Druitt et al., 1999; Huijsmans, 1985). Furthermore, because distal tephra occurrences in the Aegean Arc during MIS 12–10 are yet unknown, their dispersal areas have remained elusive.

Apart from the Italian and Aegean volcanoes, there are other volcanic centers in the greater Eastern Mediterranean region (Fig. 1) that were likely active during MIS 12–10 and were able to distribute tephra via seasonally occurring northerly and southeasterly winds reaching Tenaghi Philippon. These include (i) the alkaline Gölcük volcano in Western Anatolia (c. 650 km SE of Tenaghi Philippon; e.g., Nemec et al., 1998; Platevoet et al., 2008, 2014), (ii) the calcalkaline volcanic complexes of Central Anatolia (Acigöl, Erciyes and Hasan Dagi, c. 900–1000 km ESE of Tenaghi Philippon; e.g., Bigazzi et al, 1993; Deniel et al., 1998; Druitt et al., 1995; Schmitt et al., 2011; Şen et al., 2003), and (iii) the Eastern Carpathians in Romania (Ciomadul, c. 600 km N of Tenaghi Philippon; e.g., Harangi et al., 2015; Karátson et al., 2016; Molnár et al., 2018; Seghedi et al., 2004; Szakács et al., 2015). However, because pyroclastics from these regions still lack detailed chronological and glass-geochemical information, it has not yet been possible to trace them distally. Finally, more distant and hence less likely volcanic sources are located in Eastern Anatolia (e.g., Nemrut and Süphan Dagi, c. 1600 km E of Tenaghi Philippon; Schmincke and Sumita, 2014; Sumita and Schmincke, 2013a, b) and France (Sancy volcano, Mont-Dore, c. 1800 km W of Tenaghi Philippon; e.g., Nomade et al., 2012; Pastre and Cantagrel, 2001).

4 Material and methods

4.1 The Tenaghi Philippon peatland core "TP-2009"

Core TP-2009 (coordinates: 40° 57' 39.5" N, 24° 16' 03.1" E, 40 m a.s.l.), spanning from 50 to 200 m depth (c. 260 to 1350 ka), was recovered in 2009 and is located 4.4 km and 1.0 km ESE of the previously drilled sites TP-2005 and TF-II, respectively (see Pross et al., 2015, for a review). The investigated core interval from 82 to 63 m depth corresponds to an age of c. 480–350 ka based on the correlation of low-resolution pollen data to marine

isotope stages (Pross et al., 2015) and consists of peat, peaty mud and lake marls (Fig. 2).

4.2 Proximal correlative tephra samples

We sampled seven pumice and scoria fall deposits on Santorini in 2015 (see Supplement 1) and used data from the literature in order to correlate tephras found in core TP-2009 on the basis of their composition with proximal tephras in the region.

4.3 Tephra preparation and analysis

4.3.1 Tephra extraction and processing

To detect cryptotephra layers in the studied core material, extraction and analysis of volcanic glass shards were first performed on 10-cm-long contiguous sub-samples. Intervals in which glass shards were detected were then inspected in 1-cm increments in order to refine the stratigraphic positions of the identified cryptotephras. The volumes of the low- and high-resolution tephra samples were 10 cm^3 and 1 cm^3, respectively. In both cases, the sample material was taken from the central part of the cores to avoid potential tephra cross-contamination.

Extraction of glass shards from peat was performed using standard techniques (e.g., Gehrels et al., 2008) including removal of organic matter and carbonate material, enrichment of glass shards by density separation, as well as handpicking and mounting of glass shards in Epofix™ resin, and subsequent polishing for microanalytics (see Supplement 1). The documented cryptotephras were labeled following the scheme previously introduced for Tenaghi Philippon (Wulf et al., 2018); in this scheme, the abbreviation of the coring campaign (TP09) is followed by the mid-point of the sample depth interval (in meters) in which a cryptotephra was found (e.g., cryptotephra TP09-65.95).

The proximal samples from Santorini composed of pumice/scoria clasts were crushed, sieved into a 20-100 µm fraction and mounted onto stubs using Epofix™ resin prior to grinding and polishing for geochemical analysis.

4.3.2 Geochemical analysis of glass shards

4.3.2.1 Electron probe microanalysis (EPMA)

Major-element compositions of single glass shards were determined using a wavelength-dispersive (WDS) electron microprobe JEOL JXA-8500F at the German Research Centre for Geosciences in Potsdam. The instrument used an accelerating voltage of 15 kV, a 10 nA beam current, and a 3–10 µm beam with count times of 20 s for the elements Mg, P, Cl, Ti, Mn, and Fe, and 10 s for F, Ca, Al, Si, K, and Na (analyzed first). A range of MPI-DING reference glasses including GOR128-G (komatiite), GOR132-G (komatiite), ATHO-G (rhyolite) and StHs6/80 (andesite) (Jochum et al., 2006) as well as natural Lipari obsidian (Hunt and Hill, 1996; Kuehn et al., 2011) were employed as secondary glass standards, and measured once prior to sample analyses in order to maintain inter-laboratory consistency of analytical data (Supplements 2, 3). The EPMA data were normalized to 100% total oxides on a volatile-free basis to allow data comparison. Low values (<90% for rhyolitic and <95% for other glasses) of total oxides were rejected, except for one tephra for which better quality data were not available.

4.3.2.2 Secondary Ion Mass Spectrometry (SIMS)

Trace-element compositions of selected glass shards were analyzed at Heidelberg University using a CAMECA IMS 3f ion probe. The operating conditions were a current intensity of 10 nA, a spot diameter of 10 µm, a width of the energy slit of 50 eV, and a voltage offset applied to the sample accelerating voltage (+4.5 kV) of -105 V.

Pre-sputtering time was 120 s, and five acquisition cycles with the following count times per cycle were obtained: Si (2 s), Rb (5 s), Sr (5 s), Y (5 s), Zr (5 s), Nb (5 s), Ba (5 s), La (5 s), Ce (5 s), Th (20 s), and U (20 s). As an internal (primary) standard for the instrument, the NIST-SRM 610 glass standard was used, and the rhyolitic ATHO-G, the andesitic StHs6/80-G, and the basaltic GOR132-G glass standards (Jochum et al., 2006) were used as secondary reference materials.

4.4 Pollen analysis

In the present study, pollen data were used as a reference dataset in order to provide age constraints for the detected cryptotephras. For this purpose, the previously published, low-resolution pollen dataset of Pross et al. (2015) was augmented by an additional 100 new pollen samples for the 82.00–62.50 m depth interval of the TP-2009 core that were taken every 13 to 28 cm (mean: c. 20 cm) corresponding to an average temporal resolution of 0.8–1.8 ka. Palynological processing followed the methods given in Pross et al. (2015); for details see Supplement 1. At least 300 pollen grains were counted per sample whenever possible, excluding Poaceae, Cyperaceae, aquatic plants, and fern spores.

Arboreal pollen (AP) percentages were used to identify glacial-interglacial cycles in the study interval, on the basis that forest expansion at Tenaghi Philippon occurs under interglacial boundary conditions and *vice versa* (Pross et al., 2015; Tzedakis et al., 2006). Specifically, we have aligned our new palynological data from core TP-2009 to the old palynological record from Tenaghi Philippon (TF-II; Van der Wiel and Wijmstra, 1987; Wijmstra and Smit, 1976) using the orbitally tuned age model of Tzedakis et al. (2006). The two records were aligned using minima, maxima and inflection points of the tree-pollen percentages using the AnalySeries software (Paillard et al., 1996; see Table S1-1 in Supplement 1 for details).

5 Results

5.1 Identification of cryptotephra layers

Glass-shard extraction across the 82–63 m depth interval of core TP-2009 yielded 20 cryptotephra layers for which EPMA analysis was carried out (Table 1; Fig. 2). An additional five samples also contained glass shards; however, due to the extremely low concentrations (1 shard per 10 cm^3 of peat) and small sizes (<50 µm) of the shards in these samples, no geochemical analysis was possible (Table 1). Trace-element compositions were analyzed in 13 of the 20 cryptotephras; the remaining seven cryptotephras consisted of glass shards that were too small and/or vesicular to expose sufficiently large polished surfaces for the 10 µm beam of the SIMS apparatus.

Representative EPMA and SIMS data of the identified cryptotephras are given in Table 2, whereas full geochemical data are provided in Supplement 2. Normalized (volatile-free) EPMA glass data as plotted on the total alkali *vs*. silica (TAS) classification diagram (Le Bas et al., 1986) are shown in Fig. 3a. Tephra-shard counts range from 1 to 27 shards per cryptotephra sample (volume: 1–10 cm^3). Because of the scarcity of volcanic glass in all samples, shard concentrations per gram dry weight were not calculated. In the following, we give an account of the cryptotephras encountered, starting with the oldest cryptotephras of MIS 12 and finishing with the youngest cryptotephras of MIS 10.

5.1.1 MIS 12 cryptotephras (82–75 m core depth)

5.1.1.1 Cryptotephras TP09-77.95 to TP09-75.75 (eight layers)

Eight consecutive samples between 78.00 and 75.70 m core depth contained glass shards of similar rhyolitic composition. The number of shards, partly measured by EPMA (Table 2), varied from seven (TP09-77.65) to one (TP09-76.95 and TP09-77.35) in each

sample (Table 1). SIMS analysis was possible for all samples but TP09-76.05 and TP09-76.75, and the number of analyzed shards varied from four to one per sample (Table 2). Their major-element compositions define the cryptotephras as low-silica rhyolites (72.4–75.7 wt% SiO_2; normalized data) with high-K calcalkaline affinity (3.4–6.4 wt% K_2O) (Fig. 3a, b). Na_2O concentrations are much lower (0.36–1.20 wt%) than K_2O values, resulting in high alkali (K_2O/Na_2O) ratios of 3.80–12.83 (Fig. 3c). MgO (1.3–2.9 wt%) and CaO (1.6–7.3 wt%) show high values with a greater degree of scatter. Trace-element data support compositional homogeneity of the tephras (Supplement 2).

5.1.2 MIS 11 cryptotephras (75–66 m core depth)

5.1.2.1 Cryptotephra TP09-74.75

Cryptotephra TP09-74.75 consists of two shards; one of them was analyzed by EPMA and SIMS and yielded a composition reminiscent of that of the older cryptotephras TP09-77.95 to TP09-75.75 as described above (Table 2). The TP09-74.75 cryptotephra is defined as a low-silica rhyolite (73.3 wt% SiO_2), however, unlike the older cryptotephras, it has calcalkaline affinity due to the slightly lower K_2O concentrations (3.0 wt% K_2O) (Fig. 3a, b). At the same time the Na_2O content is higher (2.1 wt%) and the alkali ratio is lower (1.41) than in the older cryptotephras (Fig. 3c).The trace-element concentrations of cryptotephra TP09-74.75 are compatible with those of the older cryptotephras (Supplement 2).

5.1.2.2 Cryptotephra TP09-70.45

Cryptotephra TP09-70.45 is represented by a single shard of trachytic composition (Fig. 3a). One more shard was detected in the high-resolution sample TP09-70.405, but could not be extracted for geochemical analysis. Due to the lack of EPMA data proving that this

shard represents the same cryptotephra as in the low-resolution sample, the stratigraphic position of cryptotephra TP09-70.45 cannot be constrained more precisely.

The composition of cryptotephra TP09-70.45 is defined by 63.4 wt% SiO_2, 7.2 wt% Na_2O, 4.8 wt% K_2O, 0.83 wt% CaO, 0.33 wt% MgO, and 0.82 wt% Cl (Table 2). The alkali ratio of 0.67 classifies it as sodium-rich (Fig. 3c). In comparison with other trachytic tephras in the MIS 12–10 interval of core TP-2009, this tephra exhibits lower contents of K_2O and CaO as well as a lower K_2O/Na_2O ratio.

5.1.2.3 Cryptotephra TP09-68.95

Cryptotephra TP09-68.95 is represented by a single glass shard detected in a 10-cm resolution sample. Based on EPMA data (Table 2), TP09-68.95 can be classified as a calcalkaline low-silica rhyolitic tephra with SiO_2 values of 69.8 wt% (Fig. 3a). It straddles the boundary between medium and high K_2O concentrations (3.1 wt%) (Fig. 3b). The Na_2O content (4.6 wt%) is higher than the K_2O content, yielding an alkali ratio of 0.68 (Fig. 3c).

5.1.2.4 Cryptotephras TP09-67.15, -67.05 and -66.95

The dacitic cryptotephra TP09-67.15 and the rhyolitic cryptotephras TP09-66.95 and TP09-67.05 were isolated from three consecutive low-resolution samples. Cryptotephra TP09-67.15 is represented by 27 glass shards, which makes it the best documented tephra in the examined interval of core TP-2009. Four and three glass shards were analyzed by EPMA and SIMS, respectively. From the rhyolitic cryptotephras, three and two shards were counted, respectively, and one shard of each cryptotephra was analyzed by EPMA and SIMS.

Cryptotephra TP09-67.15 is a calcalkaline dacite (Fig. 3a, b) and has a well-constrained compositional range of major-element concentrations, e.g., SiO_2 (63.6–64.0 wt%), Na_2O

(4.5–4.7 wt%), and K_2O (2.1 wt%) (Table 2). The alkali ratios are 0.45–0.47 (Fig. 3c). Trace-element compositions of three glass shards also show narrow ranges of element concentrations (Supplement 2).

Cryptotephras TP09-66.95 and TP09-67.05 are both calcalkaline to high-K calcalkaline low-silica rhyolites (Fig. 3a, b), with major-element compositions that are similar to that of the previously described cryptotephra TP09-68.95 (Table 2). The respective concentrations of some major elements are 69.6 and 69.9 wt% SiO_2, 4.3 and 4.6 wt% Na_2O, and 3.7 and 3.1 wt% K_2O (Supplement 2). Both tephras have Na_2O values exceeding K_2O values, resulting in alkali ratios of 0.66–0.86 (Fig. 3c). Trace-element data confirm the similarity between cryptotephras TP09-66.95 and TP09-67.05 (Table 2).

5.1.3 MIS 10 cryptotephras (66–63 m core depth)

5.1.3.1 Cryptotephras TP09-65.95, -65.835a and -65.835b

Three glass shards were detected in a 10-cm resolution sample at 65.9–66.0 m depth, one of which was analyzed by EPMA. Despite the low analytical total, we use the EPMA data of the only available glass shard of this sample for further discussion.

One more glass shard was found in the adjacent low-resolution sample at 65.8–65.9 m depth. Detection of four more glasses at 65.83–65.84 m depth further refined the stratigraphic position of the cryptotephra. EPMA and SIMS compositions of two glasses from the 1-cm resolution sample are distinctly different, and thereby two cryptotephras were distinguished at the same depth (TP09-65.835a and TP09-65.835b).

The major-element composition of cryptotephra TP09-65.95 indicates a calcalkaline dacite (Table 2; Fig. 3a, b) with concentrations of 66.7 wt% SiO_2, 2.7 wt% K_2O and 4.4 wt% Na_2O, yielding a K_2O/Na_2O ratio of 0.61 (Fig. 3c).

Cryptotephra TP09-65.835a shows trachytic affinity with 62.1 wt% SiO_2 and a K_2O/Na_2O ratio of 1.2 indicative of shoshonites (Fig. 3a, c). It contains 7.0 wt% K_2O, 6.0 wt% Na_2O,

2.3 wt% CaO, 0.34 wt% MgO, and 0.82 wt% Cl. SIMS analysis of cryptotephra TP09-65.835a yielded trace-element data (Table 2).

Cryptotephra TP09-65.835b is a calcalkaline rhyolite with high contents of SiO_2 (76.8 wt%) and K_2O (5.0 wt%) (Fig. 3a, b) whereby K_2O is more abundant than Na_2O (K_2O/Na_2O = 1.94) (Fig. 3c). Trace-element data further define its composition (Table 2).

5.1.3.2 Cryptotephras TP09-63.05, -63.015a and -63.015b

Twelve glass shards were detected in the 63.0–63.1 m depth range of core TP-2009. Nine of them were analyzed by EPMA and revealed three different compositions. Cryptotephra TP09-63.05 comprises three glass shards of trachytic composition. Four more trachytic glass shards were found during high-resolution tephra search. They are, however, geochemically different from the ones found in the low-resolution sample and therefore form a separate cryptotephra (i.e., TP09-63.015a). The third cryptotephra of rhyolitic affinity was first detected in the low-resolution sample and then constrained to the same depth as the trachytic cryptotephra TP09-63.015a. It is represented by two glass shards and was labeled TP09-63.015b. Two more tephra shards from another high-resolution sample TP09-63.005 appear to be from a sodium-rich trachyte, but were not considered further because they yielded Na values that were considerably higher (8.27–8.62 wt%) than those typical for sodium-rich trachytes. SIMS data were obtained only from two glasses of cryptotephra TP09-63.05.

The trachytic cryptotephra TP09-63.05 has a tight compositional range (60.6–61.7 wt% SiO_2, 7.6–7.8 wt% K_2O, 3.8–4.5 wt% Na_2O, 2.7–2.9 wt% CaO, 0.77–0.88 wt% MgO, and 0.32–0.37 wt% Cl) and is characterized by an alkali ratio of 1.7–2.0 indicating potassium-rich rocks (Table 2; Fig. 3a, c). SIMS trace-element concentrations of two glass shards also show homogenous compositions (Supplement 2).

Cryptotephra TP09-63.015a straddles the trachyte-phonolite boundary and has comparable SiO_2 contents (61.5–62.0 wt%), but lower alkali ratios (0.9–1.0) relative to cryptotephra TP09-63.05, which assigns it to shoshonites (Fig. 3a, c). Lower concentrations of K_2O, FeO, CaO and MgO (5.9–7.1, 2.9–3.1, 1.2–1.8, and 0.34–0.37 wt%, respectively) and higher Na_2O and Cl values (6.9–7.2 and 0.79–0.84 wt%, respectively) of cryptotephra TP09-63.015a further discriminate it from cryptotephra TP09-63.05.

The rhyolitic cryptotephra TP09-63.015b has 71.4–72.5 wt% SiO_2 and straddles the boundary between medium and high K_2O values (3.2–3.3 wt%) (Fig. 3a, b). One of the analyzed shards shows a very low Na_2O content, apparently resulting from Na loss during EPMA analysis. The other glass shard is characterized by higher Na_2O than K_2O concentrations and has an alkali ratio of 0.70 (Fig. 3c).

6 Discussion

6.1 Sources of identified cryptotephras

The cryptotephras identified in the MIS 12–10 interval of the TP-2009 core were grouped into five main geochemical populations (POP#) with the first one (POP1) subdivided in three sub-populations (POP1A to POP1C) based on their major-element glass compositions (Table 1; Fig. 3) and compared with previously published glass-compositional data of proximal and distal tephra deposits from the Mediterranean region. The compositional groups were discriminated using classification diagrams (Fig. 3) as well as other major- and trace-element plots presented in Figs. 4 to 8 (see also figures in Supplement 4). These populations have the potential to represent different provenances of the identified cryptotephras. In the following, we therefore provide a detailed discussion on the proposed volcanic sources and tephra correlations for the trachytic population

POP1 (see Section 6.1.1), the dacitic population POP2 and the rhyolitic population POP3 (Section 6.1.2.1), and the rhyolitic populations POP4 and POP5 (Section 6.1.2.2).

6.1.1 Sources of trachytic cryptotephras

During the Quaternary, Italian volcanism produced numerous compositionally diverse pyroclastics ranging from mafic to felsic and from sub-alkaline to ultra-alkaline (e.g., Peccerillo, 2017). Its distinctive characteristics within the Mediterranean magmatic realm are the high abundance of sodic and particularly potassic alkaline volcanics (Peccerillo, 2017), a feature that we also observe in the four trachytic TP-2009 cryptotephra layers of POP1 (TP09-63.05, -63.015a, -65.835a, and -70.45). Given that trachytic pyroclastics were massively produced by the Roccamonfina, Sabatini, Vico and Vulsini volcanoes in Italy during the studied time interval (Marra et al., 2014; Palladino et al., 2014; Rouchon et al., 2008), these Italian volcanoes are the most likely sources for these tephras.

Trachytes are also common eruptive products of the Campanian Province (e.g., Ischia, Campi Flegrei), which was characterized by violent explosive activity during the Late Pleistocene. The oldest volcanic rocks exposed on Ischia and within the Campi Flegrei are dated at c. 150 and 60 ka, respectively (e.g., Poli et al., 1987; Pappalardo et al., 1999), whereas outside the Campanian Plain, in the western foothills of the Apennine Mountains, ignimbrites produced by Campanian activity yielded ages from 290 to 116 ka (De Vivo et al., 2001; Rolandi et al., 2003). Therefore, based on the evidence from proximal sites Campanian tephra deposits are too young to be present in our record. In contrast, however, several much older tephras from marine and lacustrine sediment records in central-southern Italy and on the Balkan Peninsula that yielded geochemical signatures of Campanian provenance suggest that Campanian volcanoes might potentially be older than previously thought. These tephras include the V5/Parmenide tephra (c. 723 ka) found in the Montalbano Jonico sequence as well as in the Crotone

and Sulmona basins (Giaccio et al., 2013b; Petrosino et al., 2015), the V7 tephra (c. 687 ka) from Montalbano Jonico (Petrosino et al., 2015), the A12/A11 and SC2 tephras (514.2±5.6 ka) from the Acerno and Mercure basins (Giaccio et al., 2014; Petrosino et al., 2014), which are equivalent to tephra OH-DP-2017 in Lake Ohrid (SW Balkan Peninsula; Leicher et al., 2016), and the TAV2 tephra from the Mercure basin (c. 494–438 ka; Giaccio et al., 2014). Another potential Campanian tephra, the exceptionally thick Morphi ash fall deposit in western Epirus (SW Balkan Peninsula), dates to 374±7 ka (Pyle et al., 1998). Based on major-element characteristics and Sr isotope ratios of the SC2 and TAV2 tephras, Giaccio et al. (2014) have proposed an alternative correlation of these tephras with trachytes from Ponza Island off the Italian Campania-Latium coast. Because, however, of the older ages of its volcanic products (final volcanic activity ~1 Ma; Cadoux et al., 2005) we can firmly exclude Ponza as a source for our cryptotephras during MIS 12–10. We therefore consider Campanian volcanoes as potential sources for the trachytic cryptotephras in the MIS 12–10 section of the TP-2009 core.

6.1.1.1 Cryptotephras TP09-63.015a (trachytic component) and TP09-63.05

The chemical composition of cryptotephra TP09-63.015a lies at the boundary between the Campi Flegrei and the Ischia compositional fields, while cryptotephra TP09-63.05 falls within the overlap of the Roccamonfina and Campi Flegrei compositional fields (Figs. 4, S4-2). All glass-based major-element compositions of cryptotephra TP09-63.05 match those of the upper flow unit of the Campanian Ignimbrite (CI, 39.85±0.14 ka; Giaccio et al., 2017a), while two shards of cryptotephra TP09-63.015a match the CI basal fall and lower and intermediate flow units with respect to their major-element chemistry (Figs. 4b, 5, S4-3). The SIMS trace-element data obtained from two glass shards of cryptotephra TP09-63.05 confirm that it fits both LA-ICPMS (Tomlinson et al., 2012a) and SIMS (Wulf et al., 2018) compositions of the CI upper flow unit (Figs. 5, S4-3). The CI occurs as a 23-

cm-thick tephra layer further upcore at 12.87 m depth in the Tenaghi Philippon sequence (Müller et al., 2011), and coring-related re-deposition from that tephra in the top core segments of the 40-130 ka part of the sequence has been reported (Wulf et al., 2018). We therefore interpret both the TP09-63.05 and -63.015a shards to be re-worked from the CI.

6.1.1.2 Cryptotephra TP09-65.835a (trachytic component)

The trachytic glass component TP09-65.835a of the bimodal cryptotephra layer at 65.835 m core depth can be assigned to Campanian volcanic activity, which is shown by the CaO/FeO *vs*. Cl plot (Giaccio et al., 2017b) where it matches the Campi Flegrei compositional field (Fig. 4b). It falls partly within the geochemical envelope of the basal fall and lower and intermediate flow units of CI on major- and trace-element plots (Figs. 5, S4-3). However, it can be discriminated from the CI on the basis of the lower Cl to CaO/FeO ratio (Fig. 4b). Consequently, we consider cryptotephra TP09-65.835a a primary fallout deposit of Campanian origin.

TP09-65.835a plots close to, but does not overlap with the trachytic Middle Pleistocene tephra layers that have been attributed to the Campanian Province by several authors (e.g., Giaccio et al., 2014; Petrosino et al., 2015; Leicher et al., 2016) based on their major-element chemistry (Figs. 5, S4-3). Only one of these tephras is defined in terms of trace-element composition (V5; Petrosino et al., 2015); it shows a considerably lower Nb content than TP09-65.835a (Fig. 5). Two eruptions that occurred during MIS 12–10 are those causing the Morphi (374±7 ka, Pyle et al., 1998) and TAV2 tephras (c. 494–438 ka, Giaccio et al., 2014). Published EPMA data of the Morphi and TAV2 tephras show major-element concentrations that are strongly similar to that of TP09-65.835a, but reveal differences in their MgO, CaO and Na_2O contents (Figs. 5, S4-3). The TAV2 tephra can be clearly discriminated from TP09-65.835a in the Cl *vs*. CaO/FeO diagram (Fig. 4b).

Hence, at this stage we cannot correlate the TP09-65.835a cryptotephra with a dated eruptive event, but we suggest an origin from an unknown MIS 10 eruption in the Campanian Province.

6.1.1.3 Cryptotephra TP09-70.45

The sodium-rich trachytic glass composition of cryptotephra TP09-70.45 differs from that of the three younger trachytic cryptotephras found by a substantially lower alkali ratio (0.67), slightly lower K_2O (4.8 wt% compared to 5.9–7.8 wt%) and CaO values (0.83 wt% compared to 1.2–2.9 wt%), and higher SiO_2 concentrations (63.4 wt% compared to 60.6–62.1 wt%) (Figs. 4a, 5, S4-3). Together with the relatively high Cl content (0.82 wt%) and the very low CaO/FeO ratio (0.27) matching the Ischia compositional field (Fig. 4b), this composition suggests a Campanian provenance. A correlation of cryptotephra TP09-70.45 with the Morphi tephra (374±7 ka, Pyle et al., 1998) or the TAV2 tephra (c. 494–438 ka, Giaccio et al., 2014) is not supported by the major-element compositions (Figs. 5, S4-3). Therefore, we propose that cryptotephra TP09-70.45 represents an unknown eruption from the Campanian Province during MIS 11.

6.1.2 Sources of dacitic and rhyolitic cryptotephras

A total of 16 cryptotephra layers from the studied interval of the TP-2009 core show either calcalkaline dacitic or rhyolitic glass compositions of either Aegean Arc or yet undefined Eastern Mediterranean provenance (Figs. 3a, d, 6, S4-1, S4-4). Out of these, the two dacitic layers (TP09-65.95 and TP09-67.15) and four rhyolitic layers of glass population POP3 (cryptotephras TP09-63.015b, TP09-66.95, TP09-67.05 and TP09-68.95) show compositions that are typical for Santorini tephras (see Section 6.1.2.1). Cryptotephra TP09-65.835b (glass population POP4) and nine older layers of glass population POP5 have high-silica rhyolitic glass compositions that either overlap with the tephra

compositions of Aegean Arc volcanoes, or partly overlap with those of Aegean Arc/Eastern Carpathian volcanoes; they cannot yet be assigned to individual volcanic sources (see Section 6.1.2.2).

6.1.2.1 Tephras of Santorini provenance

The six TP09 cryptotephras of Santorini provenance exhibit two different glass compositions. Cryptotephras TP09-65.95 and TP09-67.15 are calcalkaline dacites and can be grouped into glass population POP2. In contrast, cryptotephras TP09-63.015b, TP09-66.95, TP09-67.05 and TP09-68.95 are calcalkaline to high-K calcalkaline low-silica rhyolites and represent glass population POP3 (Figs. 3, 6, S4-4).

Santorini is the most explosive caldera-forming volcano within the Southern Aegean Arc and has been active since at least 650 ka (Druitt et al., 1999). Its younger activity is divided into two main explosive cycles, and a total of twelve major and numerous minor pyroclastic eruptions (labeled as M1 to M12; Druitt et al., 1999). Most of the major explosive eruptions are characterized by some degree of magma heterogeneity and/or zoning, and two types of compositional zoning present in magma reservoirs based on bulk-rock (XRF) compositional data can be distinguished (Druitt et al., 1999): (i) a predominantly silicic (rhyodacitic) magmas (66.3–71.4 wt% SiO_2) with a subordinate basaltic-andesitic component (47–62 wt% SiO_2) showing large compositional gaps, and (ii) a predominantly intermediate (andesitic-dacitic) composition (56-64 wt% SiO_2) with a minor, more evolved dacitic component (61.8–67.0 wt% SiO_2) showing large as well as small compositional gaps and zoning.

6.1.2.1.1 Cryptotephra TP09-63.015b (rhyolitic component)

The rhyolitic cryptotephra TP09-63.015b of glass population POP3 with SiO_2 contents of c. 72 wt% is comparable with the bulk composition of the first group of predominantly

rhyodacitic eruptions of Santorini (Fig. S4-5). It best matches the newly obtained EPMA glass composition of the pumice fall deposit of the Cape Therma 2 (CT-2) eruption (sample SAN15-28, Supplements 1, 3; Figs. 7, S4-6). The CT-2 pumice fall has not yet been dated directly, but its age (c. 224 ka) can be constrained by the directly overlying rhyodacitic lava flows of Cape Alonaki that yielded a K-Ar age of 224±5 ka (Druitt et al., 1999). Given the compositional similarity and the absence of a paleosol between the CT-2 pumice fall and the Cape Alonaki lavas, they were probably produced by a single eruption (Druitt et al., 1999). Because cryptotephra TP09-63.015b is older than the CT-2 eruption by more than 100 ka (see Section 6.2), it may potentially represent reworked material from an undetected primary CT-2 tephra layer in the yet unstudied interval upcore in the Tenaghi Philippon record. This interpretation is strongly supported by the reworked CI material in the same sample (see Section 6.1.1).

6.1.2.1.2 Cryptotephras TP09-65.95 and TP09-67.15

The dacitic glass population POP2 (63.6–66.7 wt% SiO_2) best matches the bulk composition of more evolved components of the second group of predominantly intermediate eruptions of Santorini (Fig. S4-5). Potential explosive Santorini eruptions with dacitic compositions that occurred during the studied time interval are the Cape Therma 1 (CT-1) and younger Cape Therma 3 (CT-3) eruptions (Druitt et al., 1999). Comparisons of newly obtained EPMA glass data of basal pumice fall and ignimbrite deposits from the CT-3 (sample SAN15-26) and CT-1 eruptions (samples SAN15-33, SAN15-34, and SAN15-36, Supplements 1, 3) show strong similarities and a close match with both the TP09-65.95 and the less evolved TP09-67.15 cryptotephras (Figs. 7, S4-6). The age of the CT-3 eruption is bracketed between those of the preceding CT-2 (c. 224 ka; Druitt et al., 1999) and the post-dating Lower Pumice 1 (c. 184 ka; Gertisser et al., 2009) eruptions of Santorini, and thus appears to be considerably younger than the

studied time interval. The published age of the CT-1 eruption of ≤360 ka is based on dating of andesites at Cape Alai that underlie CT-1; they yielded values ranging from 145±64 to 425±39 ka based on K/Ar, and 456±138 ka based on $^{40}Ar/^{39}Ar$ dating (Druitt et al., 1999). This age is compatible with those of both cryptotephras TP09-65.95 and TP09-67.15 (see Section 6.2), and we therefore correlate them with the CT-1 eruption. The trace-element glass data of cryptotephra TP09-67.15 compared to the only available bulk trace-element compositions of the CT-3 and CT-1 eruptions further support this interpretation; on most bivariate plots it falls either within the CT-1 geochemical envelope or within the overlap of the CT-1 and CT-3 envelopes (Figs. 7, S4-6). Although TP09-67.15 contains a much larger number of glass shards (n=27) compared to TP09-65.95 (n=3), we consider the latter to represent the primary layer because its age is more compatible with that of the proximal CT-1 deposits, and TP09-67.15 to be likely reworked material that has been displaced by post-depositional processes. An alternative interpretation of cryptotephra TP09-67.15 is that it might represent a yet unknown interplinian eruption within the minor pyroclastic sequence M1 below the CT-1 deposits on Santorini (Druitt et al., 1999).

6.1.2.1.3 Cryptotephras TP09-66.95, TP09-67.05 and TP09-68.95

The three remaining rhyolitic TP09 cryptotephras of glass population POP3 with SiO_2 contents of c. 70 wt% also derive from predominantly rhyodacitic magmas of Santorini eruptions (Fig. S4-5) and are stratigraphically older than the CT-1 eruption. However, little information is yet available on the pyroclastic activity that predated the first explosive cycle at Santorini (Druitt et al., 1999). Peristeria volcanic deposits, which predate (530–430 ka, Druitt et al., 1999) the Thera pyroclastics on Santorini, are predominantly basaltic to andesitic, rarely dacitic, lavas with subordinate tuffs. A correlation of MIS 11 cryptotephras from the TP-2009 core with Peristeria deposits is precluded not only by the

age discrepancy, but also the lack of published glass EPMA data on Peristeria pyroclastic units.

At Cape Plaka (Santorini), two white and well-sorted pumice fall deposits underlie the CT-1 pyroclastic unit, namely layer SAN15-35 (directly underlying CT-1) and SAN15-37 (underlying SAN15-35; Supplement 1); they most likely relate to the yet undated minor pyroclastic unit M1 of Druitt et al. (1999). Newly obtained major-element glass data of these two deposits (Supplement 3) reveal a rhyolitic composition that is similar to that of cryptotephras TP09-66.95, -67.05 and -68.95. In general, SAN15-35 and SAN15-37 are both less evolved than CT-2, with SAN15-37 partly overlapping the CT-2 composition. Cryptotephras TP09-66.95, -67.05 and -68.95 plot compositionally between SAN15-35 (67.7–69.4 wt% SiO_2) and SAN15-37 (70.3–72.3 wt% SiO_2), and some element concentrations (e.g., TiO_2, MgO, CaO) overlap with the SAN15-35 compositions (Figs. 7, S4-6).

The trace-element glass compositions of cryptotephras TP09-66.95 and -67.05 show a close match with the bulk trace-element data of the CT-2 eruption (Figs. 7, S4-6). Due to the lack of trace-element data for SAN15-35 and SAN15-37 we can only establish a tentative correlation of the identified cryptotephras with unit SAN15-35. All three cryptotephra layers most likely derive from one single volcanic event, of which TP09-66.95 is interpreted as the primary layer (three glass shards). TP09-67.05 and TP09-68.95 are most likely reworked material derived from the primary layer that have been displaced downward by post-depositional processes within the Tenaghi Philippon peat sequence.

6.1.2.2 Tephras of undefined provenance

A total of ten TP09 cryptotephra layers have high-silica rhyolitic compositions of undefined provenance. Cryptotephra TP09-65.835b of glass population POP4 can only

tentatively be assigned to Aegean Arc activity (Figs. 3d, 6, S4-1, S4-4). The nine cryptotephras of glass population POP5 show compositions that do not match any known potential volcanic sources (Figs. 3d, 6, S4-1, S4-4).

6.1.2.2.1 Cryptotephra TP09-65.835b (rhyolitic component)

The major-element data of cryptotephra TP09-65.835b of glass population POP4 overlaps with the geochemical compositions of Quaternary tephras from Aegean Arc volcanoes (excluding Santorini) as well as with that of younger rhyolitic tephras from the Aeolian Arc (<55 ka), the Eastern Carpathians (<53 ka), and Central Anatolia (<27 ka) (Figs. 6, S4-4).

Potential volcanic sources within the Aeolian Arc include Lipari and Salina Islands, which started their eruptive history c. 267 and c. 244 ka ago, respectively (Peccerillo, 2017). However, the earliest eruptive epochs of these islands are exclusively characterized by effusive and explosive eruptions with basaltic and basalt-andesitic compositions, while rhyolitic magmatism only commenced during the latest eruptive epochs (<55 ka; Albert et al., 2017; Forni et al., 2013; Lucchi et al., 2013). Furthermore, the trace-element glass compositions of younger rhyolitic tephra deposits from Lipari and Salina are distinct from that of cryptotephra TP09-65.835b (Figs. 6a, S4-4). Despite its compositional similarity with Late Pleistocene tephras with regard to major elements and partly also trace elements (Figs. 6b, S4-4), we cannot correlate cryptotephra TP09-65.835b with Eastern Carpathian and Central Anatolian volcanic eruptions because of the scarcity of tephrostratigraphic information available for these centers. A more likely source of cryptotephra TP09-65.835b is the Aegean Arc, which also provides the best match for the cryptotephra on the basis of both major- and trace-element concentrations (Figs. 6a, S4-4). Apart from Santorini, other volcanoes of the Aegean Arc are also known to have erupted during MIS 12–10 (Figs. 8, S4-7). These are (i) the volcanic archipelago of Milos,

with the Trachilas complex of the Island of Milos and the entire Island of Antimilos emplaced at c. 370–320 ka (Fytikas et al., 1986b); (ii) the peninsula of Methana with volcanics of the Chelona Series dated at c. 380–290 ka (Fytikas et al., 1976; Gaitanakis and Dietrich, 1995; Matsuda et al., 1999), and (iii) Kos Island with the pyroclastics of the Kefalos Series, dated at c. 550 ka, but considered to be potentially younger (Bachmann et al., 2010; Pasteels et al., 1986). However, reliable correlations of these pyroclastics with cryptotephra TP09-65.835b are hindered by the scarcity of glass compositional data of proximal products, since bulk chemical data may provide false information. This can be best demonstrated by the comparison of bulk chemical data of the Chelona pyroclastics of Methana (Fytikas et al., 1986a; Mitropoulos et al., 1987) with interstitial glass data of older cognate xenoliths (Pe, 1974): the former shows compositional ranges from basaltic andesites to dacites, while the latter displays a rhyolitic affinity (73.9–78.4 wt% SiO_2). With regard to its composition (e.g., SiO_2, MgO, FeO and CaO), the interstitial glass is partially similar to the single-glass composition of cryptotephra TP09-65.835b (Figs. 8, S4-7).

One bulk-pumice analysis of the Kefalos Tuff from Kos (Dalabakis and Vougioukalakis, 1993) yielded a high-SiO_2 rhyolitic composition (77.6 wt% SiO_2), which approximates the glass composition of cryptotephra TP09-65.835b (Figs. 8, S4-7). EPMA glass data available from the younger Kos Plateau Tuff (c. 161 ka) indicate a high-silica rhyolitic association with SiO_2 contents of 76.5–78.3 wt% (Aksu et al., 2008; Zouzias and St. Seymour, 2013), while bulk pumice analyses yield less SiO_2-rich values of 73.2–77.0 wt% (Pe-Piper and Moulton, 2008; Zouzias and St. Seymour, 2008) (Fig. 8). Cryptotephra TP09-65.835b plots within the Kos glass geochemical envelope on all bivariate plots, except for the Na_2O *vs*. SiO_2 diagram where it shows lower Na_2O contents (Figs. 8, S4-7). The rhyolites of the Kos Plateau Tuff and the Kefalos Series are similar in composition and mineralogy, and both were probably generated by fractional crystallization from

magmas similar to the Kefalos dacites (Bachmann and Schnyder, 2006). This would support a tentative correlation of cryptotephra TP09-65.835b with the Kefalos Series from Kos.

Although pyroclastic deposits were documented on Antimilos (Fytikas et al., 1986b), only bulk analyses of lava flows and domes are available from this center (Fytikas et al., 1986b; Marinos, 1959), precluding a possible correlation with cryptotephra TP09-65.835b. In contrast, more compositional data are available from the Island of Milos including few EDS-EPMA analyses of perlite from the Trachilas tuff ring. These data indicate highly evolved magmas with SiO_2 values between 76.7 wt% and 80.8 wt% (Filippou, 2014; Fytikas et al., 1986b; Koukouzas and Dunham, 1998). Cryptotephra TP09-65.835b falls into the geochemical field of Milos and particularly of Trachilas in all bivariate plots (Figs. 8, S4-7). Only its Na_2O content is lower than that of Milos, which may be related to sodium loss during EPMA. In addition to the similarity in chemical composition, K/Ar dates of 370±90 ka and 320±50 ka for the rhyolites of Trachilas and Antimilos, respectively (Fytikas et al., 1986b), broadly correspond to the stratigraphic position of cryptotephra TP09-65.835b within MIS 10 (358 ka). They suggest that one of these volcanic centers could also be the source of the cryptotephra. In summary, the limited availability of glass chemical data of Aegean Arc volcanoes allows only a tentative correlation of cryptotephra TP09-65.835b with volcanic centers from either Kos or Milos.

6.1.2.2.2 Cryptotephras TP09-74.75 to TP09-77.95 (nine layers)

The nine cryptotephra layers of glass population POP5 have a rhyolitic composition that is distinctly different from all volcanic sources discussed so far. They are characterized by SiO_2 (72.4–75.7 wt%), K_2O (3.0–6.4 wt%), FeO (0.30–1.56 wt%), TiO_2 (0.05–0.26 wt%), and Al_2O_3 (12.9–15.4 wt%) concentrations that best match Aegean Arc and Carpathian tephra compositions; however, they show considerably higher CaO and MgO

concentrations as well as lower Na_2O concentrations (Figs. 6, S4-4). Trace-element glass and even bulk data for tephras from this time range are lacking from the Eastern Carpathians and are very rare from the Aegean Arc. Middle Pleistocene tephra deposits from the Aegean Arc are yet characterized by bulk trace-element analyses only, and single-glass analyses are only available for few Late Pleistocene tephras from that region. Nevertheless, the available data demonstrate that population POP5 does not overlap with Aegean Arc (Santorini, Nysiros) and Central Anatolian (Acigöl, Erciyes Dagi) compositional fields in most trace-element plots (Figs. 3d, 6, S4-1, S4-4). The plots, however, indicate that this population derives from a volcano in a subduction-related tectonic setting, although it is not clear whether it relates to an active- or a post-subdaction setting (Figs. 3d, S4-1). Hence, the sources of the cryptotephras within the POP5 glass population remain yet unknown.

6.2 Ages of the MIS 12–10 cryptotephras at Tenaghi Philippon

Although the detected cryptotephras from the 460–335 ka interval at Tenaghi Philippon have distinct geochemical signatures, their correlations with well-dated volcanic eruptions remain difficult. This is because the eruptive history of the Mediterranean region during the Middle Pleistocene is as yet largely unexplored (Leicher et al., 2016; Petrosino et al., 2015). Moreover, Middle Pleistocene volcanic eruptions in the Eastern Mediterranean region lack accurate chronologies because of limited dating of proximal deposits (Bachmann et al., 2010; Sumita and Schmincke, 2013b). This is illustrated by the fact that for the only cryptotephra from the MIS 12–10 interval at Tenaghi Philippon that could be confidently assigned to a known eruption (i.e., TP09-65.95) no accurate dates exist that are derived from its proximal correlative. Instead, the available age estimate for its proximal correlative, i.e., the CT-1 eruption, is ≤360 ka (Druitt et al., 1999), which only confirms that the TP09-65.95 cryptotephra was deposited during the Middle Pleistocene.

To circumvent these limitations, we here provide tentative ages of the identified cryptotephras based on the alignment of the TF-II and TP-2009 pollen datasets from Tenaghi Philippon (Fig. 9). The cryptotephras TP09-77.95 to TP09-75.75 are situated within an interval characterized by tree-pollen percentages <20 %, which implies that they were deposited during the MIS 12 glacial between 438 and 427 ka (Table 1; Fig. 9). Cryptotephras TP09-74.75 to TP09-66.95 are located within an interval characterized by high (>80 %) tree-pollen percentages, implying that they were deposited during the MIS 11 interglacial (Fig. 9). More specifically, cryptotephra TP09-74.75 occurs close to the onset of the interglacial and has a pollen-derived age of c. 419 ka. Cryptotephras TP09-70.45, -68.95, -67.15, -67.05, and -66.95 have been deposited during the younger interval of MIS 11 between 391 and 367 ka (Table 1; Fig. 9). The cryptotephras TP09-65.95 and -835a,b are associated with relatively low tree-pollen percentages (~50 %) at the transition to the MIS 10 glacial (c. 359–358 ka; Table 1; Fig. 9). Finally, the cryptotephras TP09-63.05 and -63.015a,b are located within an interval of increasing tree-pollen percentages that marks the transition to the MIS 9 interglacial; they then can be assigned a pollen-based age of c. 336 ka (Table 1; Fig. 9).

The age assignments for the cryptotephra layers as derived from tree-pollen percentages provide a stratigraphic framework that is essential for correlation with other paleoclimatic records. Although the age model of the TF-II pollen dataset (Tzedakis et al., 2006; Van der Wiel and Wijmstra, 1987; Wijmstra and Smit, 1976) has received general acclaim and is regularly used in comparisons with terrestrial (e.g., Gasse et al., 2015; Litt et al., 2014; Sadori et al., 2016; Wagner et al., 2017) and marine (e.g., Bahr et al., 2018; Martrat et al., 2007) paleoclimate records from the Middle Pleistocene, it may be somewhat compromised by tuning uncertainties, which would by extension affect the palynologically derived ages of the cryptotephras. This holds particularly true for the younger parts of MIS 11. Specifically, the first strong forest contraction at Tenaghi Philippon during MIS

11 occurred at c. 380 ka as documented by the decline in tree-pollen abundances by c. 40–50 % (Fig. 9). This post-dates the first strong cooling event in the North Atlantic by c. 10 ka (e.g., Barker et al., 2015; Bassinot et al., 1994; Voelker et al., 2010) (Fig. 9). Considering the extremely sensitive response of the Tenaghi Philippon pollen record to northern hemisphere climate dynamics (e.g., Müller et al., 2011; Pross et al., 2009), the difference in the timing of the two events cannot be attributed to natural processes, but instead is to be sought in age-model uncertainties. This interpretation is supported by a new, chronologically well-constrained high-resolution MIS 11 palynological record from Lake Ohrid (SW Balkan Peninsula; Kousis et al., 2018). On this basis, the ages of the cryptotephra layers TP09-70.45 to TP09-66.95 can be c. 10 ka older than those deduced from the alignment of the TF-II and TP-2009 pollen records. The tentative ages of the remainder of the cryptotephra layers appear better constrained considering the good agreement between the Tenaghi Philippon pollen record with marine proxy records (e.g., ODP Site 983, Fig. 1; Barker et al., 2015) for the MIS 12 and 10 glacials as well as the MIS 12/11 and MIS 10/9 transitions (compare Fig. 9).

6.3 Implications for MIS 12–10 tephrostratigraphy of the Mediterranean region

High-fidelity synchronization of climate archives across the Mediterranean region hinges critically on the availability of a tephrostratigraphic framework (Blockley et al., 2014; Lowe et al., 2015). Notably, such an effort requires connecting the regional tephrostratigraphies of the Central and Eastern Mediterranean regions, i.e., those of Italy, the Aegean Arc and Anatolia (Zanchetta et al., 2011). In this respect, the Eastern Mediterranean region plays a key role as it is situated downwind of the Italian volcanoes, which enables tephras of Italian origin to be widely distributed eastwards as far as the Levantine Sea (Federman and Carey, 1980; Keller et al., 1978; Vinci, 1985) and the Black Sea (Cullen et al., 2014). Tephras from the Aegean Arc, in turn, are restricted to the Eastern Mediterranean region

and have not yet been detected in the Central Mediterranean (e.g., Matthews et al., 2015; Wulf et al., 2004), as this would require transport against the mostly prevailing wind directions. Tephras from Anatolian sources have yet rarely been reported beyond Asia Minor, although recent studies suggest that there is dispersal of Anatolian tephras as far as the Levantine Sea (Hamann et al., 2010), the Dead Sea and the NW Arabian Peninsula (Neugebauer et al., 2017).

While studies towards the establishment of a (crypto)tephrostratigraphic scheme for the Holocene and Late Pleistocene of the Eastern Mediterranean region are well underway (e.g., Aksu et al., 2008; Karkanas et al., 2015; Keller et al., 1978; Margari et al., 2007; Zanchetta et al., 2011; Wulf et al., 2018), comparable efforts for the Middle Pleistocene are as yet at an early stage. Important progress towards extending the Eastern Mediterranean tephrochronology beyond the past ~200 ka has recently been made based on the succession from Lake Ohrid, where at least 36 (crypto)tephras have been identified in the MIS 15–1 interval (Kousis et al., 2018; Leicher et al., 2016). However, to date this record has only yielded tephras of Italian origin. As such, our study on MIS 12–10 from Tenaghi Philippon brings together for the first time regional tephrostratigraphies from the Central and Eastern Mediterranean regions for the Middle Pleistocene.

In the Central Mediterranean region, tephra records spanning the MIS 12–10 interval are to date largely known from the Italian Peninsula (Fig. 10). Four tephra layers appear to be particularly widely dispersed: Pozzolane Rosse (~457 ka), Tuffo Rosso a Scorie Nere (TRSN, ~452 ka), Rio Rava (~439 ka), and Vico β (~410 ka), produced by the Colli Albani, Sabatini, Roccamonfina and Vico volcanoes, respectively (e.g., Galli et al., 2010; Giaccio et al., 2014; Regattieri et al., 2016; Russo Ermolli et al., 2010). Moreover, Pozzolane Rosse and Vico β (previously erroneously labeled as Vico α, Fabrizio Marra, pers. comm. 2018; compare Kousis et al., 2018) were recently discovered on the western Balkan Peninsula (Kousis et al., 2018; Leicher et al., 2016). None of these tephras are present

at Tenaghi Philippon. Instead, the here discovered cryptotephras TP09-70.45 (c. 391 ka) and TP09-65.835a (c. 358 ka) represent large, previously unknown eruptions of Campanian volcanoes. They may provide valuable stratigraphic markers for the MIS 11–10 interval that allow the connection of climate records from the Central and Eastern Mediterranean regions. Moreover, several tephra layers from presumably Italian sources have been detected at ODP Site 964 as well as in the cores KC01 and KC01B from the Ionian Sea during the MIS 12–10 interval (Fig. 10; Lourens, 2004). Ongoing work aiming at geochemical characterization of these tephras (Vakhrameeva et al., in prep.) will further contribute to the establishment of land-sea correlations during MIS 12–10 in the Mediterranean region.

An important result of our study is the first discovery of the Cape Therma 1 tephra deposit outside Santorini, which is represented by cryptotephra TP09-65.95 at Tenaghi Philippon. The age of this unit was not well constrained before, and our finding thus provides it with the best age estimate so far, i.e., c. 359 ka (Fig. 9). The identification of the CT-1 tephra at Tenaghi Philippon indicates that it might be widespread in the Aegean Sea region, with the potential of being important marker horizon for MIS 10. Cryptotephra TP09-63.015b (c. 336 ka) has a similar geochemical signature to the Cape Therma 2 eruption of Santorini, but it is older by more than 100 ka (Druitt et al., 1999) and most likely re-deposited.

Moreover, although still being tentative, the correlation of cryptotephra TP09-66.95 (c. 367 ka) with a minor Santorini pyroclastic deposit that directly underlies the CT-1 tephra indicates that even eruptions that resulted in only relatively minor pyroclastic units on Santorini may have led to tephras that became widely dispersed across the Aegean region, which may allow to use them as marker beds. To further explore this possibility, more research on older pyroclastic deposits from Santorini is needed that would include collection of major- and trace-element glass data as well as dating of tephra deposits. A

refined age model for the Tenaghi Philippon archive via higher-resolution pollen data would allow to further constrain the age estimates for all identified cryptotephras. Because many cryptotephras in this study are characterized by low glass-shard abundances, replication of our findings in other tephra records will be instrumental in proving their significance.

7 Conclusions

The detailed cryptotephra analysis of core TP-2009 allowed identification and geochemical characterization of eighteen primary cryptotephra layers in the MIS 12–10 (460–335 ka) interval of the Tenaghi Philippon archive. Major- and trace-element glass compositions were used to establish correlations between the cryptotephras detected in core TP-2009 and their volcanic and eruptive sources in the Aegean Arc and Italy. Cryptotephra ages were estimated based on palynostratigraphic information from the same archive. This yielded the first distal tephrostratigraphic framework for the Eastern Mediterranean region during MIS 12–10 and notably the first record that integrates information from both the Italian and Aegean Arc volcanic provinces during that time.

With regard to eruptive sources from the Aegean Arc, six cryptotephra layers of Santorini origin were identified in the Tenaghi Philippon record. One of them represents the oldest major explosive eruption of Santorini, i.e., Cape Therma 1. Based on palynostratigraphic information from that site, its age can be estimated to c. 359 ka. One re-deposited cryptotephra with an age estimate of c. 336 ka compositionally matches the second oldest major explosive eruption of Santorini, i.e., Cape Therma 2, suggesting a deposition of the primary tephra further upcore. Another cryptotephra constrained at c. 367 ka can be tentatively correlated with the pumice fall directly underlying the Cape Therma 1 deposit on Santorini. A cryptotephra with an age of c. 358 ka most likely derives from an Aegean Arc volcano other than Santorini, probably either Kos or Milos. A more precise correlation

would require currently lacking geochronological and glass compositional data for tephra deposits from these volcanoes.

Interestingly, the oldest nine cryptotephras in our record (438–419 ka) do not match any volcanic sources in the Mediterranean region. This clearly demonstrates a yet considerable gap in our knowledge about volcanic history of the Eastern Mediterranean region. Cryptotephras with an unequivocally Italian origin have been identified at c. 391 ka and c. 358 ka; they can be attributed to major, yet unknown eruptions of Campanian volcanoes.

In light of our findings, future work towards refining the Middle Pleistocene tephrostratigraphy for the Eastern Mediterranean region should focus on (i) detailed studies involving major- and trace-element glass analyses as well as age determinations of proximal pyroclastic sequences in the volcanic regions of the Aegean Arc, Anatolia, and the Carpathians, and (ii) further (crypto)tephra analysis of marine and terrestrial records in order to identify key tephra isochrones in the Eastern Mediterranean region.

Acknowledgments

Vincenzo Amato, Jörg Keller, Niklas Leicher, Fabrizio Marra, David Pyle, and Gianluca Sottili are thanked for discussions, and Paola Petrosino for sharing geochemical data of tephra from the Boiano basin. Frederik Allstädt, Monika Doubrawa, Ilse Glass, Thomas Ludwig, and Alexander Varychev provided technical assistance. Biagio Giaccio and Steffen Kutterolf are thanked for thoughtful reviews of an earlier version of the manuscript. This study received financial support by the Deutsche Forschungsgemeinschaft (DFG) to AK and JP (grants KO4960/3, KO4960/5 and PR 651/19).

References

1. Aksu, A.E., Jenner, G., Hiscott, R.N., Isler, E.B., 2008. Occurrence, stratigraphy and geochemistry of Late Quaternary tephra layers in the Aegean Sea and the Marmara Sea. Marine Geology 252, 174-192.
2. Albert, P.G., Hardiman, M., Keller, J., Tomlinson, E.L., Smith, V.C., Bourne, A.J., Wulf, S., Zanchetta, G., Sulpizio, R., Müller, U.C., Pross, J., Ottolini, L., Matthews, I.P., Blockley, S.P.E., Menzies, M.A., 2015. Revisiting the Y-3 tephrostratigraphic marker: a new diagnostic glass geochemistry, age estimate, and details on its climatostratigraphical context. Quaternary Science Reviews 118, 105-121.
3. Albert, P.G., Tomlinson, E.L., Lane, C.S., Wulf, S., Smith, V.C., Coltelli, M., Keller, J., Lo Castro, D., Manning, C.J., Muller, W., Menzies, M.A., 2013. Late glacial explosive activity on Mount Etna: Implications for proximal-distal tephra correlations and the synchronisation of Mediterranean archives. Journal of Volcanology and Geothermal Research 265, 9-26.
4. Albert, P.G., Tomlinson, E.L., Smith, V.C., Di Roberto, A., Todman, A., Rosi, M., Marani, M., Muller, W., Menzies, M.A., 2012. Marine-continental tephra correlations: Volcanic glass geochemistry from the Marsili Basin and the Aeolian Islands, Southern Tyrrhenian Sea, Italy. Journal of Volcanology and Geothermal Research 229–230, 74-94.
5. Albert, P.G., Tomlinson, E.L., Smith, V.C., Di Traglia, F., Pistolesi, M., Morris, A., Donato, P., De Rosa, R., Sulpizio, R., Keller, J., Rosi, M., Menzies, M., 2017. Glass geochemistry of pyroclastic deposits from the Aeolian Islands in the last 50 ka: A proximal database for tephrochronology. Journal of Volcanology and Geothermal Research 336, 81-107.
6. Amato, V., Aucelli, P.P.C., Cesarano, M., Jicha, B., Lebreton, V., Orain, R., Pappone, G., Petrosino, P., Russo Ermolli, E., 2014. Quaternary evolution of the

largest intermontane basin of the Molise Apennine (central-southern Italy). Rendiconti Lincei 25, 197-216.

7. Aureli, D., Contardi, A., Giaccio, B., Jicha, B., Lemorini, C., Madonna, S., Magri, D., Marano, F., Milli, S., Modesti, V., Palombo, M.R., Rocca, R., 2015. Palaeoloxodon and human interaction: Depositional setting, chronology and archaeology at the Middle Pleistocene Ficoncella site (Tarquinia, Italy). PLoS ONE 10, e0124498.
8. Aureli, D., Contardi, A., Giaccio, B., Modesti, V., Palombo, M.R., Rozzi, R., Sposato, A., Trucco, F., 2012. Straight-tusked elephants in the Middle Pleistocene of northern Latium: Preliminary report on the Ficoncella site (Tarquinia, central Italy). Quaternary International 255, 29-35.
9. Bachmann, O., Schnyder, C., 2006. The pre-Kos Plateau Tuff volcanic rocks on Kefalos Peninsula (Kos Island, Dodecanese, Greece): Crescendo to the largest eruption of the modern Aegean Arc, Eos, Transactions, American Geophysical Union 87(52), Fall Meet. Suppl., Abstract V33C-0680.
10. Bachmann, O., Schoene, B., Schnyder, C., Spikings, R., 2010. The 40Ar/39Ar and U/Pb dating of young rhyolites in the Kos-Nisyros volcanic complex, Eastern Aegean Arc, Greece: Age discordance due to excess 40Ar in biotite. Geochemistry, Geophysics, Geosystems 11, Q0AA08.
11. Bahr, A., Kaboth, S., Hodell, D., Zeeden, C., Fiebig, J., Friedrich, O., 2018. Oceanic heat pulses fueling moisture transport towards continental Europe across the mid-Pleistocene transition. Quaternary Science Reviews 179, 48-58.
12. Barker, S., Chen, J., Gong, X., Jonkers, L., Knorr, G., Thornalley, D., 2015. Icebergs not the trigger for North Atlantic cold events. Nature 520, 333-336.

13. Bassinot, F.C., Labeyrie, L.D., Vincent, E., Quidelleur, X., Shackleton, N.J., Lancelot, Y., 1994. The astronomical theory of climate and the age of the Brunhes-Matuyama magnetic reversal. Earth and Planetary Science Letters 126, 91-108.
14. Bigazzi, G., Yegingil, Z., Ercan, T., Oddone, M., Özdogan, M., 1993. Fission track dating obsidians in Central and Northern Anatolia. Bulletin of Volcanology 55, 588-595.
15. Blockley, S.P.E., Bourne, A.J., Brauer, A., Davies, S.M., Hardiman, M., Harding, P.R., Lane, C.S., MacLeod, A., Matthews, I.P., Pyne-O'Donnell, S.D.F., Rasmussen, S.O., Wulf, S., Zanchetta, G., 2014. Tephrochronology and the extended intimate (integration of ice-core, marine and terrestrial records) event stratigraphy 8–128 ka b2k. Quaternary Science Reviews 106, 88-100.
16. Brauer, A., Wulf, S., Mangili, C., Moscariello, A., 2007. Tephrochronological dating of varved interglacial lake deposits from Piànico-Sèllere (Southern Alps, Italy) to around 400 ka. Journal of Quaternary Science 22, 85-96.
17. Bronk Ramsey, C., Albert, P.G., Blockley, S.P.E., Hardiman, M., Housley, R.A., Lane, C.S., Lee, S., Matthews, I.P., Smith, V.C., Lowe, J.J., 2015. Improved age estimates for key Late Quaternary European tephra horizons in the RESET lattice. Quaternary Science Reviews 118, 18-32.
18. Cadoux, A., Pinti, D.L., Aznar, C., Chiesa, S., Gillot, P.-Y., 2005. New chronological and geochemical constraints on the genesis and geological evolution of Ponza and Palmarola Volcanic Islands (Tyrrhenian Sea, Italy). Lithos 81, 121-151.
19. Cantner, K., Carey, S., Nomikou, P., 2014. Integrated volcanologic and petrologic analysis of the 1650AD eruption of Kolumbo submarine volcano, Greece. Journal of Volcanology and Geothermal Research 269, 28-43.

20. Cheng, H., Edwards, R.L., Sinha, A., Spötl, C., Yi, L., Chen, S., Kelly, M., Kathayat, G., Wang, X., Li, X., Kong, X., Wang, Y., Ning, Y., Zhang, H., 2016. The Asian monsoon over the past 640,000 years and ice age terminations. Nature 534, 640-646.
21. Christanis, K., Georgakopoulos, A., Fernández-Turiel, J.L., Bouzinos, A., 1998. Geological factors influencing the concentration of trace elements in the Philippi peatland, eastern Macedonia, Greece. International Journal of Coal Geology 36, 295-313.
22. Cinque, A., Civetta, L., Orsi, G., Peccerillo, A., 1988. Geology and geochemistry of the island of Ustica (Southern Tyrrhenian Sea). Rendiconti della Società Italiana di Mineralogia e Petrologia 43, 987-1002.
23. Cohen, K.M., Finney, S.C., Gibbard, P.L., Fan, J.-X., 2013. The ICS International Chronostratigraphic Chart. Episodes 36, 199-204.
24. Cullen, V.L., Smith, V.C., Arz, H.W., 2014. The detailed tephrostratigraphy of a core from the south-east Black Sea spanning the last □60 ka. Journal of Quaternary Science 29, 675-690.
25. Dalabakis, P., Vougioukalakis, G., 1993. The Kefalos Tuff Ring (W. Kos): depositional mechanisms, vent position and model of the evolution of the eruptive activity. Bulletin of the Geological Society of Greece 28, 259-273 (in Greek).
26. Davies, S.M., 2015. Cryptotephras: the revolution in correlation and precision dating. Journal of Quaternary Science 30, 114-130.
27. De Vivo, B., Rolandi, G., Gans, P.B., Calvert, A., Bohrson, W.A., Spera, F.J., Belkin, H.E., 2001. New constraints on the pyroclastic eruptive history of the Campanian volcanic Plain (Italy). Mineralogy and Petrology 73, 47-65.

28. Deniel, C., Aydar, E., Gourgaud, A., 1998. The Hasan Dagi stratovolcano (Central Anatolia, Turkey): evolution from calc-alkaline to alkaline magmatism in a collision zone. Journal of Volcanology and Geothermal Research 87, 275-302.
29. Druitt, T.H., Brenchley, P.J., Gökten, Y.E., Francaviglia, V., 1995. Late Quaternary rhyolitic eruptions from the Acigöl Complex, central Turkey. Journal of the Geological Society, London 152, 655-667.
30. Druitt, T.H., Edwards, L., Mellors, R.M., Pyle, D.M., Sparks, R.S.J., Lanphere, M., Davies, M., Barreirio, B., 1999. Santorini Volcano. Geological Society, London, Memoirs 19.
31. Engelhardt, J.F., Sudo, M., Stockhecke, M., Oberhänsli, R., 2017. Feldspar 40Ar/39Ar dating of ICDP PALEOVAN cores. Geochimica Et Cosmochimica Acta 217, 144-170.
32. Federman, A.N., Carey, S.N., 1980. Electron microprobe correlation of tephra layers from Eastern Mediterranean abyssal sediments and the Island of Santorini. Quaternary Research 13, 160-171.
33. Filippou, A., 2014. Minerochemical study of rhyolitic lavas with perlitic texture from the Island of Milos. MSc thesis, University of Patras, Patras, Greece (in Greek).
34. Forni, F., Lucchi, F., Peccerillo, A., Tranne, C.A., Rossi, P.L., Frezzotti, M.L., 2013. Stratigraphy and geological evolution of the Lipari volcanic complex (central Aeolian archipelago). Geological Society, London, Memoirs 37, 213-279.
35. Freeman, C., 2014. Egypt, Greece, and Rome: Civilizations of the Ancient Mediterranean, Third ed. Oxford University Press, Oxford, UK.
36. Fuller, S.A., 2015. Distribution of tephra from the 1650 AD submarine eruption of Kolumbo volcano, Greece. MSc thesis, University of Rhode Island, Ann Arbor, USA.

37. Fytikas, M., Giuliani, O., Innocenti, F., Marinelli, G., Mazzuoli, R., 1976. Geochronological data on recent magmatism of the Aegean Sea. Tectonophysics 31, T29-T34.
38. Fytikas, M., Innocenti, F., Kolios, N., Manetti, P., Mazzuoli, R., 1986a. The Plio-Quaternary volcanism of Saronikos area (western part of the active Aegean volcanic arc). Hellenic Journal of Geosciences 33, 23-45.
39. Fytikas, M., Innocenti, F., Kolios, N., Manetti, P., Mazzuoli, R., Poli, G., Rita, F., Villari, L., 1986b. Volcanology and petrology of volcanic products from the island of Milos and neighbouring islets. Journal of Volcanology and Geothermal Research 28, 297-317.
40. Gaitanakis, P., Dietrich, V., 1995. Geological map of Methana peninsula 1: 25 000. ETH, Zürich.
41. Galli, P., Giaccio, B., Messina, P., 2010. The 2009 central Italy earthquake seen through 0.5 Myr-long tectonic history of the L'Aquila faults system. Quaternary Science Reviews 29, 3768-3789.
42. Gasse, F., Vidal, L., Van Campo, E., Demory, F., Develle, A.-L., Tachikawa, K., Elias, A., Bard, E., Garcia, M., Sonzogni, C., Thouveny, N., 2015. Hydroclimatic changes in northern Levant over the past 400,000 years. Quaternary Science Reviews 111, 1-8.
43. Gehrels, M.J., Newnham, R.M., Lowe, D.J., Wynne, S., Hazell, Z.J., Caseldine, C., 2008. Towards rapid assay of cryptotephra in peat cores: Review and evaluation of various methods. Quaternary International 178, 68-84.
44. Gertisser, R., Preece, K., Keller, J., 2009. The Plinian Lower Pumice 2 eruption, Santorini, Greece: Magma evolution and volatile behaviour. Journal of Volcanology and Geothermal Research 186, 387-406.

45. Giaccio, B., Arienzo, I., Sottili, G., Castorina, F., Gaeta, M., Nomade, S., Galli, P., Messina, P., 2013a. Isotopic (Sr-Nd) and major element fingerprinting of distal tephras: an application to the Middle-Late Pleistocene markers from the Colli Albani volcano, central Italy. Quaternary Science Reviews 67, 190-206.
46. Giaccio, B., Castorina, F., Nomade, S., Scardia, G., Voltaggio, M., Sagnotti, L., 2013b. Revised chronology of the Sulmona lacustrine succession, central Italy. Journal of Quaternary Science 28, 545-551.
47. Giaccio, B., Galli, P., Messina, P., Peronace, E., Scardia, G., Sottili, G., Sposato, A., Chiarini, E., Jicha, B., Silvestri, S., 2012. Fault and basin depocentre migration over the last 2 Ma in the L'Aquila 2009 earthquake region, central Italian Apennines. Quaternary Science Reviews 56, 69-88.
48. Giaccio, B., Galli, P., Peronace, E., Arienzo, I., Nomade, S., Cavinato, G.P., Mancini, M., Messina, P., Sottili, G., 2014. A 560-440 ka tephra record from the Mercure Basin, southern Italy: volcanological and tephrostratigraphic implications. Journal of Quaternary Science 29, 232-248.
49. Giaccio, B., Hajdas, I., Isaia, R., Deino, A., Nomade, S., 2017a. High-precision ^{14}C and $^{40}Ar/^{39}Ar$ dating of the Campanian Ignimbrite (Y-5) reconciles the time-scales of climatic-cultural processes at 40 ka. Scientific Reports 7, 45940.
50. Giaccio, B., Niespolo, E.M., Pereira, A., Nomade, S., Renne, P.R., Albert, P.G., Arienzo, I., Regattieri, E., Wagner, B., Zanchetta, G., Gaeta, M., Galli, P., Mannella, G., Peronace, E., Sottili, G., Florindo, F., Leicher, N., Marra, F., Tomlinson, E.L., 2017b. First integrated tephrochronological record for the last similar to 190 kyr from the Fucino Quaternary lacustrine succession, central Italy. Quaternary Science Reviews 158, 211-234.
51. Giannetti, B., Luhr, J.F., 1983. The White Trachytic Tuff of Roccamonfina volcano (Roman region, Italy). Contributions to Mineralogy and Petrology 84, 235-252.

52. Giraudi, C., Giaccio, B., 2015. Middle Pleistocene glaciations in the Apennines, Italy: new chronological data and preservation of the glacial record. Geological Society, London, Special Publications 433, 161-178.
53. Grant, K.M., Rohling, E.J., Westerhold, T., Zabel, M., Heslop, D., Konijnendijk, T., Lourens, L., 2017. A 3 million year index for North African humidity/aridity and the implication of potential pan-African Humid periods. Quaternary Science Reviews 171, 100-118.
54. Hamann, Y., Wulf, S., Ersoy, O., Ehrmann, W., Aydar, E., Schmiedl, G., 2010. First evidence of a distal early Holocene ash layer in Eastern Mediterranean deep-sea sediments derived from the Anatolian volcanic province. Quaternary Research 73, 497-506.
55. Harangi, S., Lukács, R., Schmitt, A.K., Dunkl, I., Molnár, K., Kiss, B., Seghedi, I., Novothny, Á., Molnár, M., 2015. Constraints on the timing of Quaternary volcanism and duration of magma residence at Ciomadul volcano, east–central Europe, from combined U–Th/He and U–Th zircon geochronology. Journal of Volcanology and Geothermal Research 301, 66-80.
56. Herbert, T.D., Peterson, L.C., Lawrence, K.T., Liu, Z., 2010. Tropical ocean temperatures over the past 3.5 million years. Science 328, 1530-1534.
57. Huijsmans, J.P.P., 1985. Calc-alkaline lavas from the volcanic complex of Santorini, Aegean Sea, Greece: a petrological, geochemical and stratigraphic study. PhD thesis, Utrecht University, The Netherlands.
58. Hunt, J.B., Hill, P.G., 1996. An inter-laboratory comparison of the electron probe microanalysis of glass geochemistry. Quaternary International 34-36, 229-241.
59. Jochum, K.P., Stoll, B., Herwig, K., Willbold, M., Hofmann, A.W., Amini, M., Aarburg, S., Abouchami, W., Hellebrand, E., Mocek, B., Raczek, I., Stracke, A., Alard, O., Bouman, C., Becker, S., Dücking, M., Brätz, H., Klemd, R., de Bruin, D.,

Canil, D., Cornell, D., de Hoog, C.-J., Dalpé, C., Danyushevsky, L., Eisenhauer, A., Gao, Y., Snow, J.E., Groschopf, N., Günther, D., Latkoczy, C., Guillong, M., Hauri, E.H., Höfer, H.E., Lahaye, Y., Horz, K., Jacob, D.E., Kasemann, S.A., Kent, A.J.R., Ludwig, T., Zack, T., Mason, P.R.D., Meixner, A., Rosner, M., Misawa, K., Nash, B.P., Pfänder, J., Premo, W.R., Sun, W.D., Tiepolo, M., Vannucci, R., Vennemann, T., Wayne, D., Woodhead, J.D., 2006. MPI-DING reference glasses for in situ microanalysis: New reference values for element concentrations and isotope ratios. Geochemistry, Geophysics, Geosystems 7, Q02008.

60. Jouzel, J., Masson-Delmotte, V., Cattani, O., Dreyfus, G., Falourd, S., Hoffmann, G., Minster, B., Nouet, J., Barnola, J.M., Chappellaz, J., Fischer, H., Gallet, J.C., Johnsen, S., Leuenberger, M., Loulergue, L., Luethi, D., Oerter, H., Parrenin, F., Raisbeck, G., Raynaud, D., Schilt, A., Schwander, J., Selmo, E., Souchez, R., Spahni, R., Stauffer, B., Steffensen, J.P., Stenni, B., Stocker, T.F., Tison, J.L., Werner, M., Wolff, E.W., 2007. Orbital and millennial Antarctic climate variability over the past 800,000 years. Science 317, 793-796.
61. Karátson, D., Wulf, S., Veres, D., Magyari, E.K., Gertisser, R., Timar-Gabor, A., Novothny, A., Telbisz, T., Szalai, Z., Anechitei-Deacu, V., Appelt, O., Bormann, M., Jánosi, C., Hubay, K., Schäbitz, F., 2016. The latest explosive eruptions of Ciomadul (Csomad) volcano, East Carpathians – A tephrostratigraphic approach for the 51–29 ka BP time interval. Journal of Volcanology and Geothermal Research 319, 29-51.
62. Karkanas, P., White, D., Lane, C.S., Stringer, C., Davies, W., Cullen, V.L., Smith, V.C., Ntinou, M., Tsartsidou, G., Kyparissi-Apostolika, N., 2015. Tephra correlations and climatic events between the MIS6/5 transition and the beginning of MIS3 in Theopetra Cave, central Greece. Quaternary Science Reviews 118, 170-181.

63. Keller, J., Ryan, W.B.F., Ninkovich, D., Altherr, R., 1978. Explosive volcanic activity in the Mediterranean over the past 200,000 yr as recorded in deep-sea sediments. Geological Society of America Bulletin 89, 591-604.
64. Koukouzas, N.K., 1997. Rare earth elements in volcanic glass: A case study from Trachilas perlite deposit, Greece. Chemie der Erde 57, 351-362.
65. Koukouzas, N.K., Dunham, A.C., 1998. Glass composition of perlites from Milos, Kimolos and Kos islands (Greece). Bulletin of the Geological Society of Greece 32, 303-312.
66. Kousis, I., Koutsodendris, A., Peyron, O., Leicher, N., Francke, A., Wagner, B., Giaccio, B., Knipping, M., Pross, J., 2018. Centennial-scale vegetation dynamics and climate variability in SE Europe during Marine Isotope Stage 11 based on a pollen record from Lake Ohrid. Quaternary Science Reviews 190, 20-38.
67. Kuehn, S.C., Froese, D.G., Shane, P.A.R., 2011. The INTAV intercomparison of electron-beam microanalysis of glass by tephrochronology laboratories: Results and recommendations. Quaternary International 246, 19-47.
68. Le Bas, M.J., Le Maitre, R.W., Streckeisen, A., Zanettin, B., 1986. A chemical classification of volcanic rocks based on the total alkali-silica diagram. Journal of Petrology 27, 745-750.
69. Leicher, N., Zanchetta, G., Sulpizio, R., Giaccio, B., Wagner, B., Nomade, S., Francke, A., Del Carlo, P., 2016. First tephrostratigraphic results of the DEEP site record from Lake Ohrid (Macedonia and Albania). Biogeosciences 13, 2151-2178.
70. Lionello, P., Abrantes, F., Congedi, L., Dulac, F., Gacic, M., Gomis, D., Goodess, C., Hoff, H., Kutiel, H., Luterbacher, J., Planton, S., Reale, M., Schröder, K., Vittoria Struglia, M., Toreti, A., Tsimplis, M., Ulbrich, U., Xoplaki, E., 2012. Introduction: Mediterranean Climate—Background Information, in: Lionello, P. (Ed.), The Climate of the Mediterranean Region. Elsevier, Oxford, pp. xxxv-xc.

71. Lisiecki, L.E., Raymo, M.E., 2005. A Pliocene-Pleistocene stack of 57 globally distributed benthic $\delta^{18}O$ records. Paleoceanography 20, PA1003.
72. Litt, T., Pickarski, N., Heumann, G., Stockhecke, M., Tzedakis, P.C., 2014. A 600,000 year long continental pollen record from Lake Van, eastern Anatolia (Turkey). Quaternary Science Reviews 104, 30-41.
73. Loulergue, L., Schilt, A., Spahni, R., Masson-Delmotte, V., Blunier, T., Lemieux, B., Barnola, J.-M., Raynaud, D., Stocker, T.F., Chappellaz, J., 2008. Orbital and millennial-scale features of atmospheric CH_4 over the past 800,000 years. Nature 453, 383-386.
74. Lourens, L.J., 2004. Revised tuning of Ocean Drilling Program Site 964 and KC01B (Mediterranean) and implications for the $\delta^{18}O$, tephra, calcareous nannofossil, and geomagnetic reversal chronologies of the past 1.1 Myr. Paleoceanography 19, PA3010.
75. Lowe, D.J., 2011. Tephrochronology and its application: A review. Quaternary Geochronology 6, 107-153.
76. Lowe, J., Barton, N., Blockley, S., Ramsey, C.B., Cullen, V.L., Davies, W., Gamble, C., Grant, K., Hardiman, M., Housley, R., Lane, C.S., Lee, S., Lewis, M., MacLeod, A., Menzies, M., Müller, W., Pollard, M., Price, C., Roberts, A.P., Rohling, E.J., Satow, C., Smith, V.C., Stringer, C.B., Tomlinson, E.L., White, D., Albert, P., Arienzo, I., Barker, G., Borić, D., Carandente, A., Civetta, L., Ferrier, C., Guadelli, J.-L., Karkanas, P., Koumouzelis, M., Müller, U.C., Orsi, G., Pross, J., Rosi, M., Shalamanov-Korobar, L., Sirakov, N., Tzedakis, P.C., 2012. Volcanic ash layers illuminate the resilience of Neanderthals and early modern humans to natural hazards. Proceedings of the National Academy of Sciences 109, 13532-13537.
77. Lowe, J.J., Bronk Ramsey, C., Housley, R.A., Lane, C.S., Tomlinson, E.L., RESET Team, RESET Associates, 2015. The RESET project: constructing a European

tephra lattice for refined synchronisation of environmental and archaeological events during the last c. 100 ka. Quaternary Science Reviews 118, 1-17.

78. Lucchi, F., Gertisser, R., Keller, J., Forni, F., De Astis, G., Tranne, C.A., 2013. Eruptive history and magmatic evolution of the island of Salina (central Aeolian archipelago). Geological Society, London, Memoirs 37, 155-211.
79. Macdonald, R., Sumita, M., Schmincke, H.U., Bagiński, B., White, J.C., Ilnicki, S.S., 2015. Peralkaline felsic magmatism at the Nemrut volcano, Turkey: impact of volcanism on the evolution of Lake Van (Anatolia) IV. Contributions to Mineralogy and Petrology 169, 34.
80. Margari, V., Pyle, D.M., Bryant, C., Gibbard, P.L., 2007. Mediterranean tephra stratigraphy revisited: Results from a long terrestrial sequence on Lesvos Island, Greece. Journal of Volcanology and Geothermal Research 163, 34-54.
81. Marinos, G., 1959. The Antimilos volcano in Aegean Sea. Bulletin of the Geological Society of Greece 4, 38-50 (in Greek).
82. Marra, F., Sottili, G., Gaeta, M., Giaccio, B., Jicha, B., Masotta, M., Palladino, D.M., Deocampo, D.M., 2014. Major explosive activity in the Monti Sabatini Volcanic District (central Italy) over the 800-390 ka interval: geochronological-geochemical overview and tephrostratigraphic implications. Quaternary Science Reviews 94, 74-101.
83. Martrat, B., Grimalt, J.O., Shackleton, N.J., de Abreu, L., Hutterli, M.A., Stocker, T.F., 2007. Four climate cycles of recurring deep and surface water destabilizations on the Iberian margin. Science 317, 502-507.
84. Matsuda, J.-i., Senoh, K., Maruoka, T., Sato, H., Mitropoulos, P., 1999. K-Ar ages of the Aegean volcanic rocks and their implication for the arc-trench system. Geochemical Journal 33, 369-377.

85. Matthews, I.P., Trincardi, F., Lowe, J.J., Bourne, A.J., MacLeod, A., Abbott, P.M., Andersen, N., Asioli, A., Blockley, S.P.E., Lane, C.S., Oh, Y.A., Satow, C.S., Staff, R.A., Wulf, S., 2015. Developing a robust tephrochronological framework for Late Quaternary marine records in the Southern Adriatic Sea: new data from core station SA03-11. Quaternary Science Reviews 118, 84-104.
86. Melles, M., Brigham-Grette, J., Minyuk, P.S., Nowaczyk, N.R., Wennrich, V., DeConto, R.M., Anderson, P.M., Andreev, A.A., Coletti, A., Cook, T.L., Haltia-Hovi, E., Kukkonen, M., Lozhkin, A.V., Rosén, P., Tarasov, P., Vogel, H., Wagner, B., 2012. 2.8 Million years of Arctic climate change from Lake El'gygytgyn, NE Russia. Science 337, 315-320.
87. Mitropoulos, P., Tarney, J., Saunders, A.D., Marsh, N.G., 1987. Petrogenesis of Cenozoic volcanic rocks from the Aegean island arc. Journal of Volcanology and Geothermal Research 32, 177-193.
88. Molnár, K., Harangi, S., Lukács, R., Dunkl, I., Schmitt, A.K., Kiss, B., Garamhegyi, T., Seghedi, I., 2018. The onset of the volcanism in the Ciomadul Volcanic Dome Complex (Eastern Carpathians): Eruption chronology and magma type variation. Journal of Volcanology and Geothermal Research 354, 39-56.
89. Müller, U.C., Pross, J., Tzedakis, P.C., Gamble, C., Kotthoff, U., Schmiedl, G., Wulf, S., Christanis, K., 2011. The role of climate in the spread of modern humans into Europe. Quaternary Science Reviews 30, 273-279.
90. Nappi, G., Antonelli, F., Coltorti, M., Milani, L., Renzulli, A., Siena, F., 1998. Volcanological and petrological evolution of the Eastern Vulsini District, Central Italy. Journal of Volcanology and Geothermal Research 87, 211-232.
91. Nappi, G., Capaccioni, B., Mattioli, M., Mancini, E., Valentini, L., 1994. Plinian fall deposits from Vulsini Volcanic District (Central Italy). Bulletin of Volcanology 56, 502-515.

92. Nemec, W., Kazanci, N., Mitchell, J.G., 1998. Pleistocene explosions and pyroclastic currents in west-central Anatolia. Boreas 27, 311-332.
93. Neugebauer, I., Wulf, S., Schwab, M.J., Serb, J., Plessen, B., Appelt, O., Brauer, A., 2017. Implications of S1 tephra findings in Dead Sea and Tayma palaeolake sediments for marine reservoir age estimation and palaeoclimate synchronisation. Quaternary Science Reviews 170, 269-275.
94. Nomade, S., Scaillet, S., Pastre, J.-F., Nehlig, P., 2012. Pyroclastic chronology of the Sancy stratovolcano (Mont-Dore, French Massif Central): New high-precision 40Ar/39Ar constraints. Journal of Volcanology and Geothermal Research 225-226, 1-12.
95. Paillard, D., Labeyrie, L., Yiou, P., 1996. Macintosh Program performs time-series analysis. Eos, Transactions, American Geophysical Union 77, 379-379.
96. Palladino, D.M., Gaeta, M., Giaccio, B., Sottili, G., 2014. On the anatomy of magma chamber and caldera collapse: The example of trachy-phonolitic explosive eruptions of the Roman Province (central Italy). Journal of Volcanology and Geothermal Research 281, 12-26.
97. Pappalardo, L., Civetta, L., D'Antonio, M., Deino, A., Di Vito, M., Orsi, G., Carandente, A., de Vita, S., Isaia, R., Piochi, M., 1999. Chemical and Sr-isotopical evolution of the Phlegraean magmatic system before the Campanian Ignimbrite and the Neapolitan Yellow Tuff eruptions. Journal of Volcanology and Geothermal Research 91, 141-166.
98. Past Interglacials Working Group of Pages, 2016. Interglacials of the last 800,000 years. Reviews of Geophysics 54, 162-219.
99. Pasteels, P., Kolios, N., Boven, A., Saliba, E., 1986. Applicability of the K/Ar method to whole-rock samples of acid lava and pumice: Case of the Upper

Pleistocene domes and pyroclasts on Kos Island, Aegean Sea, Greece. Chemical Geology 57, 145-154.

100. Pastre, J., Cantagrel, J., 2001. The Mont Dore tephrostratigraphy (Massif Central, France). Quaternaire 12, 249-267.

101. Pe, G.G., 1974. Volcanic rocks of Methana, South Aegean arc, Greece. Bulletin Volcanologique 38, 270-290.

102. Pe-Piper, G., Moulton, B., 2008. Magma evolution in the Pliocene–Pleistocene succession of Kos, South Aegean arc (Greece). Lithos 106, 110-124.

103. Peccerillo, A., 2017. Cenozoic volcanism in the Tyrrhenian Sea region. Springer International Publishing, Cham, Switzerland.

104. Peccerillo, A., Taylor, S.R., 1976. Geochemistry of Eocene calc-alkaline volcanic rocks from the Kastamonu area, northern Turkey. Contributions to Mineralogy and Petrology 58, 63-81.

105. Perini, G., Conticelli, S., Francalanci, L., Davidson, J.P., 2000. The relationship between potassic and calc-alkaline post-orogenic magmatism at Vico volcano, central Italy. Journal of Volcanology and Geothermal Research 95, 247-272.

106. Petrosino, P., Jicha, B.R., Mazzeo, F.C., Ciaranfi, N., Girone, A., Maiorano, P., Marino, M., 2015. The Montalbano Jonico marine succession: An archive for distal tephra layers at the Early-Middle Pleistocene boundary in southern Italy. Quaternary International 383, 89-103.

107. Petrosino, P., Jicha, B.R., Mazzeo, F.C., Russo Ermolli, E., 2014. A high resolution tephrochronological record of MIS 14-12 in the Southern Apennines (Acerno Basin, Italy). Journal of Volcanology and Geothermal Research 274, 34-50.

108. Platevoet, B., Elitok, Ö., Guillou, H., Bardintzeff, J.-M., Yagmurlu, F., Nomade, S., Poisson, A., Deniel, C., Özgür, N., 2014. Petrology of Quaternary volcanic rocks and related plutonic xenoliths from Gölcük volcano, Isparta Angle, Turkey: Origin and evolution of the high-K alkaline series. Journal of Asian Earth Sciences 92, 53-76.

109. Platevoet, B., Scaillet, S., Guillou, H., Blamart, D., Nomade, S., Massault, M., Poisson, A., Elitok, Ö., Özgür, N., Yagmurlu, F., 2008. Pleistocene eruptive chronology of the Gölcük volcano, Isparta Angle, Turkey. Quaternaire 19, 147-156.

110. Poli, S., Chiesa, S., Gillot, P.-Y., Gregnanin, A., Guichard, F., 1987. Chemistry versus time in the volcanic complex of Ischia (Gulf of Naples, Italy): evidence of successive magmatic cycles. Contributions to Mineralogy and Petrology 95, 322-335.

111. Pross, J., Kotthoff, U., Müller, U., Peyron, O., Dormoy, I., Schmiedl, G., Kalaitzidis, S., Smith, A., 2009. Massive perturbation in terrestrial ecosystems of the Eastern Mediterranean region associated with the 8.2 kyr B.P. climatic event. Geology 37, 887-890.

112. Pross, J., Koutsodendris, A., Christanis, K., Fischer, T., Fletcher, W.J., Hardiman, M., Kalaitzidis, S., Knipping, M., Kotthoff, U., Milner, A.M., Müller, U.C., Schmiedl, G., Siavalas, G., Tzedakis, P.C., Wulf, S., 2015. The 1.35-Ma-long terrestrial climate archive of Tenaghi Philippon, northeastern Greece: Evolution, exploration, and perspectives for future research. Newsletters on Stratigraphy 48, 253-276.

113. Pyle, D.M., van Andel, T.H., Paschos, P., van den Bogaard, P., 1998. An exceptionally thick Middle Pleistocene tephra layer from Epirus, Greece. Quaternary Research 49, 280-286.

114. Regattieri, E., Giaccio, B., Galli, P., Nomade, S., Peronace, E., Messina, P., Sposato, A., Boschi, C., Gemelli, M., 2016. A multi-proxy record of MIS 11-12 deglaciation and glacial MIS 12 instability from the Sulmona basin (central Italy). Quaternary Science Reviews 132, 129-145.

115. Rolandi, G., Bellucci, F., Heizler, M.T., Belkin, H.E., De Vivo, B., 2003. Tectonic controls on the genesis of ignimbrites from the Campanian Volcanic Zone, southern Italy. Mineralogy and Petrology 79, 3-31.

116. Rouchon, V., Gillot, P.Y., Quidelleur, X., Chiesa, S., Floris, B., 2008. Temporal evolution of the Roccamonfina volcanic complex (Pleistocene), Central Italy. Journal of Volcanology and Geothermal Research 177, 500-514.

117. Russo Ermolli, E., Aucelli, P.P.C., Di Rollo, A., Mattei, M., Petrosino, P., Porreca, M., Rosskopf, C.M., 2010. An integrated stratigraphical approach to the Middle Pleistocene succession of the Sessano basin (Molise, Italy). Quaternary International 225, 114-127.

118. Sadori, L., Koutsodendris, A., Panagiotopoulos, K., Masi, A., Bertini, A., Combourieu-Nebout, N., Francke, A., Kouli, K., Joannin, S., Mercuri, A.M., Peyron, O., Torri, P., Wagner, B., Zanchetta, G., Sinopoli, G., Donders, T.H., 2016. Pollen-based paleoenvironmental and paleoclimatic change at Lake Ohrid (south-eastern Europe) during the past 500 ka. Biogeosciences 13, 1423-1437.

119. Satow, C., Tomlinson, E.L., Grant, K.M., Albert, P.G., Smith, V.C., Manning, C.J., Ottolini, L., Wulf, S., Rohling, E.J., Lowe, J.J., Blockley, S.P.E., Menzies, M.A., 2015. A new contribution to the Late Quaternary tephrostratigraphy of the Mediterranean: Aegean Sea core LC21. Quaternary Science Reviews 117, 96-112.

120. Schmincke, H.-U., Sumita, M., 2014. Impact of volcanism on the evolution of Lake Van (eastern Anatolia) III: Periodic (Nemrut) vs. episodic (Süphan)

explosive eruptions and climate forcing reflected in a tephra gap between ca. 14 ka and ca. 30 ka. Journal of Volcanology and Geothermal Research 285, 195-213.

121. Schmitt, A.K., Danišík, M., Evans, N.J., Siebel, W., Kiemele, E., Aydin, F., Harvey, J.C., 2011. Acigöl rhyolite field, Central Anatolia (part 1): high-resolution dating of eruption episodes and zircon growth rates. Contributions to Mineralogy and Petrology 162, 1215-1231.

122. Seghedi, I., Downes, H., Szakács, A., Mason, P.R.D., Thirlwall, M.F., Roşu, E., Pécskay, Z., Márton, E., Panaiotu, C., 2004. Neogene–Quaternary magmatism and geodynamics in the Carpathian–Pannonian region: a synthesis. Lithos 72, 117-146.

123. Şen, E., Kürkcüoğlu, B., Aydar, E., Gourgaud, A., Vincent, P.M., 2003. Volcanological evolution of Mount Erciyes stratovolcano and origin of the Valibaba Tepe ignimbrite (Central Anatolia, Turkey). Journal of Volcanology and Geothermal Research 125, 225-246.

124. Smith, V.C., Isaia, R., Pearce, N.J.G., 2011. Tephrostratigraphy and glass compositions of post-15 kyr Campi Flegrei eruptions: implications for eruption history and chronostratigraphic markers. Quaternary Science Reviews 30, 3638-3660.

125. St. Seymour, K., Christanis, K., Bouzinos, A., Papazisimou, S., Papatheodorou, G., Moran, E., Denes, G., 2004. Tephrostratigraphy and tephrochronology in the Philippi peat basin, Macedonia, Northern Hellas (Greece). Quaternary International 121, 53-65.

126. Sumita, M., Schmincke, H.-U., 2013a. Impact of volcanism on the evolution of Lake Van I: evolution of explosive volcanism of Nemrut Volcano (eastern Anatolia) during the past >400,000 years. Bulletin of Volcanology 75, Art. No. 714.

127. Sumita, M., Schmincke, H.-U., 2013b. Impact of volcanism on the evolution of Lake Van II: Temporal evolution of explosive volcanism of Nemrut Volcano (eastern Anatolia) during the past ca. 0.4 Ma. Journal of Volcanology and Geothermal Research 253, 15-34.

128. Szakács, A., Seghedi, I., Pécskay, Z., Mirea, V., 2015. Eruptive history of a low-frequency and low-output rate Pleistocene volcano, Ciomadul, South Harghita Mts., Romania. Bulletin of Volcanology 77, Art. No. 12.

129. Tamburrino, S., Insinga, D.D., Sprovieri, M., Petrosino, P., Tiepolo, M., 2012. Major and trace element characterization of tephra layers offshore Pantelleria Island: insights into the last 200 ka of volcanic activity and contribution to the Mediterranean tephrochronology. Journal of Quaternary Science 27, 129-140.

130. Tomlinson, E.L., Albert, P.G., Wulf, S., Brown, R.J., Smith, V.C., Keller, J., Orsi, G., Bourne, A.J., Menzies, M.A., 2014. Age and geochemistry of tephra layers from Ischia, Italy: constraints from proximal-distal correlations with Lago Grande di Monticchio. Journal of Volcanology and Geothermal Research 287, 22-39.

131. Tomlinson, E.L., Arienzo, I., Civetta, L., Wulf, S., Smith, V.C., Hardiman, M., Lane, C.S., Carandente, A., Orsi, G., Rosi, M., Muller, W., Menzies, M.A., 2012a. Geochemistry of the Phlegraean Fields (Italy) proximal sources for major Mediterranean tephras: Implications for the dispersal of Plinian and co-ignimbritic components of explosive eruptions. Geochimica Et Cosmochimica Acta 93, 102-128.

132. Tomlinson, E.L., Kinvig, H.S., Smith, V.C., Blundy, J.D., Gottsmann, J., Müller, W., Menzies, M.A., 2012b. The Upper and Lower Nisyros Pumices: Revisions to the Mediterranean tephrostratigraphic record based on micron-beam

glass geochemistry. Journal of Volcanology and Geothermal Research 243, 69-80.

133. Tomlinson, E.L., Smith, V.C., Albert, P.G., Aydar, E., Civetta, L., Cioni, R., Cubukcu, E., Gertisser, R., Isaia, R., Menzies, M.A., Orsi, G., Rosi, M., Zanchetta, G., 2015. The major and trace element glass compositions of the productive Mediterranean volcanic sources: tools for correlating distal tephra layers in and around Europe. Quaternary Science Reviews 118, 48-66.

134. Tzedakis, P.C., Hooghiemstra, H., Pälike, H., 2006. The last 1.35 million years at Tenaghi Philippon: revised chronostratigraphy and long-term vegetation trends. Quaternary Science Reviews 25, 3416-3430.

135. Van der Wiel, A.M., Wijmstra, T.A., 1987. Palynology of the lower part (78–120 m) of the core Tenaghi Philippon II, Middle Pleistocene of Macedonia, Greece. Review of Palaeobotany and Palynology 52, 73-88.

136. Villa, V., Pereira, A., Chaussé, C., Nomade, S., Giaccio, B., Limondin-Lozouet, N., Fusco, F., Regattieri, E., Degeai, J.-P., Robert, V., Kuzucuoglu, C., Boschian, G., Agostini, S., Aureli, D., Pagli, M., Bahain, J.J., Nicoud, E., 2016. A MIS 15-MIS 12 record of environmental changes and Lower Palaeolithic occupation from Valle Giumentina, central Italy. Quaternary Science Reviews 151, 160-184.

137. Vinci, A., 1985. Distribution and chemical-composition of tephra layers from Eastern Mediterranean abyssal sediments. Marine Geology 64, 143-155.

138. Voelker, A.H.L., Rodrigues, T., Billups, K., Oppo, D., McManus, J., Stein, R., Hefter, J., Grimalt, J.O., 2010. Variations in mid-latitude North Atlantic surface water properties during the mid-Brunhes (MIS 9–14) and their implications for the thermohaline circulation. Climate of the Past 6, 531-552.

139. Wagner, B., Wilke, T., Francke, A., Albrecht, C., Baumgarten, H., Bertini, A., Combourieu-Nebout, N., Cvetkoska, A., D'Addabbo, M., Donders, T.H., Föller, K., Giaccio, B., Grazhdani, A., Hauffe, T., Holtvoeth, J., Joannin, S., Jovanovska, E., Just, J., Kouli, K., Koutsodendris, A., Krastel, S., Lacey, J.H., Leicher, N., Leng, M.J., Levkov, Z., Lindhorst, K., Masi, A., Mercuri, A.M., Nomade, S., Nowaczyk, N., Panagiotopoulos, K., Peyron, O., Reed, J.M., Regattieri, E., Sadori, L., Sagnotti, L., Stelbrink, B., Sulpizio, R., Tofilovska, S., Torri, P., Vogel, H., Wagner, T., Wagner-Cremer, F., Wolff, G.A., Wonik, T., Zanchetta, G., Zhang, X.S., 2017. The environmental and evolutionary history of Lake Ohrid (FYROM/Albania): interim results from the SCOPSCO deep drilling project. Biogeosciences 14, 2033-2054.

140. Wijmstra, T., Smit, A., 1976. Palynology of the middle part (30–78 metres) of the 120 m deep section in northern Greece (Macedonia). Acta Botanica Neerlandica 25, 297-312.

141. Wulf, S., Hardiman, M., Staff, R.A., Koutsodendris, A., Appelt, O., Blockley, S.P.E., Lowe, J.J., Manning, C.J., Ottolini, L., Schmitt, A.K., Smith, V.C., Tomlinson, E.L., Vakhrameeva, P., Knipping, M., Kotthoff, U., Milner, A.M., Müller, U.C., Christanis, K., Kalaitzidis, S., Tzedakis, C., Schmiedl, G., Pross, J., 2018. The marine isotope stage 1–5 cryptotephra record of Tenaghi Philippon, Greece: Towards a detailed tephrostratigraphic framework for the Eastern Mediterranean region. Quaternary Science Reviews 186, 236–262.

142. Wulf, S., Keller, J., Paterne, M., Mingram, J., Lauterbach, S., Opitz, S., Sottili, G., Giaccio, B., Albert, P.G., Satow, C., Tomlinson, E.L., Viccaro, M., Brauer, A., 2012. The 100–133 ka record of Italian explosive volcanism and revised tephrochronology of Lago Grande di Monticchio. Quaternary Science Reviews 58, 104-123.

143. Wulf, S., Kraml, M., Brauer, A., Keller, J., Negendank, J.F.W., 2004. Tephrochronology of the 100 ka lacustrine sediment record of Lago Grande di Monticchio (southern Italy). Quaternary International 122, 7-30.

144. Zanchetta, G., Giaccio, B., Bini, M., Sarti, L., 2018. Tephrostratigraphy of Grotta del Cavallo, Southern Italy: Insights on the chronology of Middle to Upper Palaeolithic transition in the Mediterranean. Quaternary Science Reviews 182, 65-77.

145. Zanchetta, G., Sulpizio, R., Roberts, N., Cioni, R., Eastwood, W.J., Siani, G., Caron, B., Paterne, M., Santacroce, R., 2011. Tephrostratigraphy, chronology and climatic events of the Mediterranean basin during the Holocene: An overview. The Holocene 21, 33-52.

146. Zouzias, D., St. Seymour, K., 2008. Consanguineous geochemistry of the Kos Plateau and Tilos D and E Pumices, Aegean Volcanic Arc, Hellas. Neues Jahrbuch für Mineralogie – Abhandlungen 184, 231-241.

147. Zouzias, D., St. Seymour, K., 2013. Kos Plateau Tuff (KPT) on Kalymnos island, Aegean volcanic arc: A geochemical approach. Journal of Volcanology and Seismology 7, 293-312.

Figure captions

Figure 1: Map of the Central and Eastern Mediterranean regions showing the location of Tenaghi Philippon and other Middle Pleistocene tephra archives considered in this study: 1 – Piánico paleolake; 2 – Ficoncella site; 3 – Campo Felice basin; 4 – Paganica-San Demetrio-Castelnuovo basin; 5 – Sulmona basin; 6 – Sessano basin; 7 – Boiano basin; 8 – Mercure basin; 9 – ODP Site 964; 10 – Lake Ohrid; 11 – Lake Van. The main volcanic centers active (or possibly active) during MIS 12–10 are also marked: A, Aeolian Islands; Ac, Acigöl; C, Ciomadul; CA, Colli Albani; CF, Campi Flegrei; Ch, Christiana Islands; E,

Etna; ED, Erciyes Dagi; G, Gölcük; HD, Hasan Dagi; Is, Ischia; K, Kos; M, Milos and Antimilos; Me, Methana; N, Nemrut; P, Pantelleria; Pz, Ponza Island; R, Roccamonfina; S, Sabatini; Sn, Sancy; St, Santorini; Sü, Süphan; U, Ustica; V, Vico; Vs, Vulsini; Vt, Monte Vulture. The inset map shows the location of ODP Site 983 (12) in the North Atlantic.

Figure 2: Lithostratigraphy, arboreal pollen record (AP) and distribution of cryptotephras with glass-shard counts in the 82–63 m depth interval of the Tenaghi Philippon TP-2009 core. Cryptotephras are color-coded according to their provenance as inferred in this study.

Figure 3: Individual cryptotephra layers in core TP-2009 plotted in (**A**) total alkali *vs*. silica diagram (Le Bas et al., 1986); (**B**) K_2O *vs*. SiO_2 diagram (Peccerillo and Taylor, 1976); (**C**) K_2O/Na_2O *vs*. SiO_2 diagram with a close-up part of the diagram showing classification of Italian volcanic rocks on the basis of the K_2O/Na_2O ratio (modified after Peccerillo, 2017); (**D**) tectonic setting discrimination diagrams Rb *vs.* Y+Nb and Nb/Rb *vs.* Th/Rb (Tomlinson et al., 2015) for anorogenic, active-subduction and post-subduction settings. Tephras are grouped into geochemical populations and indicated by colors. Rock types: A – andesite; B – basalt; BA – basaltic andesite; BTA – basaltic trachyandesite; D – dacite; F – foidite; L – latite; P – phonolite; PB – picrobasalt; PT – phonotephrite; R – rhyolite; S – shoshonite; SB – shoshonitic basalt; TB – tephrite or basanite; TP – tephriphonolite; Tr – trachyte; TrA – trachyandesite; TrB – trachybasalt; TrD – trachydacite.

Figure 4: (**A**) Major-element plots and (**B**) Cl *vs*. CaO/FeO plot (Giaccio et al., 2017b) showing comparison of trachytic TP09 cryptotephras with potential Italian source

volcanoes. Geochemical envelopes corresponding to the basal fall, lower and intermediate flow units, and the upper flow unit of CI are plotted as well. A N_2O/K_2O ratio of 0.6 is used to discriminate the two components of CI following Tomlinson et al. (2012a). The TAV2 tephra of Campanian provenance (Giaccio et al., 2014) is shown as a potential correlative for cryptotephras from Tenaghi Philippon. Data sources: Campi Flegrei – Leicher et al. (2016), Margari et al. (2007), Müller et al. (2011) Smith et al. (2011), Tomlinson et al. (2012a); Campanian Ignimbrite – Leicher et al. (2016), Margari et al. (2007), Müller et al. (2011), Tomlinson et al. (2012a); Etna – Albert et al. (2013), Wulf et al. (2004, 2012); Ischia – Tomlinson et al. (2014, 2015); Pantelleria – Leicher et al. (2016), Margari et al. (2007), Tamburrino et al. (2012), Tomlinson et al. (2015); Roccamonfina – Giaccio et al. (2014), Giannetti and Luhr (1983), Leicher et al. (2016), Regattieri et al. (2016); Sabatini – Aureli et al. (2012), Giaccio et al. (2014), Leicher et al. (2016), Marra et al. (2014), Palladino et al. (2014), Petrosino et al. (2014); Ustica (bulk analyses) – Cinque et al. (1988); Vico – Leicher et al. (2016), Marra et al. (2014), Palladino et al. (2014), Perini et al. (2000), Regattieri et al. (2016); Vulsini – Leicher et al. (2016), Nappi et al. (1994, 1998), Palladino et al. (2014).

Figure 5: Major- and trace-element plots refining the correlation of trachytic cryptotephras from Tenaghi Philippon with Italian source volcanoes and individual eruptions during the MIS 12–10 interval. * Old Campanian Tephras – tephras with Campanian geochemical fingerprints that are older than proximal Campanian volcanics (~290 ka), including the Morphi and TAV2 tephras; see text for details on particular tephra layers. SIMS (purple dotted/dashed lines) and LA-ICPMS (dark blue dotted/dashed lines) data of CI on trace-element plots are shown separately. Data sources: Ischia – Tomlinson et al. (2014, 2015)[1,2]; Campanian Ignimbrite – Leicher et al. (2016)[1], Margari et al. (2007)[1], Tomlinson et al. (2012a)[1,2], Wulf et al. (2018)[1,2,3]; pre- and post-Campanian Ignimbrite series of

Campi Flegrei – Smith et al. (2011)[1,2], Tomlinson et al. (2012a)[1,2]; Old Campanian Tephras – Giaccio et al. (2013b, 2014)[1], Leicher et al. (2016)[1], Petrosino et al. (2014[1], 2015[1,2]), Pyle et al. (1998)[1]. Analytical techniques used in the data sources: 1 – EPMA; 2 – LA-ICP-MS; 3 – SIMS.

Figure 6: Major- and trace-element plots showing comparison of dacitic and rhyolitic cryptotephras from Tenaghi Philippon with potential volcanic sources: (**A**) Aegean Arc, including only Quaternary rocks of Methana, Milos, Kolumbo, Kos, Nisyros, Yali, and (plotted separately) Santorini; Aeolian Islands, including Salina and Lipari; (**B**) Western (Gölcük), Central (Acigöl; Erciyes Dagi) and Eastern (Nemrut, Süphan) Anatolia, Carpathians (Ciomadul), and Pianico (T21d) tephra. Data sources: Aegean Arc – Aksu et al. (2008)[1], Dalabakis and Vougioukalakis (1993)[3], Federman and Carey (1980)[1], Cantner et al. (2014)[1], Filippou (2014)[3], Fuller (2015)[1], Fytikas et al. (1986a,b)[3], Koukouzas (1997)[3], Koukouzas and Dunham (1998)[3], Margari et al. (2007)[1], Mitropoulos et al. (1987)[3], Pe (1974)[3], Pe-Piper and Moulton (2008)[3], Tomlinson et al. (2012b)[1,2], Vinci (1985)[1], Zouzias and St. Seymour (2008, 2013)[1,3]; Santorini – Druitt et al. (1999)[3], Huijsmans (1985)[3], Margari et al. (2007)[1], Satow et al. (2015)[1], Tomlinson et al. (2015)[1,2], this study[1]; Salina and Lipari – Albert et al. (2012, 2017)[1,2]; Western and Central Anatolia – Tomlinson et al. (2015)[1,2]; Eastern Anatolia – Macdonald et al. (2015)[1], Schmincke and Sumita (2014)[1], Sumita and Schmincke (2013a,b)[1,3]; Carpathians – Karátson et al. (2016)[1], Molnár et al. (2018)[3]; Pianico (T21d) – Brauer et al. (2007)[1]. Analytical techniques used in the data sources: 1 – EPMA; 2 – LA-ICP-MS; 3 – bulk analyses.

Figure 7: Major- and trace-element plots showing comparison of dacitic (POP2) and rhyolitic (POP3) cryptotephras from Tenaghi Philippon with potential Santorini tephra

equivalents: Cape Therma 1, 2 and 3; 1st and 2nd pumice falls below Cape Therma 1. Bulk trace-element data are from Druitt et al. (1999).

Figure 8: Major-element plots showing comparison of rhyolitic cryptotephras from Tenaghi Philippon (POP4 and POP5) with Middle Pleistocene volcanic sources of the Aegean Arc. Data sources as in Fig. 6.

Figure 9: Ages of cryptotephras from Tenaghi Philippon as estimated by aligning the pollen record from core TP-2009 to other climate records. (**A**) Percentages of the planktonic foraminifer *Neogloboquadrina pachyderma* (NPS %) from ODP Site 983 (Barker et al., 2015) tuned to the LR04 stack (Lisiecki and Raymo, 2005); (**B**) Tree-pollen percentages (AP %) from core TP-2009 (this study); (**C**) Tree-pollen percentages (AP %) from the old Tenaghi Philippon core TF-II (Van der Wiel and Wijmstra, 1987; Wijmstra and Smit, 1976) plotted on the orbitally tuned age model of Tzedakis et al. (2006). The yellow band marks an offset between the age models of the TF-II and ODP Site 983 records. The MIS boundaries shown in the figure are from the low-latitude oxygen isotope stack of Bassinot et al. (1994).

Figure 10: Tephrostratigraphic framework for the Central and Eastern Mediterranean for the MIS 12–10 (460–335 ka) interval in Tenaghi Philippon. The MIS boundaries shown in the figure are from the low-latitude oxygen isotope stack of Bassinot et al. (1994). The following tephra records are shown (from W to E): Ficoncella site (Aureli et al., 2012, 2015); Campo Felice basin (Giraudi and Giaccio, 2015); Paganica-San Demetrio-Castelnuovo basin (Galli et al., 2010; Giaccio et al., 2012); Sulmona basin (Giaccio et al., 2013b; Regattieri et al., 2016); Valle Guimentina basin (Villa et al., 2016); Sessano basin (Russo Ermolli et al., 2010); Boiano basin (Amato et al., 2014); Mercure basin (Giaccio

et al., 2014); ODP Site 964 (Lourens, 2004); Lake Ohrid (Kousis et al., 2018; Leicher et al., 2016); Tenaghi Philippon (this study); Lake Van (Engelhardt et al., 2017). The dashed lines mark tephra layers that have been found in at least two distal sequences. Tephras from ODP Site 964 and Lake Van have been included for completeness despite the absence of geochemical data.

Table titles

Table 1: Summary of cryptotephra samples in the MIS 12–10 interval of core TP-2009 including glass shard counts, geochemical affinity, likely sources and estimated ages.

Table 2: Representative EPMA (non-normalized) and SIMS glass data of cryptotephras in the MIS 12–10 interval of core TP-2009.

Supplementary files

Supplement 1: Supplementary information on peat tephra archives, material and methods, and sampling sites for proximal tephra samples on Santorini, as well as micrographs of glass shard from Tenaghi Philippon.

Supplement 2: Full EPMA and SIMS glass analytical data of cryptotephras from Tenaghi Philippon.

Supplement 3: EPMA glass data of proximal tephra samples from Santorini.

Supplement 4: Additional major- and trace-element plots supporting the interpretation.

Table 1

Tephra	TP-2009 depth range (m)	Shard counts	Shards analyzed	Geochemical population	Provenance	Age estimates (ka)	MIS
	63.00-63.01	2	0	-		336	10
TP09-63.015a	63.01-63.02	7	4	POP1B	Campi Flegrei, reworked CI	336	10
TP09-63.015b	63.01-63.02		2	POP3	Santorini, reworked CT-2?	336	10
TP09-63.05	63.00-63.10	5	3	POP1A	Campi Flegrei, reworked CI	336	10
TP09-65.835a	65.83-65.84	4	1	POP1B	Campanian Province	358	10
TP09-65.835b	65.83-65.84		1	POP4	Aegean Arc, Kos or Milos?	358	10
	65.80-65.90	1	0	-		358	10
TP09-65.95	65.90-66.00	3	1	POP2	Santorini, CT-1	359	10
	66.60-66.70	1	0	-		364	11
TP09-66.95	66.90-67.00	3	1	POP3	Santorini, SAN 35?	367	11
TP09-67.05	67.00-67.10	2	1	POP3	Santorini, reworked SAN 35?	368	11
TP09-67.15	67.10-67.20	27	4	POP2	Santorini, reworked CT-1	369	11
TP09-68.95	68.90-69.00	1	1	POP3	Santorini, reworked SAN 35?	382	11
	70.40-70.41	1	0	-		391	11
TP09-70.45	70.40-70.50	1	1	POP1C	Campanian Province	391	11
	73.70-73.80	1	0	-		412	11
TP09-74.75	74.70-74.80	2	1	POP5	Uncorrelated	419	11
TP09-75.75	75.70-75.80	5	4	POP5	Uncorrelated	427	12
TP09-75.85	75.80-75.90	2	1	POP5	Uncorrelated	428	12
TP09-76.05	76.00-76.10	2	2	POP5	Uncorrelated	430	12
TP09-76.75	76.70-76.80	2	1	POP5	Uncorrelated	433	12
TP09-76.95	76.90-77.00	1	1	POP5	Uncorrelated	434	12
TP09-77.35	77.30-77.40	1	1	POP5	Uncorrelated	436	12
TP09-77.65	77.60-77.70	7	2	POP5	Uncorrelated	437	12
TP09-77.95	77.90-78.00	2	1	POP5	Uncorrelated	438	12

Table 2a

Tephra	**TP09-63.015a**	**TP09-63.015b**	**TP09-63.05**	**TP09-65.835a**	**TP09-65.835b**	**TP09-65.95**	**TP09-66.95**	**TP09-67.05**	**TP09-67.15**	**TP09-68.95**
Provenance	Campi Flegrei, rew. CI	Santorini, rew. CT-2?	Campi Flegrei, rew. CI	Campanian Province	Aegean Arc, Kos or Milos?	Santorini, CT-1	Santorini, SAN 35?	Santorini, rew. SAN 35?	Santorini, rew. CT-1	Santorini, rew. SAN 35?
(wt%)	*n = 4*	*n = 2*	*n = 3*	*n = 1*	*n = 1*	*n = 1*	*n = 1*	*n = 1*	*n = 4*	*n = 1*
SiO_2	59.73	69.43	58.95	61.18	76.22	60.13	68.51	65.83	62.51	65.96
TiO_2	0.43	0.46	0.35	0.38	0.10	0.62	0.57	0.52	0.85	0.56
Al_2O_3	18.75	14.69	18.58	18.59	12.83	13.36	14.31	13.90	15.09	14.14
FeO	2.88	2.91	3.36	2.79	1.49	5.36	3.78	3.56	6.63	3.35
MnO	0.25	0.09	0.10	0.19	0.08	0.10	0.06	0.08	0.14	0.09
MgO	0.35	0.43	0.79	0.33	0.06	0.82	0.68	0.62	1.44	0.62
CaO	1.49	1.67	2.67	2.26	0.95	3.26	2.55	2.33	4.48	2.42
Na_2O	6.79	4.39	4.09	5.92	2.54	3.92	4.18	4.35	4.48	4.31
K_2O	6.17	3.07	7.42	6.86	4.92	2.39	3.60	2.88	2.05	2.91
P_2O_5	0.04	0.07	0.15	0.02	0.00	0.17	0.12	0.09	0.21	0.10
Cl	0.81	0.26	0.35	0.82	0.10	0.36	0.24	0.18	0.23	0.17
Total	98.51	97.71	97.16	100.15	99.39	90.85	98.84	94.51	98.33	94.80
(ppm)			*n = 2*	*n = 1*	*n = 1*		*n = 1*	*n = 1*	*n = 3*	
Rb			251.21	426.95	151.97		112.28	100.93	73.57	
Sr			300.38	20.40	48.66		77.23	90.36	146.26	
Y			18.25	54.20	39.11		45.83	45.27	48.41	
Zr			166.45	694.67	159.73		311.52	302.55	248.06	
Nb			26.63	128.89	17.93		13.79	13.46	9.51	
Ba			506.55	18.14	886.97		497.85	509.75	317.27	
La			38.42	119.33	35.37		27.52	28.37	21.21	
Ce			70.97	226.74	68.82		56.47	59.05	46.46	
Th			11.31	48.17	12.40		14.98	15.58	10.47	
U			3.83	18.24	3.64		4.65	5.13	3.42	

Table 2b

Tephra	**TP09-70.45**	**TP09-74.75**	**TP09-75.75**	**TP09-75.85**	**TP09-76.05**	**TP09-76.75**	**TP09-76.95**	**TP09-77.35**	**TP09-77.65**	**TP09-77.95**
Provenance	Campanian Province	Uncorrelated	Uncorrelated	Uncorrelated	Uncorrelated	Uncorrelated	Uncorrelated	Uncorrelated	Uncorrelated	Uncorrelated
(wt%)	*n = 1*	*n = 1*	*n = 4*	*n = 1*	*n = 2*	*n = 1*	*n = 1*	*n = 1*	*n = 2*	*n = 1*
SiO_2	61.30	72.27	72.68	73.56	72.41	71.81	72.67	74.17	73.12	73.73
TiO_2	0.42	0.12	0.08	0.05	0.08	0.26	0.10	0.09	0.07	0.06
Al_2O_3	19.06	13.77	13.44	13.36	12.87	15.13	12.87	12.77	13.02	15.34
FeO	2.96	1.48	0.49	0.32	0.41	0.48	0.68	0.38	0.44	1.55
MnO	0.20	0.03	0.02	0.02	0.00	0.00	0.00	0.02	0.02	0.00
MgO	0.32	3.59	2.25	2.52	2.22	1.70	2.38	1.25	2.10	1.37
CaO	0.81	2.17	4.59	5.44	5.29	3.91	5.15	2.90	4.11	1.60
Na_2O	6.93	2.08	0.73	0.57	0.45	0.67	0.36	0.86	0.61	1.19
K_2O	4.66	2.94	4.41	3.59	4.06	5.23	4.24	6.31	5.04	4.51
P_2O_5	0.06	0.09	0.03	0.01	0.05	0.03	0.08	0.01	0.05	0.06
Cl	0.82	0.01	0.01	0.01	0.01	0.02	0.00	0.02	0.02	0.02
Total	98.35	98.55	98.73	99.47	97.85	99.26	98.54	98.79	98.61	99.44
(ppm)		*n = 1*	*n = 4*	*n = 1*			*n = 1*	*n = 1*	*n = 2*	*n = 1*
Rb		140.42	189.47	171.47			193.37	197.69	195.42	186.90
Sr		89.14	100.82	99.05			109.84	79.44	98.71	129.17
Y		4.60	6.72	5.26			5.88	6.43	8.08	8.48
Zr		26.22	106.40	87.63			87.89	90.66	121.43	53.17
Nb		6.34	2.97	2.74			3.11	3.76	3.36	7.48
Ba		626.45	395.31	393.88			411.94	343.97	373.91	837.87
La		19.43	14.37	12.97			13.58	15.47	14.71	34.40
Ce		35.69	45.80	43.68			42.84	43.79	44.22	55.77
Th		5.48	5.62	5.10			5.01	5.82	5.23	5.97
U		1.84	1.96	1.96			1.85	1.94	1.93	2.14

Figure 1

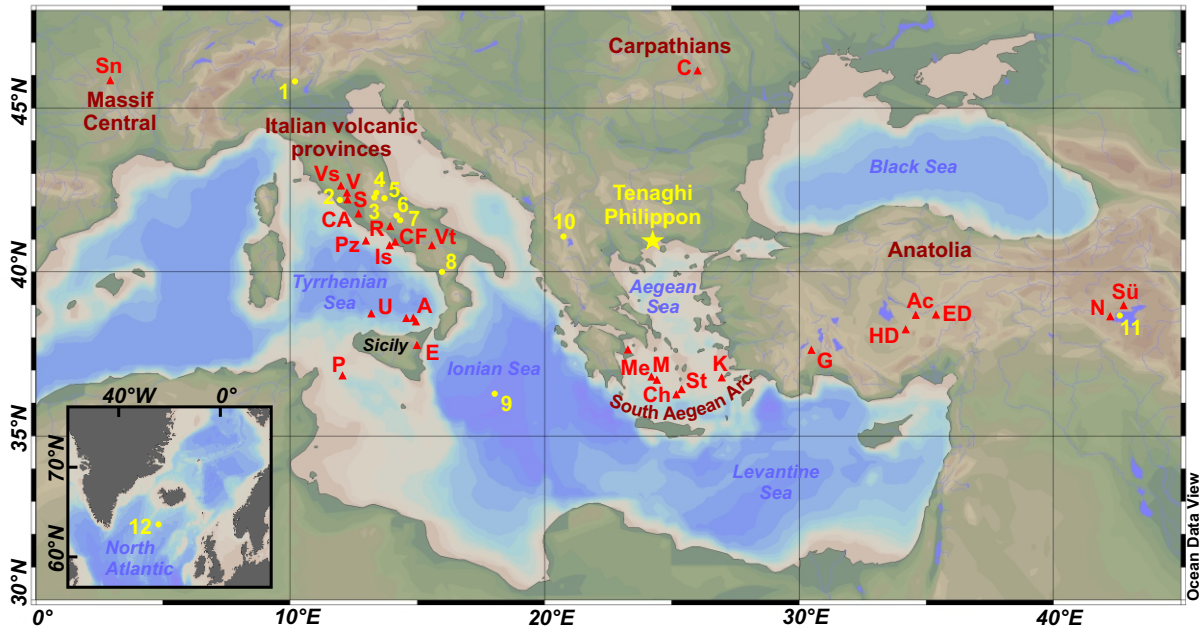
Sn
Massif Central
1
Italian volcanic provinces
Vs
V
S
CA
R
Pz
Is
CF
Vt
2
3
4
5
6
7
8
Tyrrhenian Sea
U
A
Sicily
E
P
9
Ionian Sea
10
Carpathians
C
Tenaghi Philippon
Aegean Sea
Me
M
Ch
St
K
South Aegean Arc
Black Sea
Anatolia
Ac
ED
HD
G
Sü
N
11
Levantine Sea
40°W
0°
70°N
60°N
12
North Atlantic
45°N
40°N
35°N
30°N
0°
10°E
20°E
30°E
40°E
Ocean Data View

Figure 2

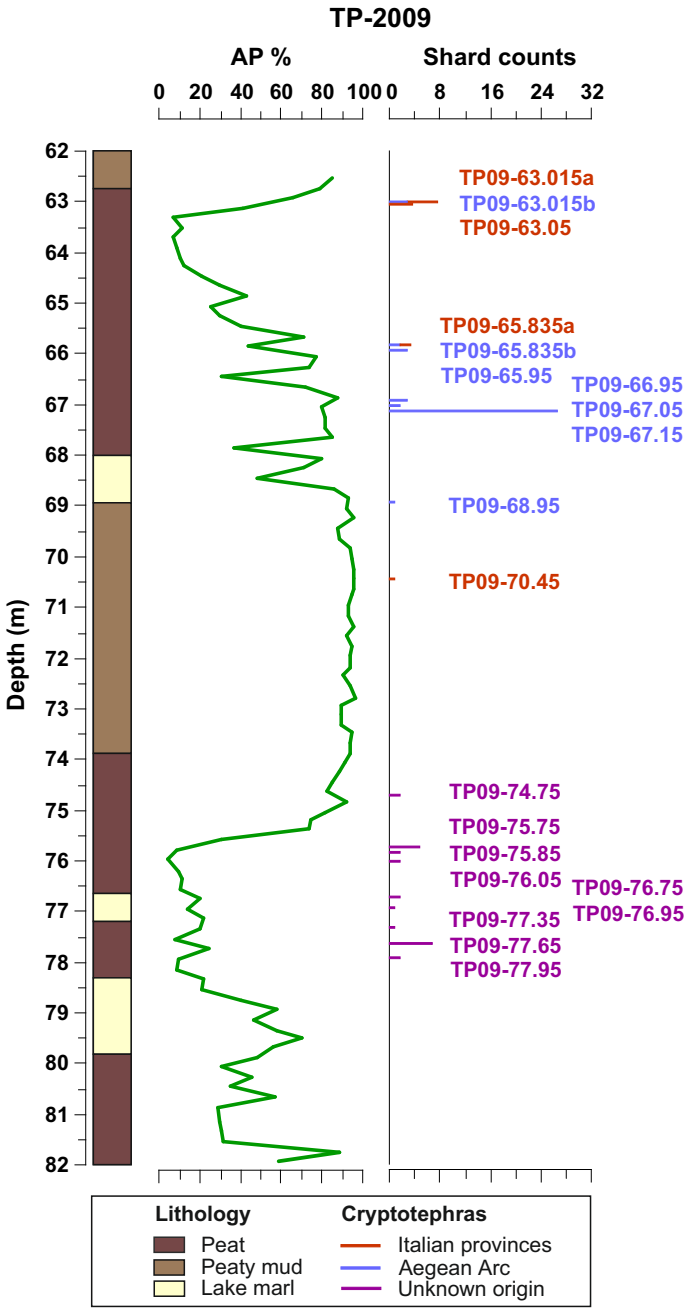
TP-2009
AP %
0 20 40 60 80 100
Shard counts
0 8 16 24 32
Depth (m)
62 63 64 65 66 67 68 69 70 71 72 73 74 75 76 77 78 79 80 81 82
TP09-63.015a
TP09-63.015b
TP09-63.05
TP09-65.835a
TP09-65.835b
TP09-65.95
TP09-66.95
TP09-67.05
TP09-67.15
TP09-68.95
TP09-70.45
TP09-74.75
TP09-75.75
TP09-75.85
TP09-76.05
TP09-76.75
TP09-76.95
TP09-77.35
TP09-77.65
TP09-77.95
Lithology
Peat
Peaty mud
Lake marl
Cryptotephras
Italian provinces
Aegean Arc
Unknown origin

Figure 3

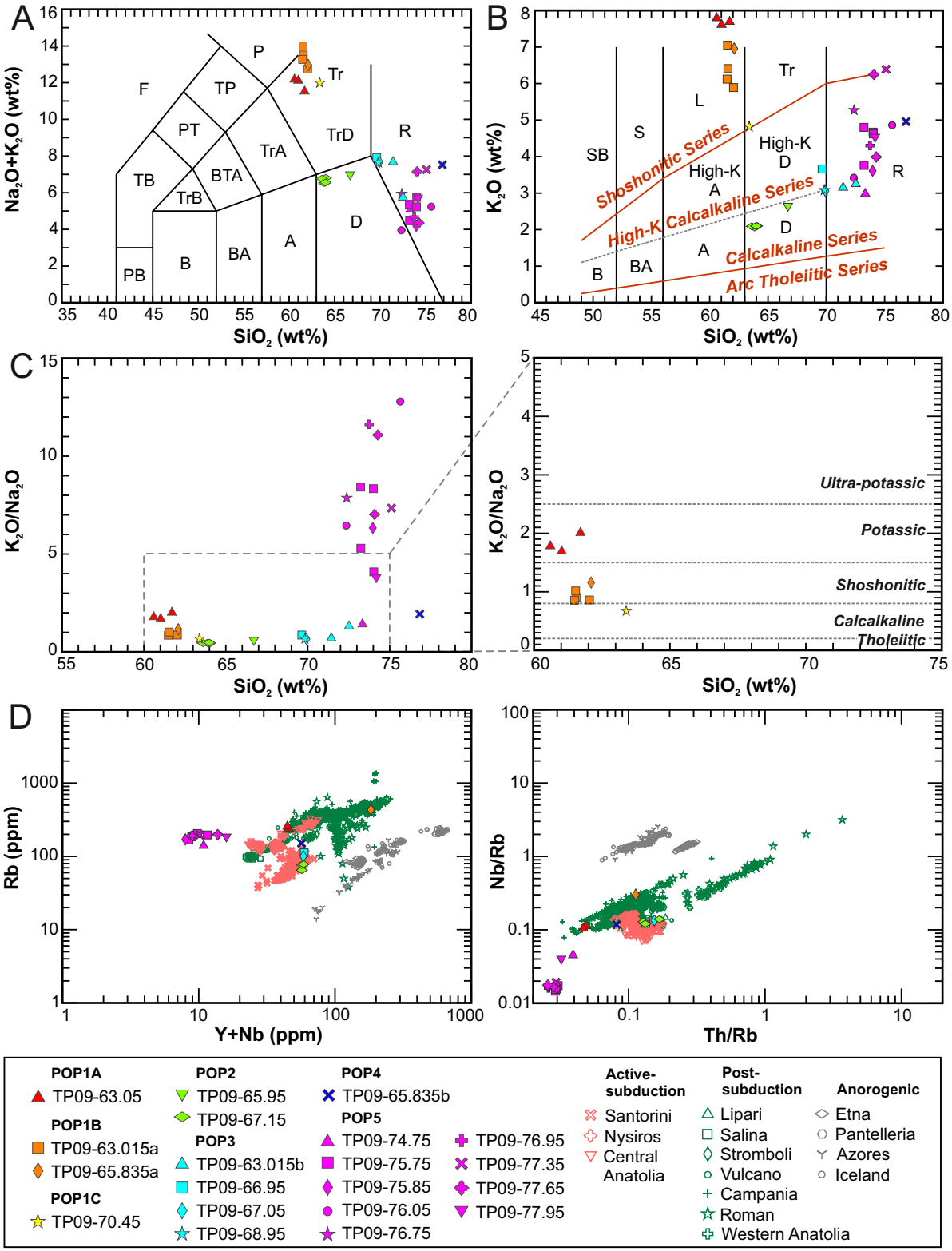
A
Na2O+K2O (wt%)
SiO2 (wt%)
F
P
TP
Tr
PT
TrA
TrD
R
TB
BTA
TrB
D
PB
B
BA
A
B
K2O (wt%)
SiO2 (wt%)
SB
S
L
Tr
High-K
D
R
Shoshonitic Series
High-K Calcalkaline Series
Calcalkaline Series
Arc Tholeiitic Series
High-K
A
D
A
B
BA
C
K2O/Na2O
SiO2 (wt%)
Ultra-potassic
Potassic
Shoshonitic
Calcalkaline
Tholeiitic
D
Rb (ppm)
Y+Nb (ppm)
Nb/Rb
Th/Rb
POP1A
TP09-63.05
POP1B
TP09-63.015a
TP09-65.835a
POP1C
TP09-70.45
POP2
TP09-65.95
TP09-67.15
POP3
TP09-63.015b
TP09-66.95
TP09-67.05
TP09-68.95
POP4
TP09-65.835b
POP5
TP09-74.75
TP09-75.75
TP09-75.85
TP09-76.05
TP09-76.75
TP09-76.95
TP09-77.35
TP09-77.65
TP09-77.95
Active-subduction
Santorini
Nysiros
Central Anatolia
Post-subduction
Lipari
Salina
Stromboli
Vulcano
Campania
Roman
Western Anatolia
Anorogenic
Etna
Pantelleria
Azores
Iceland

Figure 4

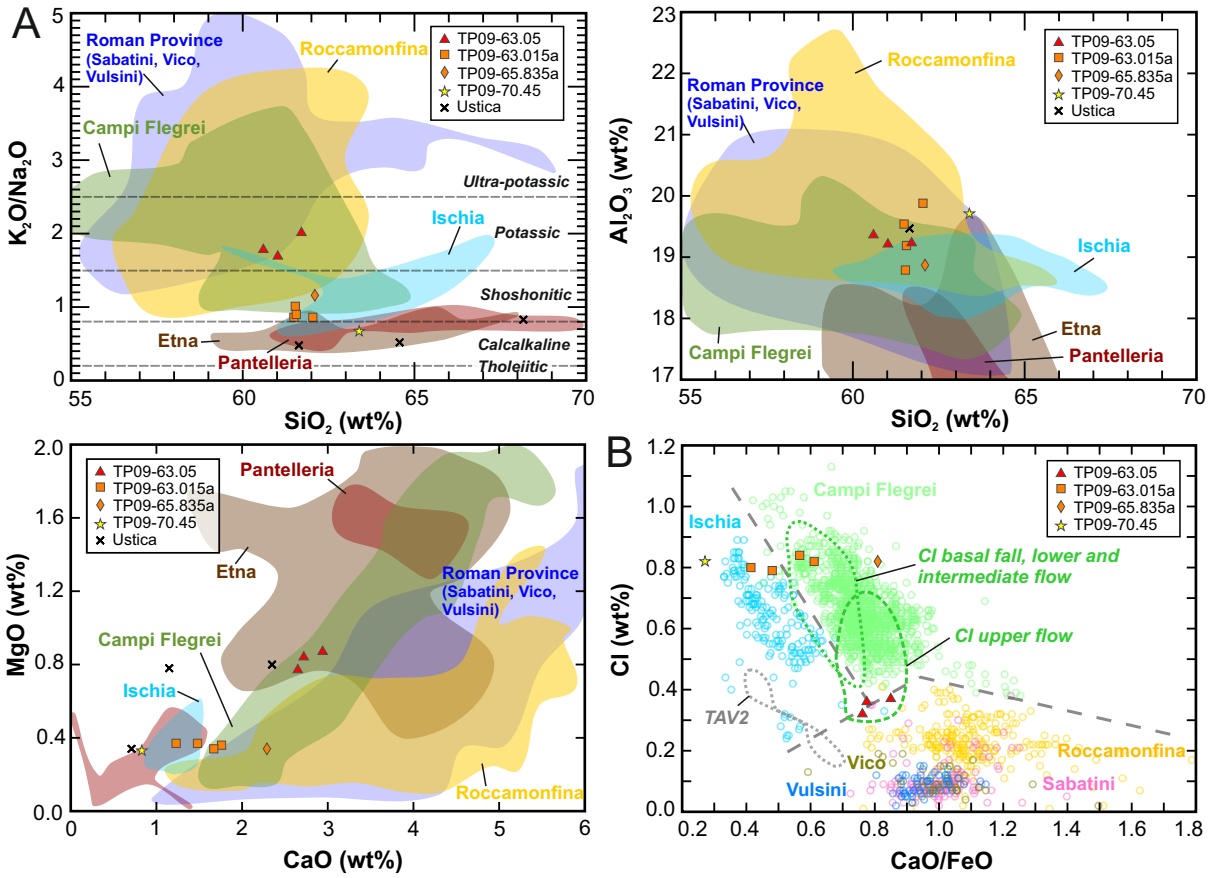
A
Roman Province (Sabatini, Vico, Vulsini)
Roccamonfina
Campi Flegrei
Ischia
Etna
Pantelleria
Ultra-potassic
Potassic
Shoshonitic
Calcalkaline
Tholeiitic
TP09-63.05
TP09-63.015a
TP09-65.835a
TP09-70.45
Ustica
K2O/Na2O
SiO2 (wt%)
Al2O3 (wt%)
MgO (wt%)
CaO (wt%)
B
Cl (wt%)
CaO/FeO
Cl basal fall, lower and intermediate flow
Cl upper flow
TAV2
Vico
Vulsini
Sabatini

Figure 5

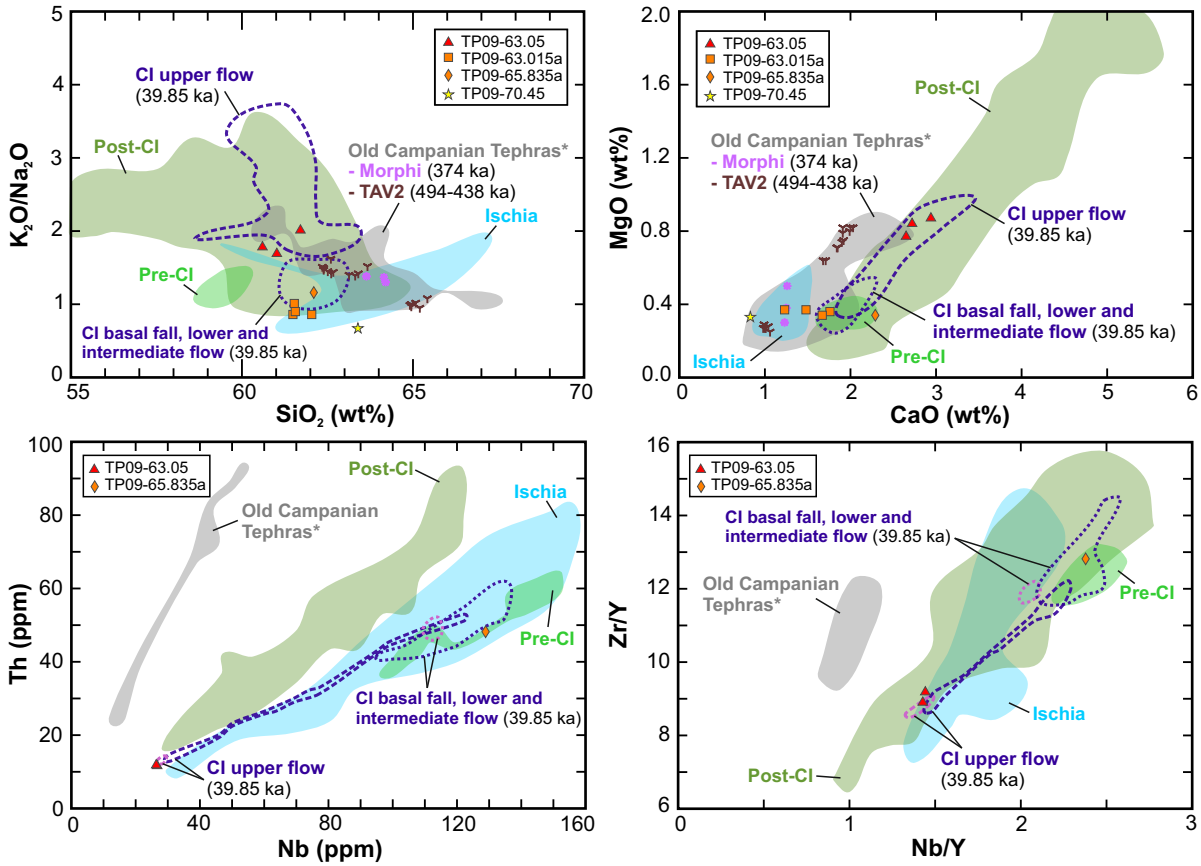
TP09-63.05
TP09-63.015a
TP09-65.835a
TP09-70.45
CI upper flow
(39.85 ka)
Post-CI
Old Campanian Tephras*
- Morphi (374 ka)
- TAV2 (494-438 ka)
Ischia
Pre-CI
CI basal fall, lower and
intermediate flow (39.85 ka)
K2O/Na2O
SiO2 (wt%)
MgO (wt%)
CaO (wt%)
Th (ppm)
Nb (ppm)
Zr/Y
Nb/Y

Figure 6

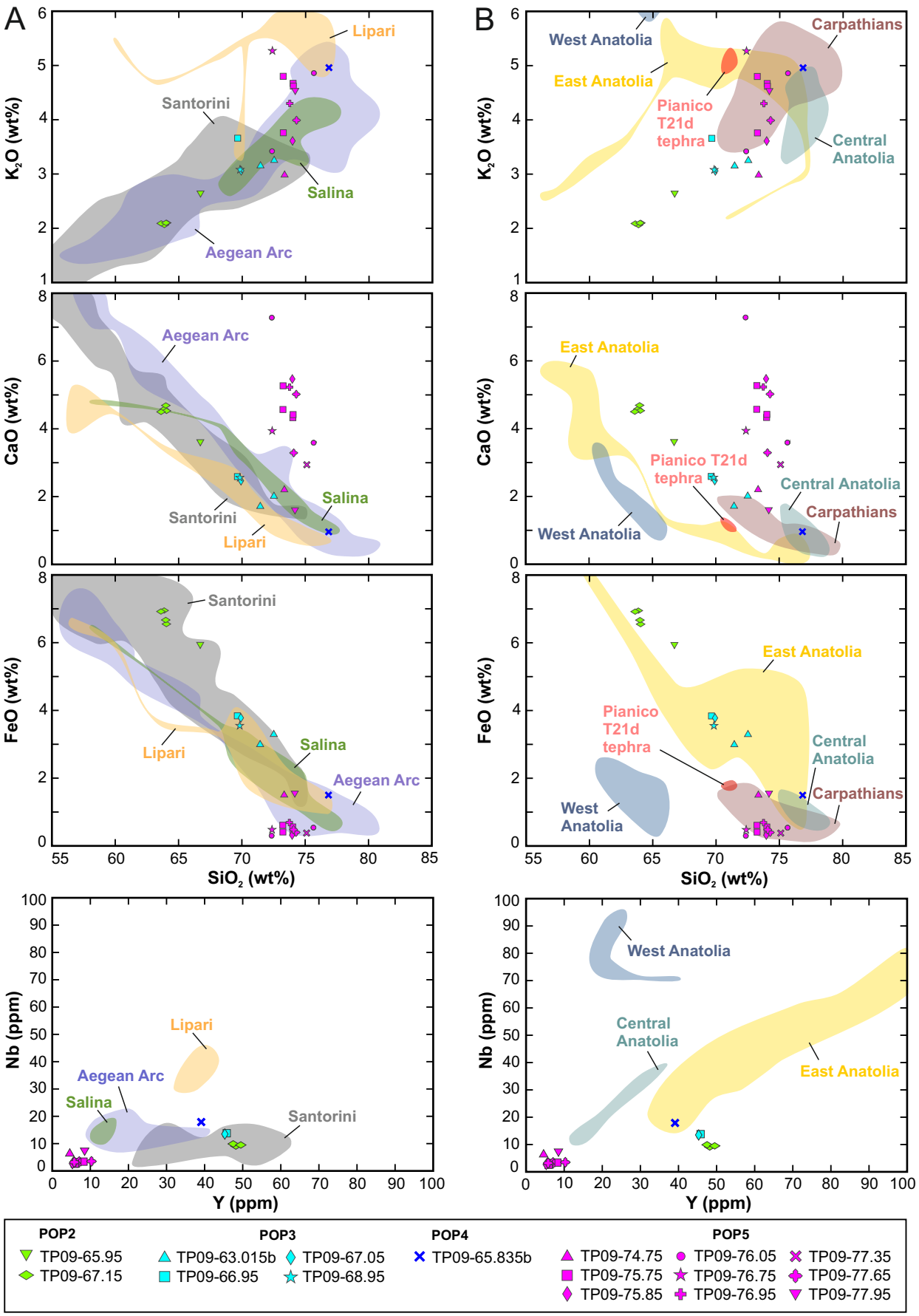
A
B
K2O (wt%)
CaO (wt%)
FeO (wt%)
SiO2 (wt%)
Nb (ppm)
Y (ppm)
Lipari
Santorini
Salina
Aegean Arc
West Anatolia
East Anatolia
Carpathians
Central Anatolia
Pianico T21d tephra
POP2
TP09-65.95
TP09-67.15
POP3
TP09-63.015b
TP09-66.95
TP09-67.05
TP09-68.95
POP4
TP09-65.835b
POP5
TP09-74.75
TP09-75.75
TP09-75.85
TP09-76.05
TP09-76.75
TP09-76.95
TP09-77.35
TP09-77.65
TP09-77.95

Figure 7

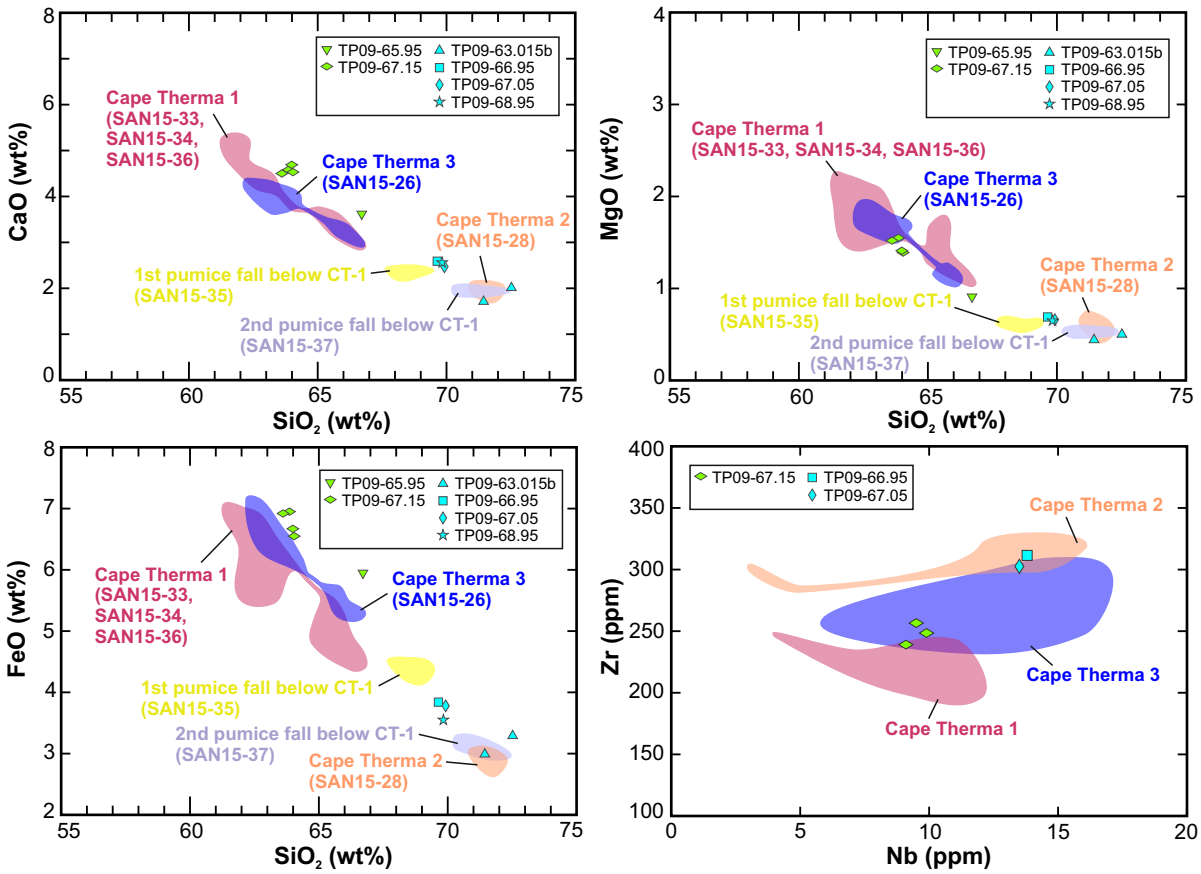
TP09-65.95
TP09-63.015b
TP09-67.15
TP09-66.95
TP09-67.05
TP09-68.95
Cape Therma 1
(SAN15-33,
SAN15-34,
SAN15-36)
Cape Therma 3
(SAN15-26)
Cape Therma 2
(SAN15-28)
1st pumice fall below CT-1
(SAN15-35)
2nd pumice fall below CT-1
(SAN15-37)
CaO (wt%)
MgO (wt%)
FeO (wt%)
Zr (ppm)
SiO2 (wt%)
Nb (ppm)

Figure 8

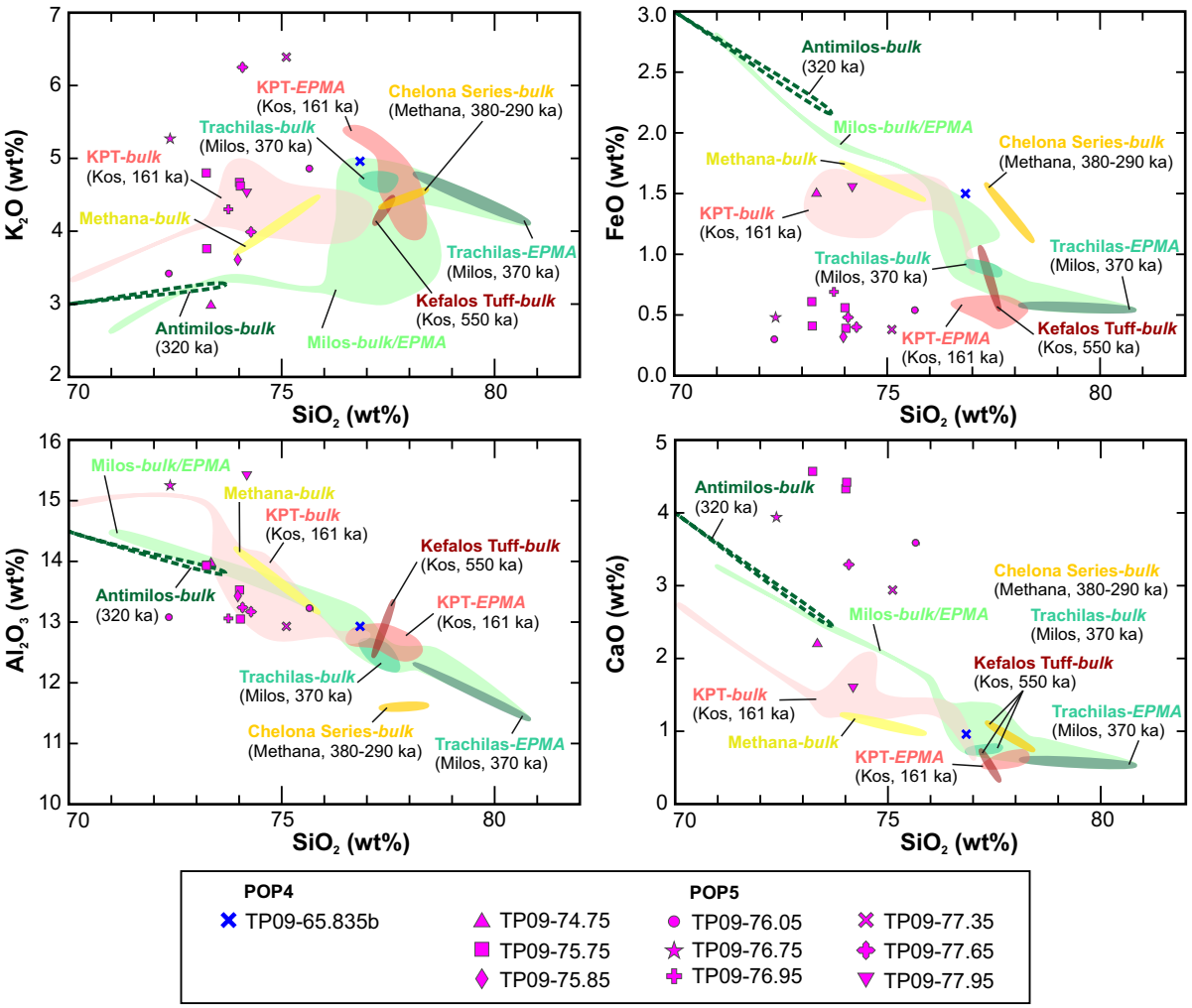
K2O (wt%)
SiO2 (wt%)
KPT-EPMA (Kos, 161 ka)
Chelona Series-bulk (Methana, 380-290 ka)
Trachilas-bulk (Milos, 370 ka)
KPT-bulk (Kos, 161 ka)
Methana-bulk
Trachilas-EPMA (Milos, 370 ka)
Kefalos Tuff-bulk (Kos, 550 ka)
Antimilos-bulk (320 ka)
Milos-bulk/EPMA
FeO (wt%)
Al2O3 (wt%)
CaO (wt%)
POP4
TP09-65.835b
TP09-74.75
TP09-75.75
TP09-75.85
POP5
TP09-76.05
TP09-76.75
TP09-76.95
TP09-77.35
TP09-77.65
TP09-77.95

Figure 9

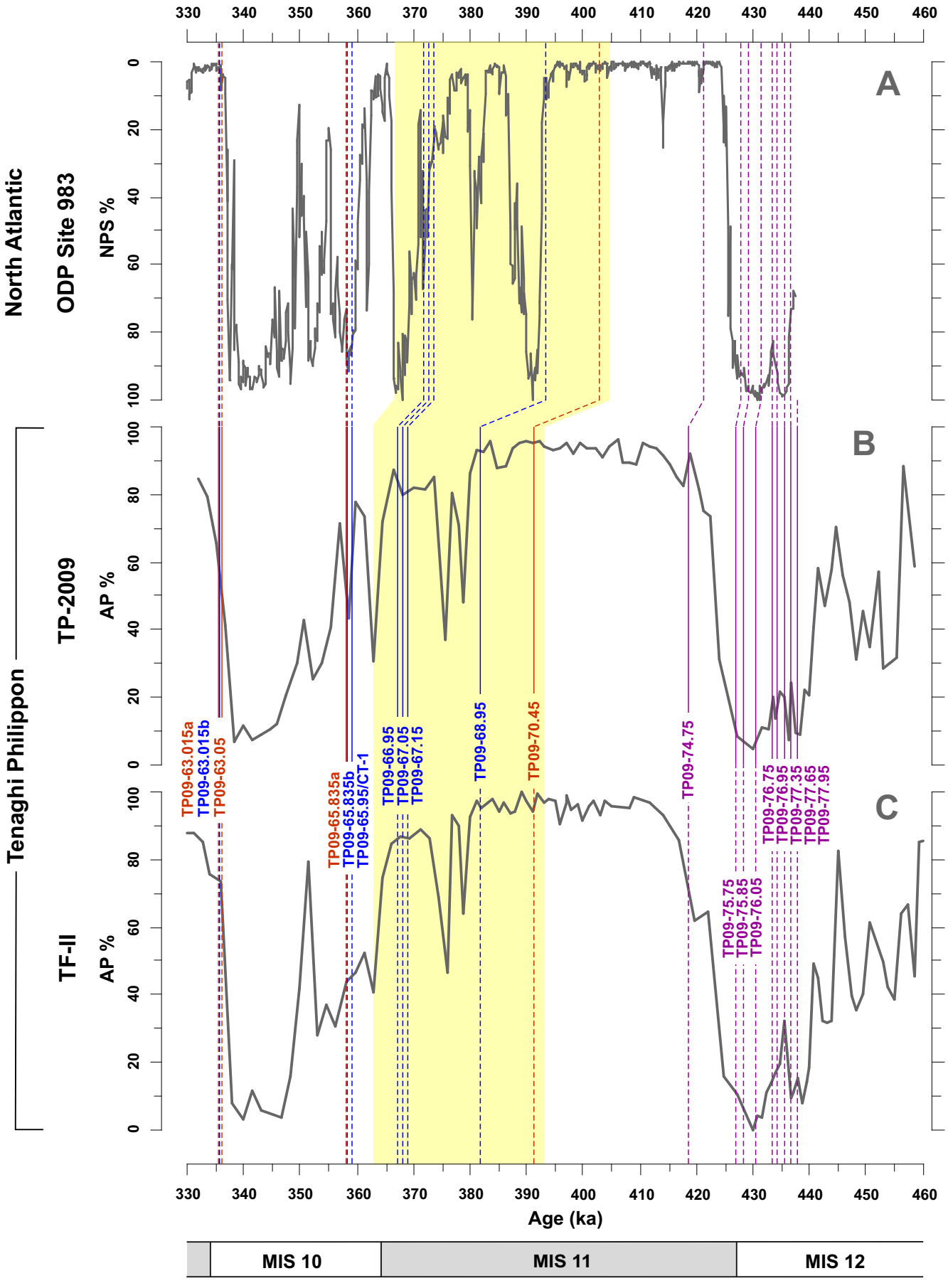
North Atlantic
ODP Site 983
NPS %
A
Tenaghi Philippon
TP-2009
AP %
B
TF-II
AP %
C
TP09-63.015a
TP09-63.015b
TP09-63.05
TP09-65.835a
TP09-65.835b
TP09-65.95/CT-1
TP09-66.95
TP09-67.05
TP09-67.15
TP09-68.95
TP09-70.45
TP09-74.75
TP09-75.75
TP09-75.85
TP09-76.05
TP09-76.75
TP09-76.95
TP09-77.35
TP09-77.65
TP09-77.95
330 340 350 360 370 380 390 400 410 420 430 440 450 460
Age (ka)
MIS 10
MIS 11
MIS 12

Figure 10

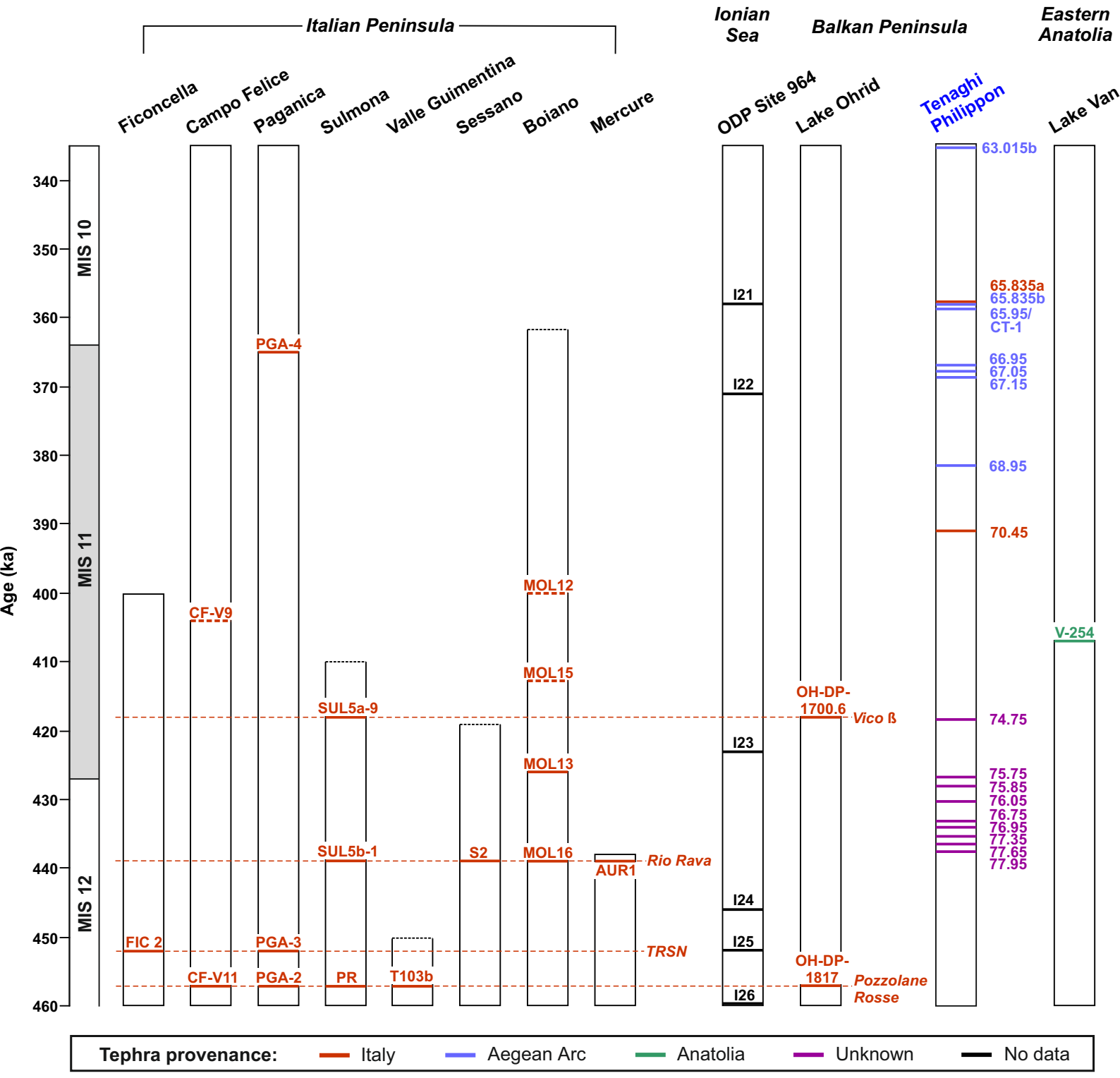
Italian Peninsula
Ionian Sea
Balkan Peninsula
Eastern Anatolia
Ficoncella
Campo Felice
Paganica
Sulmona
Valle Guimentina
Sessano
Boiano
Mercure
ODP Site 964
Lake Ohrid
Tenaghi Philippon
Lake Van
Age (ka)
340
350
360
370
380
390
400
410
420
430
440
450
460
MIS 10
MIS 11
MIS 12
PGA-4
CF-V9
MOL12
MOL15
SUL5a-9
MOL13
SUL5b-1
S2
MOL16
AUR1
Rio Rava
FIC 2
PGA-3
TRSN
CF-V11
PGA-2
PR
T103b
I21
I22
I23
I24
I25
I26
OH-DP-1700.6
Vico ß
OH-DP-1817
Pozzolane Rosse
63.015b
65.835a
65.835b
65.95/ CT-1
66.95
67.05
67.15
68.95
70.45
74.75
75.75
75.85
76.05
76.75
76.95
77.35
77.65
77.95
V-254
Tephra provenance:
Italy
Aegean Arc
Anatolia
Unknown
No data

Supplement 1

1. Peatlands as tephrostratigraphic archives

Peatland settings are ideally suited to preserve inorganic solids supplied by atmospheric deposition such as tephra fallout because of their low-energy depositional environment with negligible erosional processes and bioturbation (Davies, 2015; Watson et al., 2015). Moreover, extraction and detection of cryptotephras is more straightforward in peat than in sediments dominated by inorganic components as they typically prevail in lacustrine and marine settings (e.g., Gehrels et al., 2008). In addition, post-depositional tephra movement in peatlands related to gravitational sinking, rainfall percolation as well as fluctuations of the water table is generally minor and has little effect on the actual stratigraphic position of a tephra layer (Payne and Gehrels, 2010). However, in the case of thick visible tephra layers, both up- and downcore tephra movement in peat can occur over longer distances (Wulf et al., 2018).

2. Material and methods

Proximal correlative tephra samples from Santorini

Deposits of the Cape Therma 3 (c. 224–184 ka; Druitt et al., 1999; Gertisser et al., 2009; sample SAN15-26) and Cape Therma 1 (≤360 ka; Druitt et al., 1999; samples SAN15-33, -34, -36) eruptions were sampled from the caldera wall at Cape Plaka, whereas deposits of the Cape Therma 2 eruption (c. 224 ka; Druitt et al., 1999; sample SAN15-28) were sampled from a road cut near Athinios harbor (Table S1-2; Fig. S1-1). In addition, two samples from white pumice fall deposits that stratigraphically underlie the Cape Therma 1 deposits and derive from two different, yet unknown older Santorini eruptions (SAN15-35 and SAN15-37) were also collected in the area.

Tephra extraction and processing

To remove organic matter, samples were oven-dried for 12–24 hours at 105 °C and subsequently combusted in a muffle furnace for 4 hours at 550 °C. The weight differences between wet, dry and ashed samples were measured to calculate water and organic matter contents. The ash residues were immersed in ~15% H_2O_2 overnight to remove remaining traces of organic matter. Carbonate material was dissolved by immersion in ~7.5–10% HCl. Samples were sieved through 20 and 100 µm nylon meshs to isolate the 20–100 µm grain-size fraction. Density separation of the 20–100 µm fraction was performed with sodium polytungstate following the protocol of Turney (1998). The material was separated into two density fractions (<2.55 g/cm^3 and >2.55 g/cm^3) using the heavy liquid sodium polytungstate, and the lighter fraction was transferred into rectangular plastic lids to be examined for tephra components under a light microscope at 100x magnification. Identified glass shards were handpicked with a single-hair brush into an aluminum stub, mounted in Epofix™ resin, and subsequently sectioned and polished to allow geochemical analysis.

Pollen analysis

Palynological processing comprised sediment freeze-drying, weighing, spiking with Lycopodium marker spores, treatment with HCl (10%), NaOH (10%) and HF (when necessary; 40%), heavy-liquid separation with Na_2WO_4 x $2H_2O$ (when necessary), acetolysis, sieving through a 7 µm mesh, and slide preparation using glycerin jelly. Slides were analysed under an Imager.A2 Zeiss light microscope at 400x and 1000x magnification.

Table S1-1: Tie points for the tuning of the arboreal pollen record from core TP-2009 to that from the old Tenaghi Philippon core (TF-II; Van der Wiel and Wijmstra, 1987; Wijmstra and Smit, 1976) using the orbitally tuned age model of Tzedakis et al. (2006).

TP-2009 Depth (m)	TF-II Age (ka)
63.14	336.87
64.64	349.08
66.60	364.04
67.98	376.61
68.57	379.41
75.53	423.42
75.96	430.02
76.66	433.07
78.71	440.42
79.84	446.69
80.78	452.88
81.65	455.79
81.91	458.15

3. Sampling sites for proximal tephra samples on Santorini

Table S1-2: Details of pumice-fall sampling sites on Santorini.

Sample ID	Unit	Latitude	Longitude
SAN15-26	Cape Therma 3, basal pumice fall (Cape Plaka)	36°22'35.8" N	25°25'26.5" E
SAN15-28	Cape Therma 2, white pumice fall (street to Athinios harbour)	36°23'22.8" N	25°26'05.0" E
SAN15-33	Cape Therma 1, black non-lithified ignimbrite (Cape Plaka)	36°22'35.9" N	25°25'30.2" E
SAN15-34	Cape Therma 1, basal pumice fall, pinkish scoriae and strongly altered white pumices, base rich in lithics (Cape Plaka)	36°22'35.9" N	25°25'30.2" E
SAN15-35	white pumice fall (40-60 cm), ca. 6 m below Cape Therma 1 (Cape Plaka)	36°22'36.3" N	25°25'30.0" E
SAN15-36	Cape Therma 1, basal pink pumice fallout (Cape Plaka)	36°22'36.8" N	25°25'27.5" E
SAN15-37	white pumice fallout (20-30 cm), ca. 21 m below Cape Therma 1 (Cape Plaka)	36°22'37.6" N	25°25'24.8" E

Figure S1-1: Photoaereal map of sampling locations of pyroclastic fall deposits on Santorini.

Figure S1-2: Stratigraphic position of pumice and scoriae fall deposits sampled on Santorini. For details see Table S1-2.

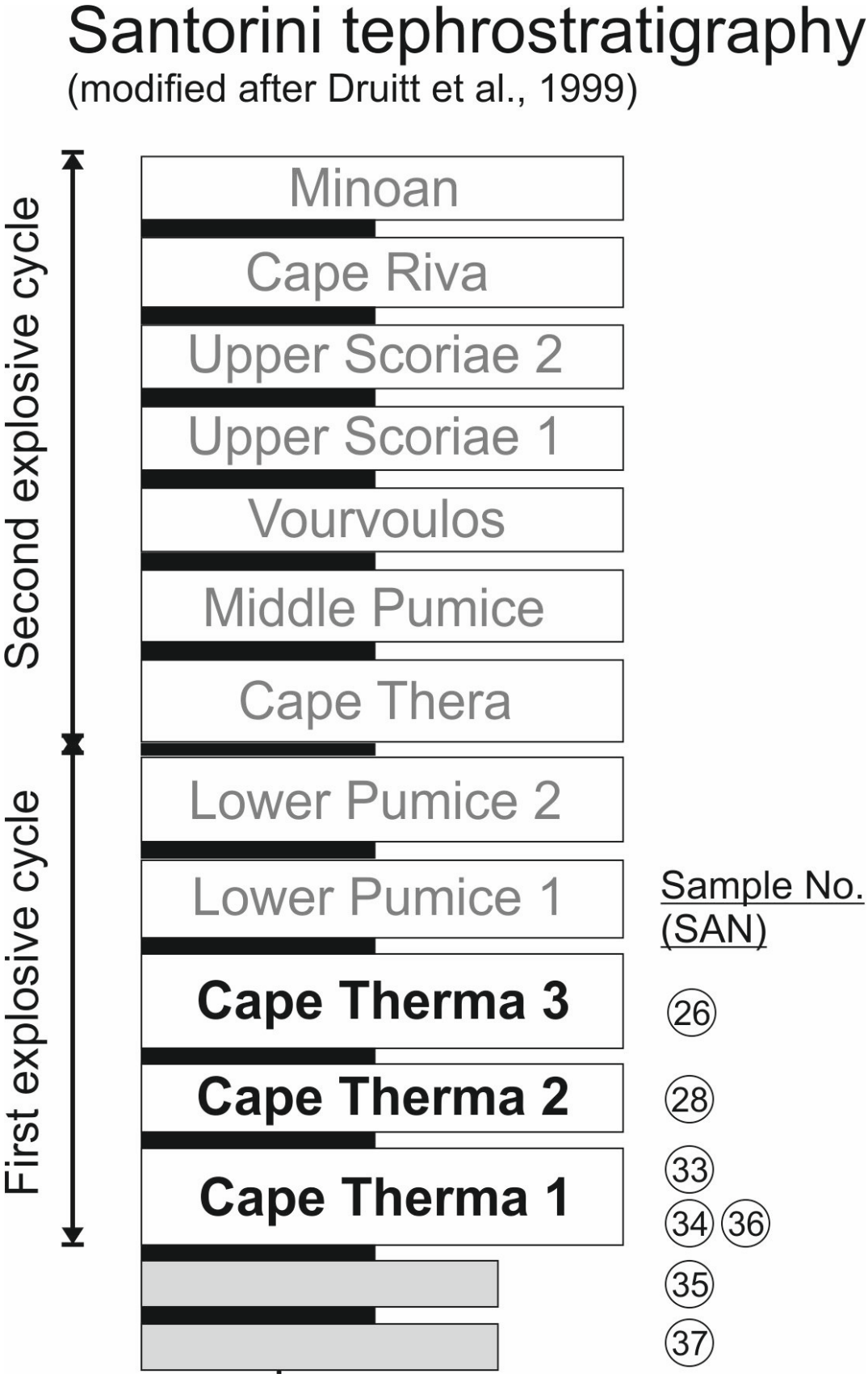

4. Glass shard micrographs

TP09-63.015a

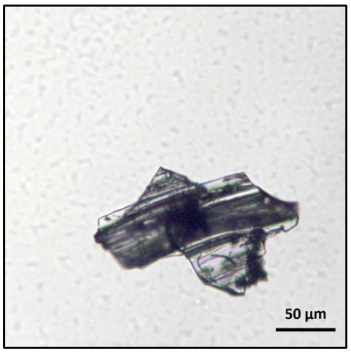

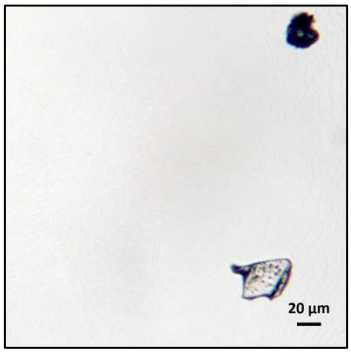

TP09-63.015b

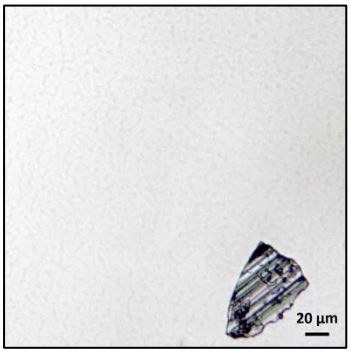

TP09-63.05

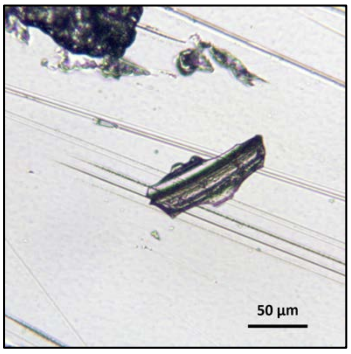

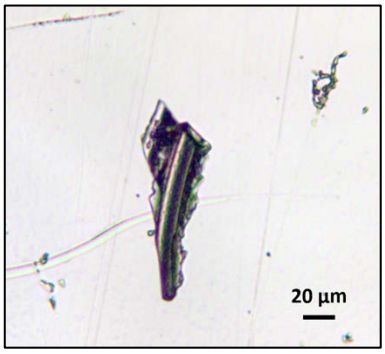

TP09-65.95

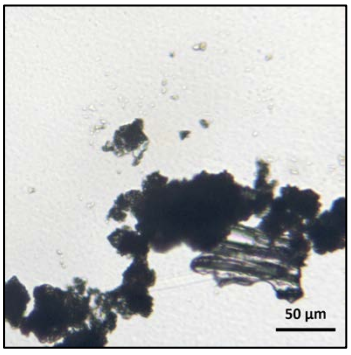

TP09-66.95

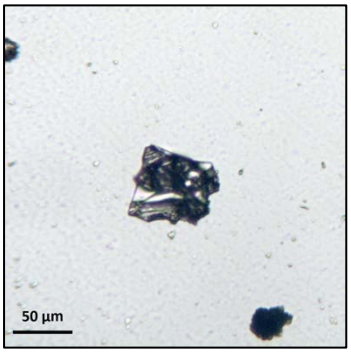

TP09-67.15

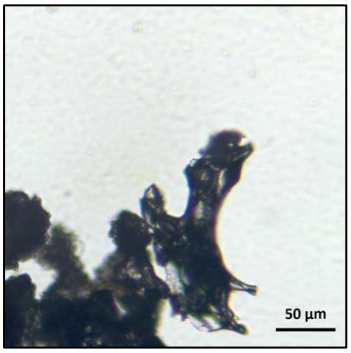

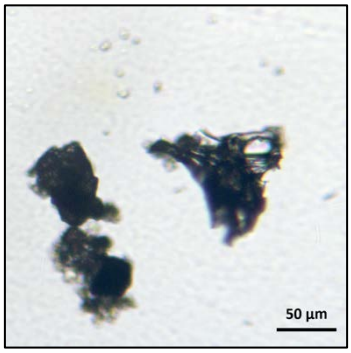

TP09-74.75

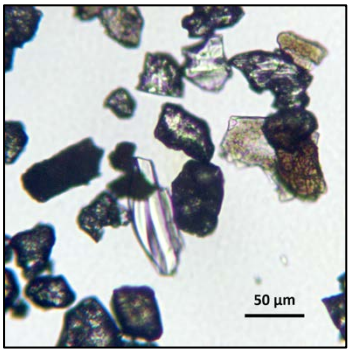

TP09-75.75

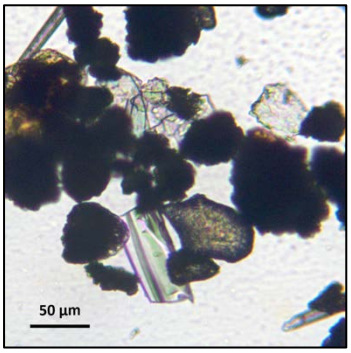

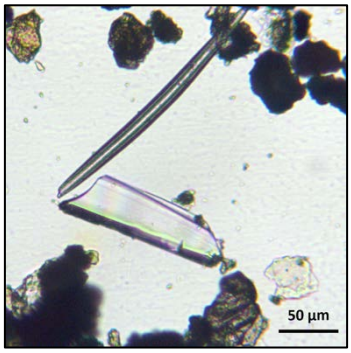

TP09-75.85

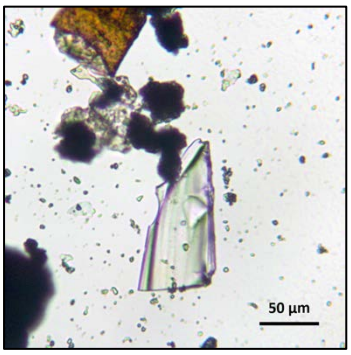

TP09-76.95

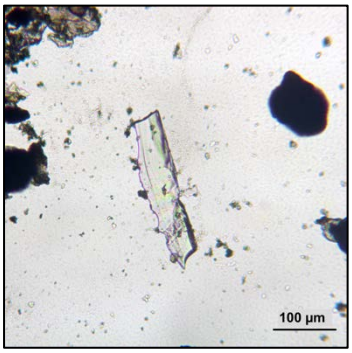

TP09-77.65

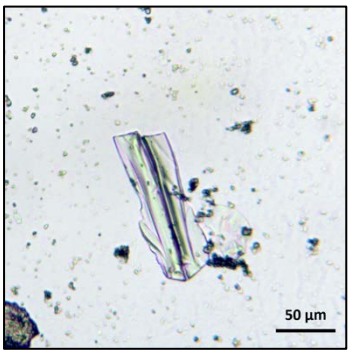

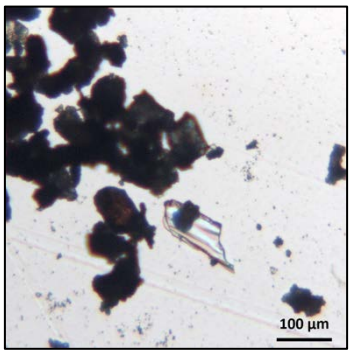

TP09-77.95

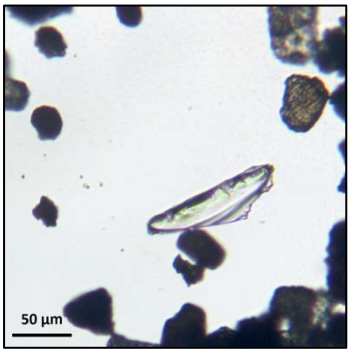

References

Davies, S.M., 2015. Cryptotephras: the revolution in correlation and precision dating. Journal of Quaternary Science 30, 114-130.

Druitt, T.H., Edwards, L., Mellors, R.M., Pyle, D.M., Sparks, R.S.J., Lanphere, M., Davies, M., Barreirio, B., 1999. Santorini Volcano. Geological Society, London, Memoirs 19.

Gehrels, M.J., Newnham, R.M., Lowe, D.J., Wynne, S., Hazell, Z.J., Caseldine, C., 2008. Towards rapid assay of cryptotephra in peat cores: Review and evaluation of various methods. Quaternary International 178, 68-84.

Gertisser, R., Preece, K., Keller, J., 2009. The Plinian Lower Pumice 2 eruption, Santorini, Greece: Magma evolution and volatile behaviour. Journal of Volcanology and Geothermal Research 186, 387-406.

Payne, R., Gehrels, M., 2010. The formation of tephra layers in peatlands: An experimental approach. Catena 81, 12-23.

Turney, C.S.M., 1998. Extraction of rhyolitic component of Vedde microtephra from minerogenic lake sediments. Journal of Paleolimnology 19, 199-206.

Tzedakis, P.C., Hooghiemstra, H., Pälike, H., 2006. The last 1.35 million years at Tenaghi Philippon: revised chronostratigraphy and long-term vegetation trends. Quaternary Science Reviews 25, 3416-3430.

Van der Wiel, A.M., Wijmstra, T.A., 1987. Palynology of the lower part (78–120 m) of the core Tenaghi Philippon II, Middle Pleistocene of Macedonia, Greece. Review of Palaeobotany and Palynology 52, 73-88.

Watson, E.J., Swindles, G.T., Lawson, I.T., Savov, I.P., 2015. Spatial variability of tephra and carbon accumulation in a Holocene peatland. Quaternary Science Reviews 124, 248-264.

Wijmstra, T., Smit, A., 1976. Palynology of the middle part (30–78 metres) of the 120 m deep section in northern Greece (Macedonia). Acta Botanica Neerlandica 25, 297-312.

Wulf, S., Hardiman, M., Staff, R.A., Koutsodendris, A., Appelt, O., Blockley, S.P.E., Lowe, J.J., Manning, C.J., Ottolini, L., Schmitt, A.K., Smith, V.C., Tomlinson, E.L., Vakhrameeva, P., Knipping, M., Kotthoff, U., Milner, A.M., Müller, U.C., Christanis, K., Kalaitzidis, S., Tzedakis, C., Schmiedl, G., Pross, J., 2018. The marine isotope stage 1–5 cryptotephra record of Tenaghi Philippon, Greece: Towards a detailed tephrostratigraphic framework for the Eastern Mediterranean region. Quaternary Science Reviews 186, 236–262.

Supplement 4

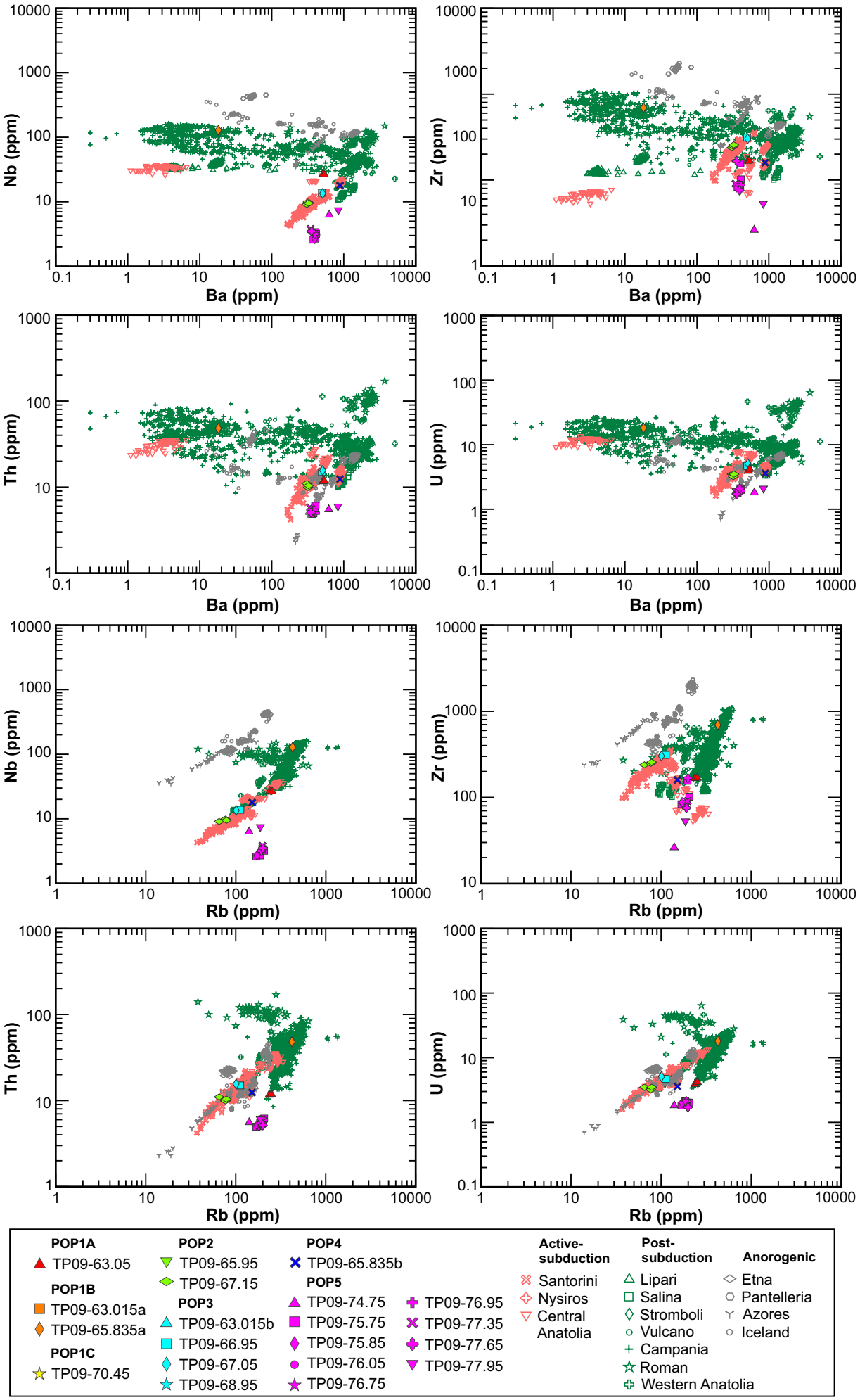

Figure S4-1: Complementary trace-element plots to Fig. 3 in the text.

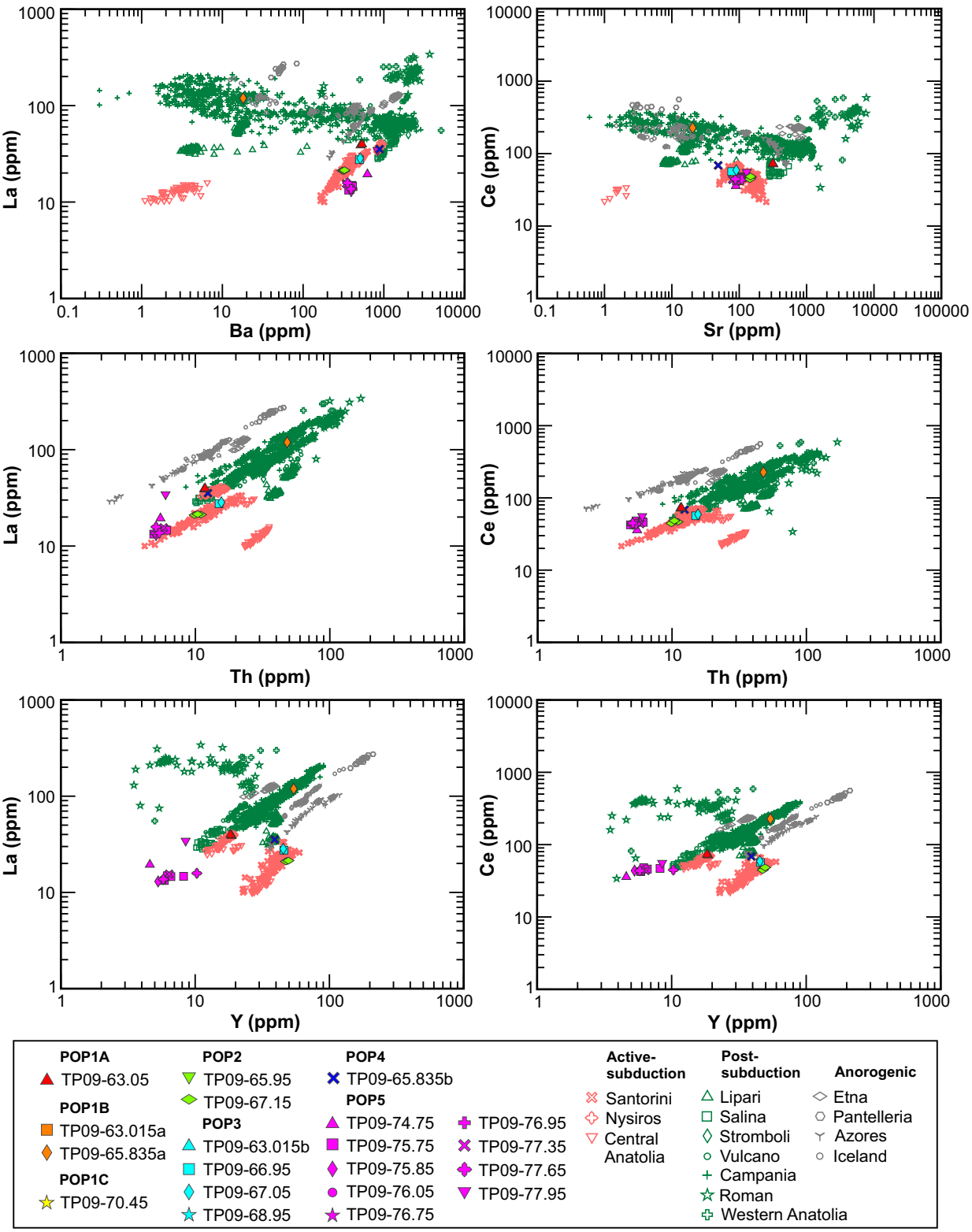

Figure S4-1: *(continued)*.

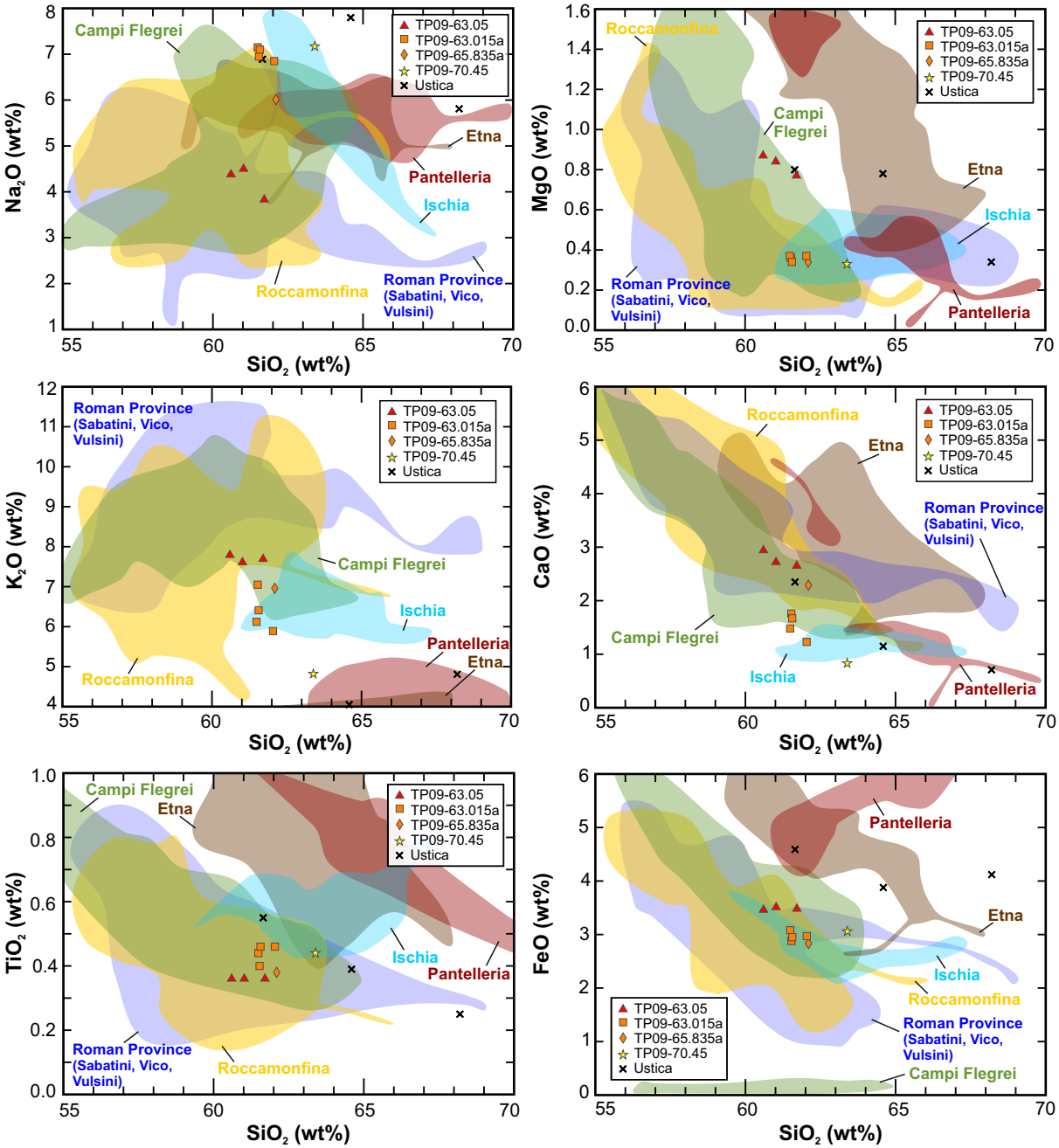

Figure S4-2: Complementary major-element plots to Fig. 4 in the text.

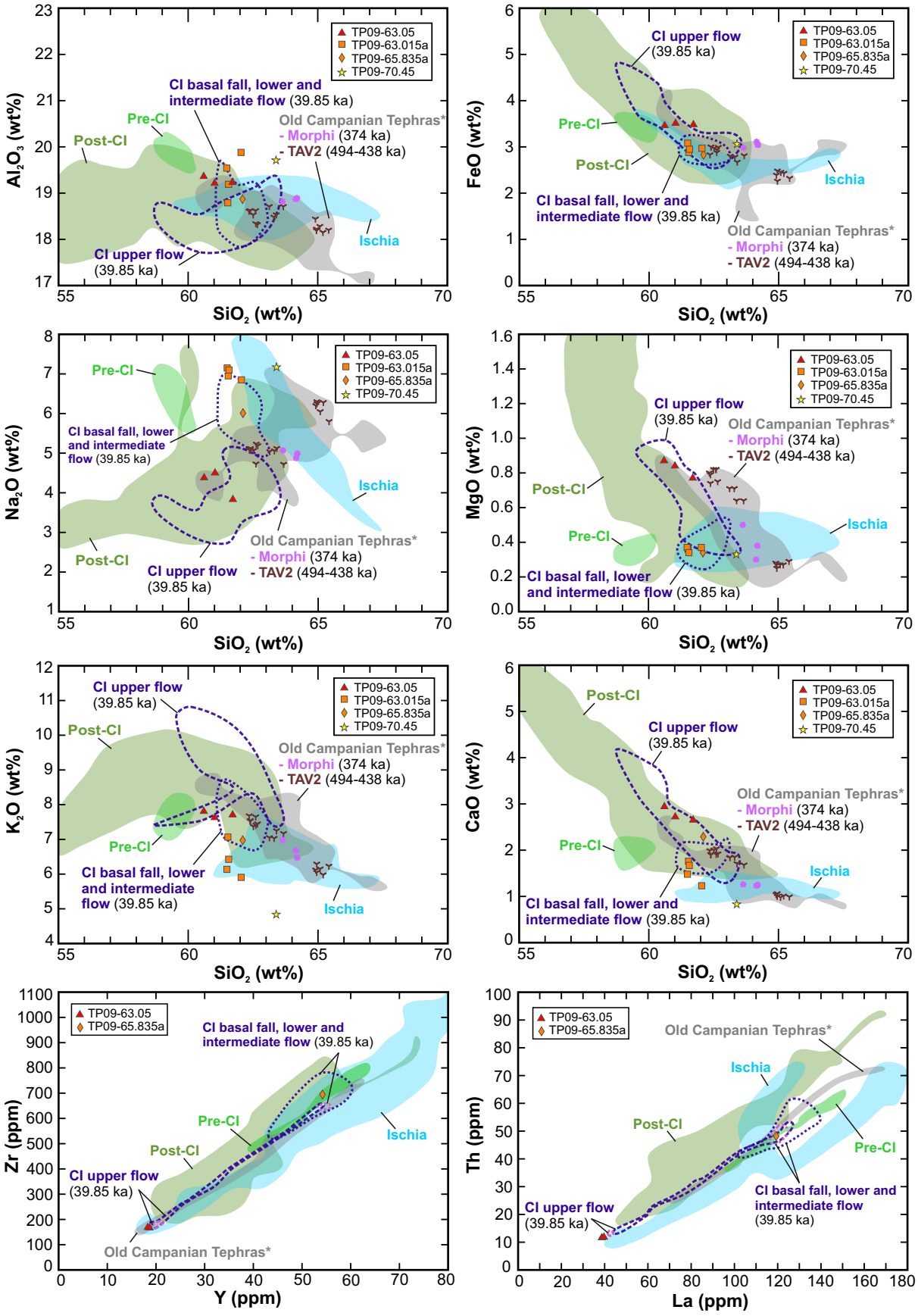

Figure S4-3: Complementary major- and trace-element plots to Fig. 5 in the text.

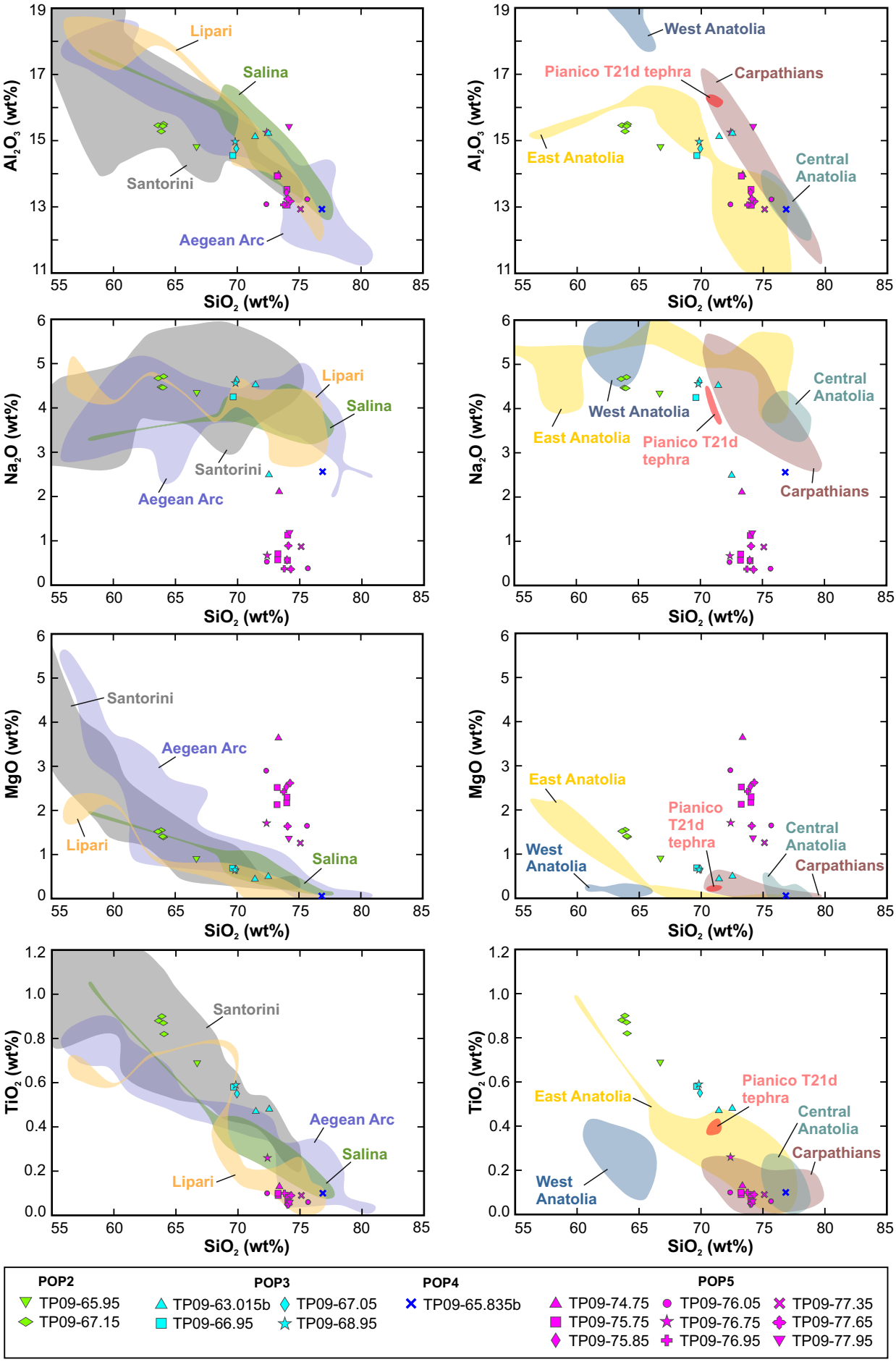

Figure S4-4: Complementary major- and trace-element plots to Fig. 6 in the text.

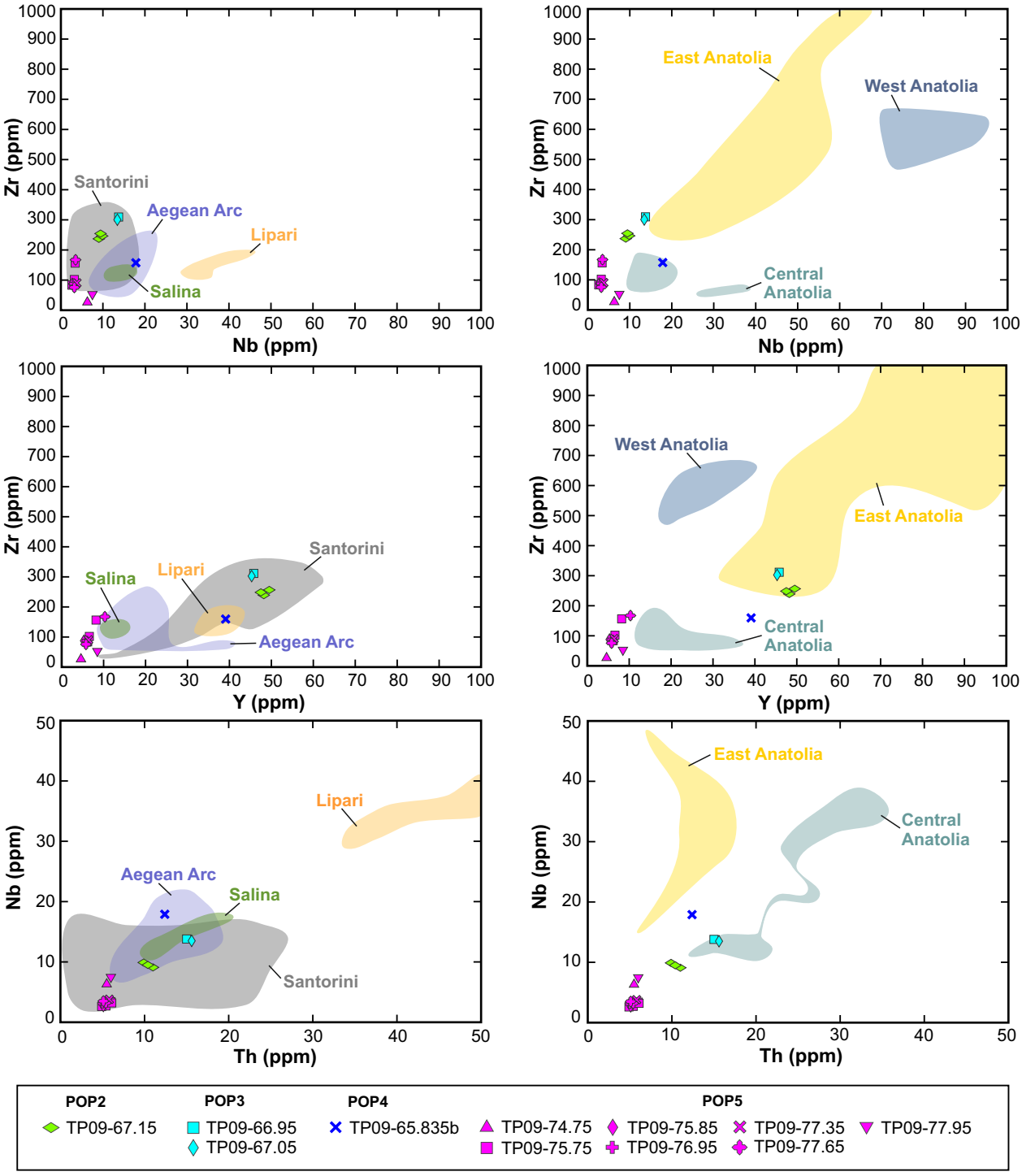

Figure S4-4: (*continued*).

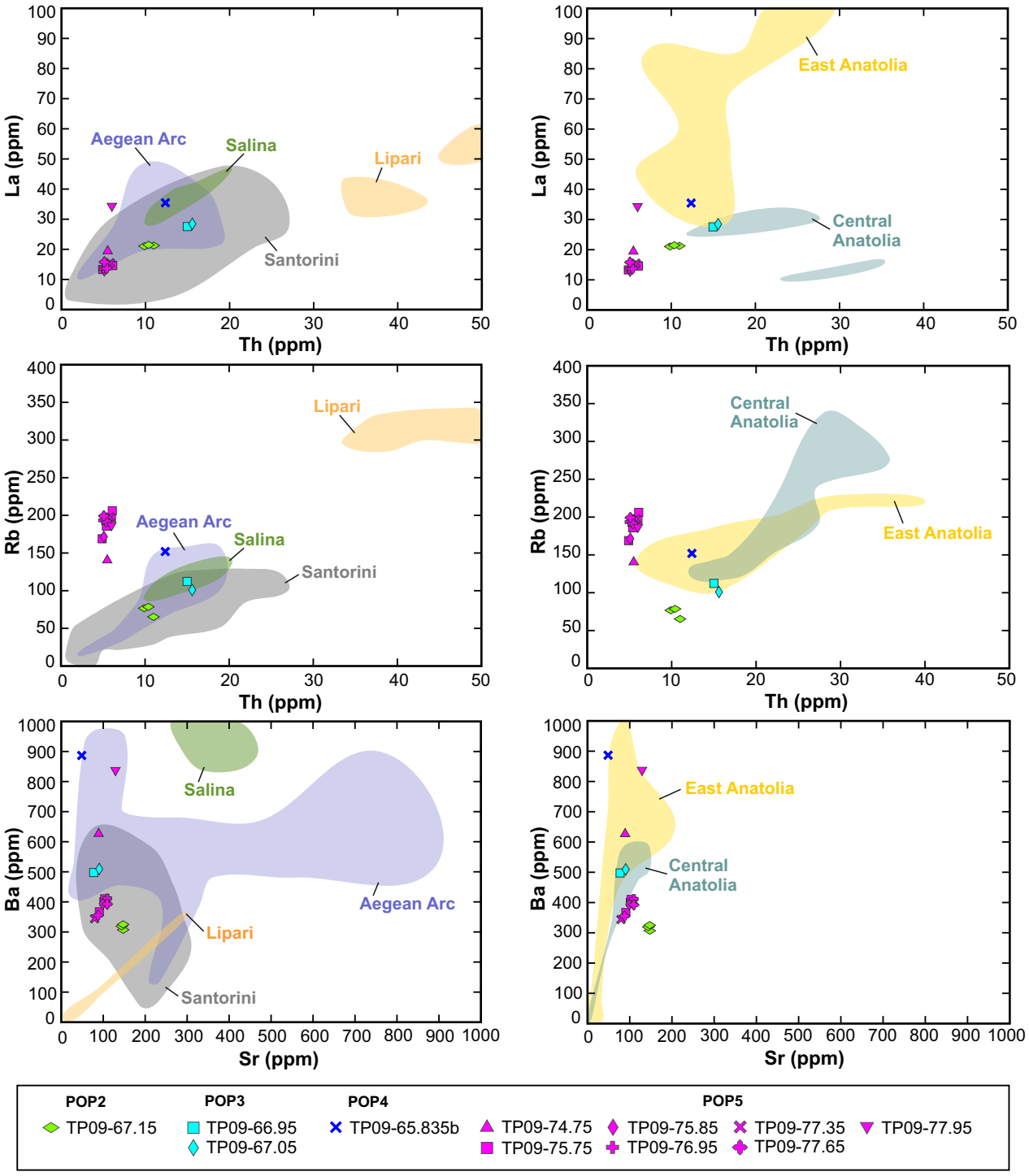

Figure S4-4: (*continued*).

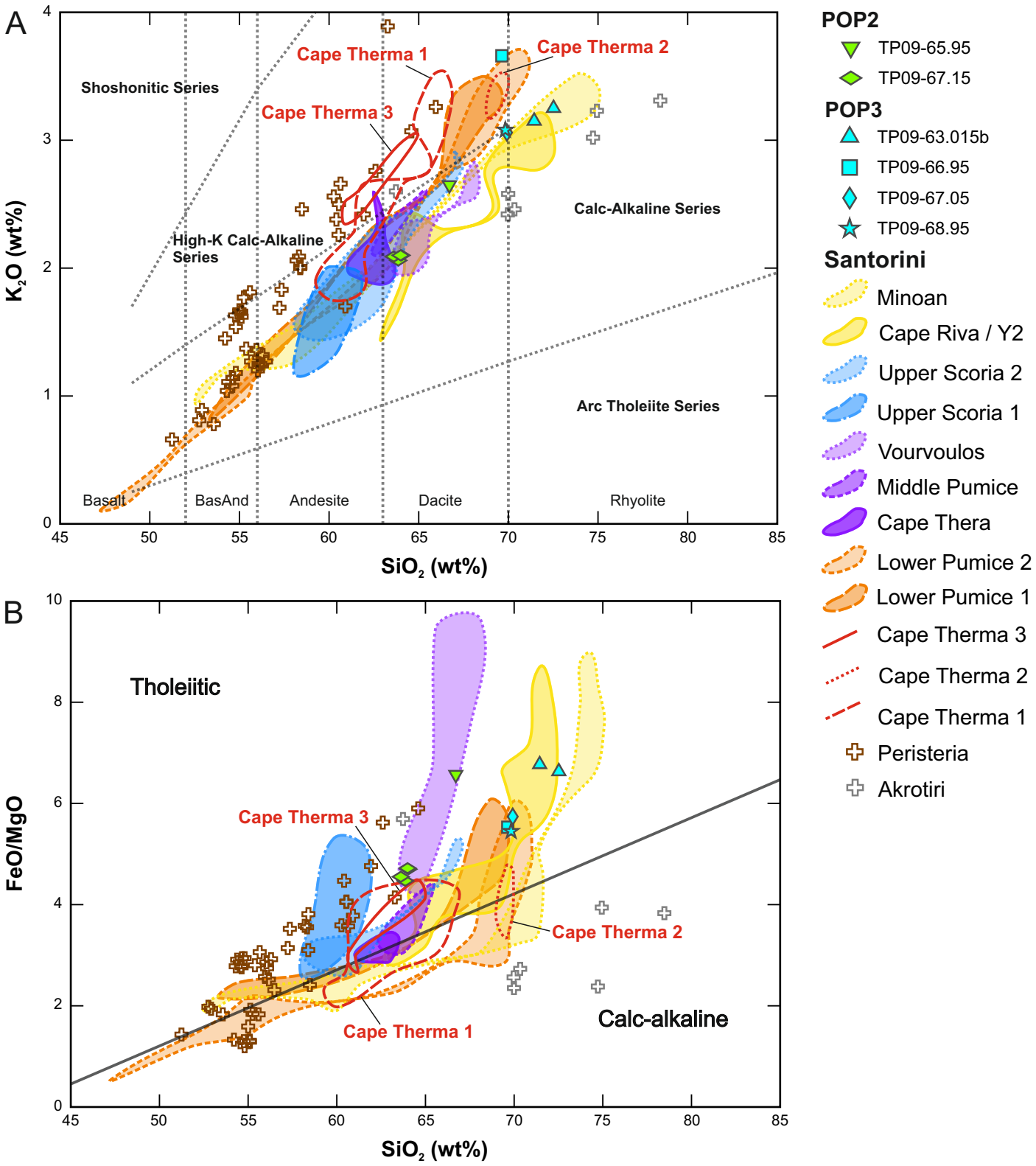

Figure S4-5: **(A)** K_2O *vs.* SiO_2 diagram (Peccerillo and Taylor, 1976) and **(B)** FeO/MgO *vs.* SiO_2 diagram (Miyashiro, 1974) showing dacitic (POP2) and rhyolitic (POP3) cryptotephras from Tenaghi Philippon in comparison with Santorini major pyroclastic units. Data sources: see Fig. 6 in the text.

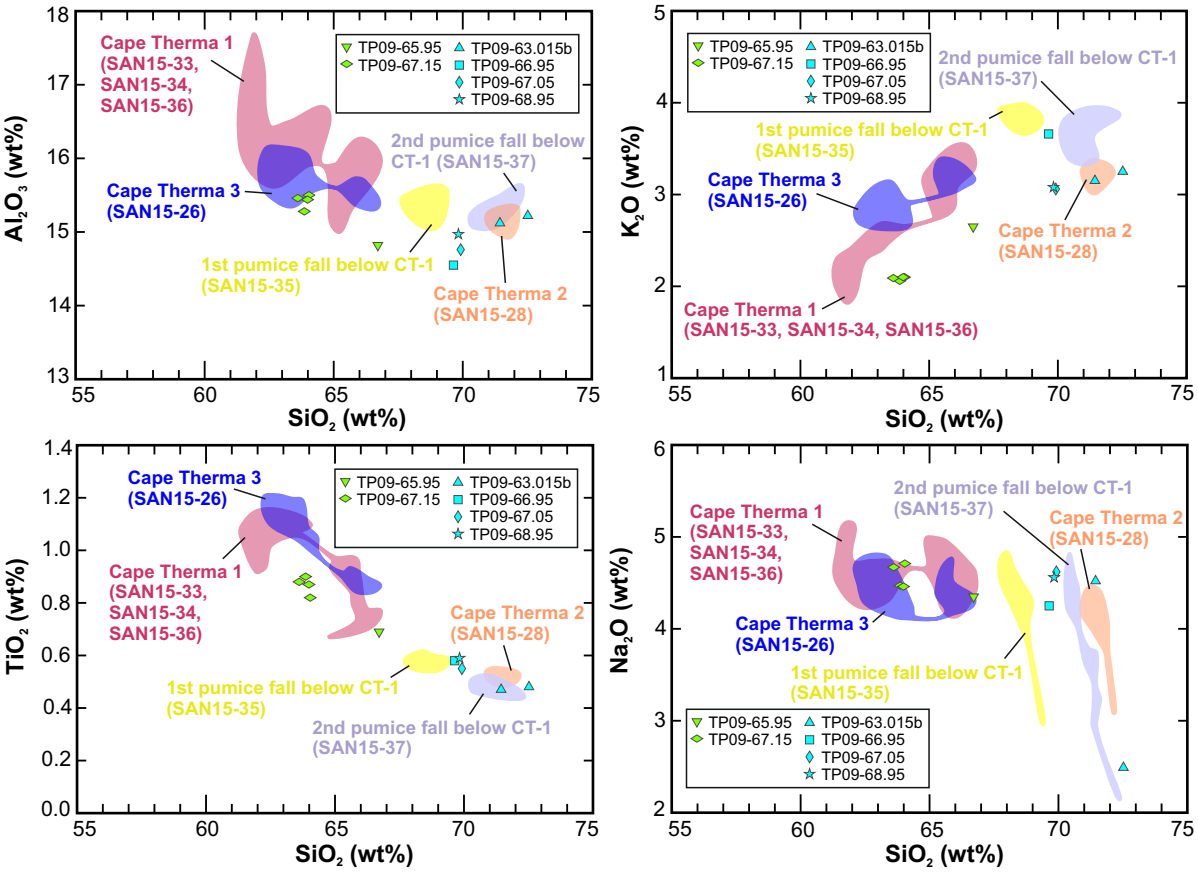

Figure S4-6: Complementary major- and trace-element plots to Fig. 7 in the text.

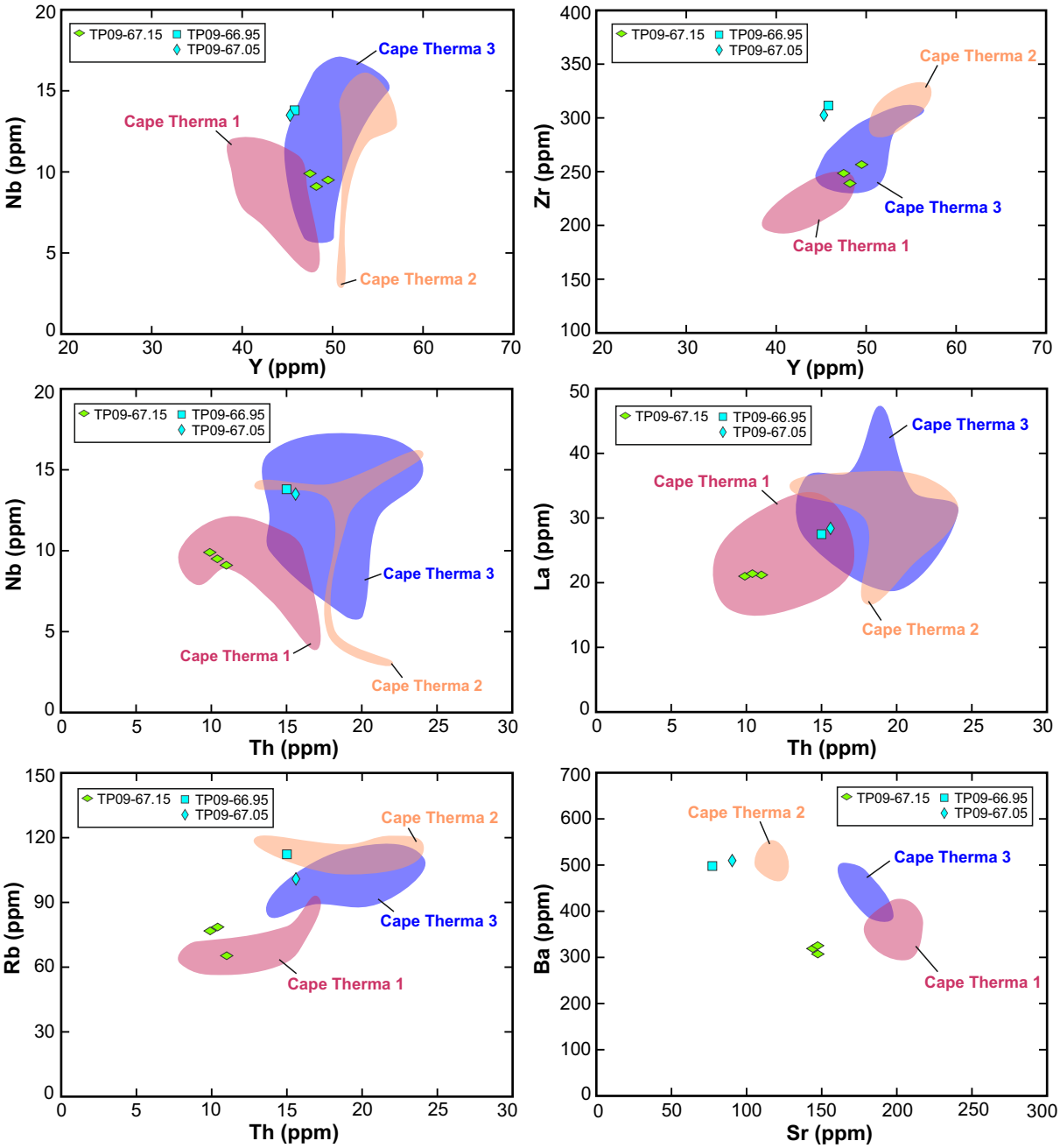

Figure S4-6: (*continued*).

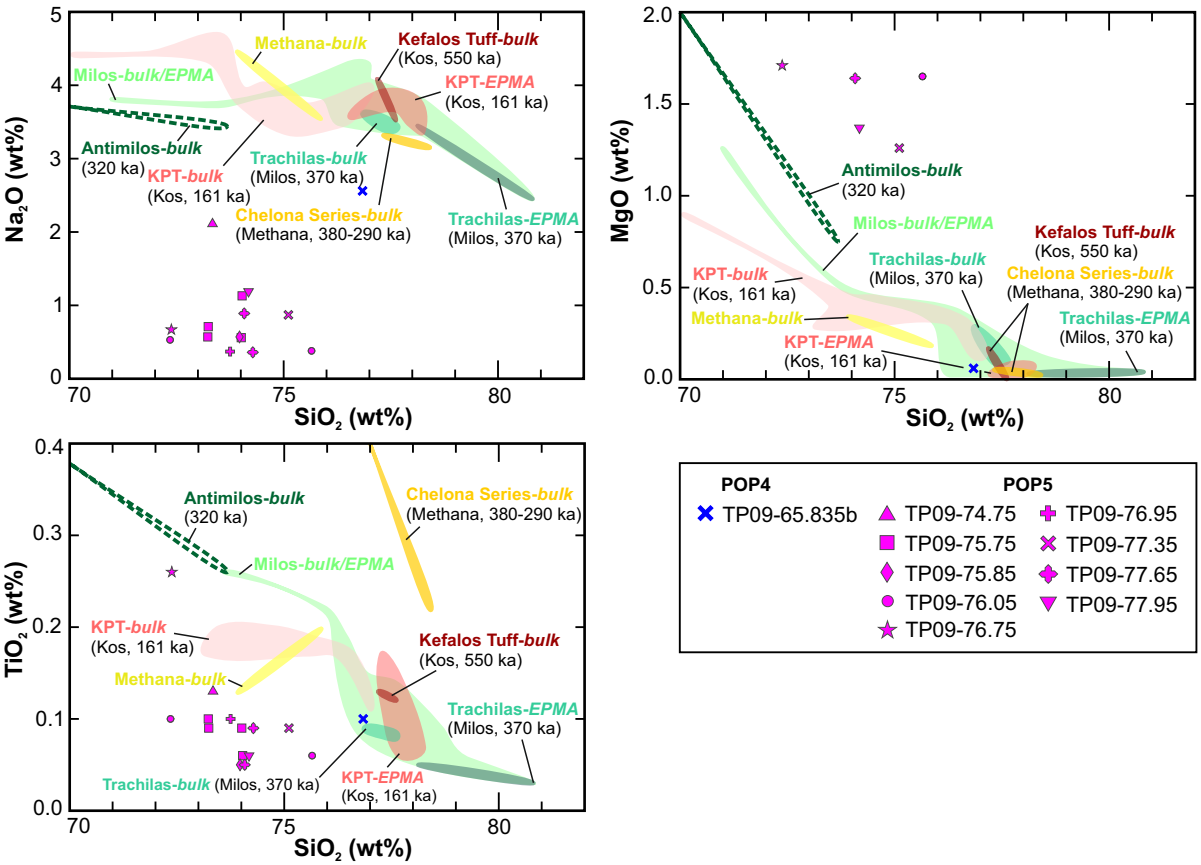

Figure S4-7: Complementary major-element plots to Fig. 8 in the text.